40Gbit/s DISPERSION MANAGED SOLITON TRANSMISSION

ROBIN ANTHONY IBBOTSON

Doctor of Philosophy

ASTON UNIVERSITY

December 2005

ASTON UNIVERSITY

40Gbit/s DISPERSION MANAGED SOLITON TRANSMISSION

ROBIN ANTHONY IBBOTSON

Doctor of Philosophy

December 2005

This thesis contains the results of experimental and numerical simulations of optical transmission systems using dispersion managed transmission techniques. Theoretical background is given on the propagation of pulses in optical fibres before extending the arguments to optical solitons, their applications and uses in communications. Dispersion management for transmission systems is introduced and then a brief explanation of quasi-linear pulse propagation is given.

Techniques for performing laboratory transmission experiments are divulged and focus on the construction and operation of a recirculating loop. Laser sources and modulators for 40Gbit/s transmission rates are discussed and techniques for acquiring information from the resultant eye are explained.

The operation of optically time division demultiplexing with a nonlinear elecro-absorption modulator is considered and then is replaced by the used of a linear electro-optic modulator and Dispersion imbalanced loop mirror (DILM). The use of nonlinearity as a positive effect for the use of processing and regenerating optical data is approached with an insight into the operation interferometers. Successful experimental results are given for the characterisation of the DILM and 40Gbit/ to 10Gbit/s demultiplexing is demonstrated.

Modelling of a terrestrial style system is performed and the methods for computer simulation are discussed. The simulations model single channel 40Gbit/s transmission, 16 x 40Gbit/s WDM transmission and WDM transmission with varying channel separation. Three modulation formats are examined over the single mode fibre span. It is found that the dispersion managed soliton is not suitable for terrestrial style systems and that return-to-zero was the optimum format for the considered system.

Additional key words and phrases

Nonlinear optics, optic fibres, optical solitons, optical networks, dispersion management, nonlinear optical loop mirrors

Acknowledgements

This is the section where I have free reign over my words; the r
vetted out, so please bear with me. I would like to thank all thr
Firstly Nick Doran, his passion and fascination about the subj
field, Igor Khruschev for his technical expertise and his val
finally Keith Blow for his immense experience and his clarity
thanks are given to the two people from whom I derived almost a
knowledge, Steven Alleston and Paul Harper. I still aspire to the
and the exacting workaholic nature of Paul, although I doubt I'l
lines around my tools, but I do have remarkably tidy colour
Russell Davey, my external supervisor for showing me professi
me with invaluable workplace experience, Yu Rong, And
exceptional technical tuition and Ed Sikora for his provoking que
Shelley Fevien, for their help in the lab and construction of the
loop mirror, Bert Biggs for maintenance of the lab and equipmer
tirelessness in running the research group and everyone else in th
Group for countless discussions and pub lunches.

I also acknowledge the financial support of BTexact and the EPS

Table of Contents

List of Figures

Chapter 1

Introduction

1.1 • Introduction

The use of optical frequencies for the transmission of information has been around for a long time. The majority of the world's communication backbone is now made up of spans of fibre, which are used to carry the billions of bits of data people use in their daily lives. Traditional telephony systems that transport the 64kbit/s voice are no longer the median. These are now required to carry services that require a higher data rate such as video conferencing, Internet streaming and many carriers are professing everyday utilisation of third generation broadband mobile technology. As the demand for these higher bandwidth telecommunication services increases, it provokes research into optical communication systems that can support the higher data rates required to sustain the consumer demands. Research in optical communications is not only confined to communication systems but also encompasses investigations into high-speed sources, detectors and bit rate independent devices.

In order to increase the information capacity, a number of solutions exist. Time division multiplexing (TDM) interleaves channels in time and can occur in both the electrical domain or in the optical domain. This introduces restrictions on the pulse width as the bit window has reduced. Electrical time division multiplexing (ETDM) places a burden on the speed of the electronics in the transmitter and receiver, whereas optical time division multiplexing (OTDM) allows simple multiplexing in the time domain, yet requires more complicated optical demultiplexing schemes. Wavelength division multiplexing (WDM) is another approach, by which the system capacity can be increased by introducing additional wavelengths carrying data. This requires additional electronics at the receiver and transmitter, although these operate at the current system modulation frequency.

1.2 • Objective of the research

The aim of the research was to examine the suitability of the dispersion managed soliton (DMS) for high speed 40Gbit/s systems. Experimentally this requires the understanding of the composition of 40Gbit/s transmitters, multiplexers, receivers, demultiplexers and the recirculating loop. Theoretically, this requires the analysis of the various linear and nonlinear effects and methods that can be used to overcome them. For the case of wavelength-division-multiplexed dispersion-managed-soliton transmission, the research must also investigate the nonlinear effects that are generated when introducing multiple copropagating signals. This understanding can then be used to look at the suitability of the dispersion managed soliton with respect to WDM terrestrial communication systems.

1.3 • Research Approach

Initially the work was experimental in nature, with work focusing on the operation of the recirculating loop test bed that would be utilised for the transmission of dispersion managed solitons. This was initially at 10Gbit/s and then increased to 40Gbit/s by the use of optical time division multiplexing (OTDM). The 40Gbit/s OTDM data was demultiplexed by an electro-absorption modulator based demultiplexer. Unfortunately, this research groups sole EAM was damaged and a new method of demultiplexing at 40Gbit/s was required. This took the shape of a nonlinear interferometer based demultiplexer.

With the contractual requirements of work for the research sponsor, BTexact, and the lack of available experimental research facilities, the research focused around the simulation of systems. A terrestrial style system was adopted as a test bed to investigate the ability of six 100km spans of single mode fibre (SMF) to sustain high speed 40Gbit/s transmission.

1.4 • Structure of the Thesis

Chapter 2 introduces the linear fibre effects of dispersion and loss, and introduces the topic of nonlinearity. The main components of the nonlinear Schrödinger wave

equation (NLSE) are introduced and they are used to examine the behaviour of group velocity dispersion (GVD) and self phase modulation (SPM). The concept of the Soliton is introduced and the negative effects that it generates are examined. This is to provide the reader with the basic understanding of linear and nonlinear effects.

In chapter 3 dispersion management and wavelength division multiplexing is investigated. Dispersion management is frequently used in systems to compensate for dispersion, therefore both the dispersion map is described and how soliton like pulses can propagate along dispersion maps is explained. A scale for this suitability, known as map strength, is given and the concept of dense dispersion management, by which a multiple repetitions of a short dispersion map are used between nodes, is introduced. The Quasi-linear region, defined as the overlap between linear and nonlinear interactions in a transmission span, is discussed and is particularly important for systems that cannot sustain dispersion managed solitons. The WDM nonlinear interactions of cross phase modulation (XPM) and four wave mixing (FWM) are explained so that they affect they have WDM systems can be greater understood.

Chapter 4 introduces the reader to the experimental domain and investigates the suitability of sources, optical time division multiplexers (OTDM) and optical time division demultiplexers (OTDD) for 40Gbit/s transmission. Initially the distributed feedback (DFB) laser is examined with attention paid to how the jitter can be reduced. The operating principles of two types of optical modulator are described and their characteristics are contrasted. These are then used to apply data to the PriTel fibre laser, which is used as a source in a chapter 5, and this source is OTDM to 40Gbit/s. The main test bed for a laboratory based transmission experiment is the recirculating loop, its salient features are described and the principle of its operation is given.

Chapter 5 examines methods for the OTDD of the 40Gbit/s system proposed in chapter 4; starting with the conventional electro-absorption-modulator (EAM) based demultiplexer. Due to the failure of the EAM, an electro optic modulator was used to replace the EAM in the demultiplexer although this was unsuitable due to its linear response. Nonlinear interferometers are introduced and the dispersion imbalanced loop mirror is used to aid the EOM in 40Gbit/s demultiplexing.

In Chapter 6 computer simulations based on a terrestrial style dispersion map are produced in order to test the suitability of this fibre map for 40Gbit/s dispersion managed solitons (DMS). The theory behind optical simulation is explained and the method adopted (including the handling output data) is presented. The features of the

simulation tool are explained and a list of the parameters for the proposed test system is given. The fibre map is then discussed and its ability to support dispersion managed solitons is examined. The simulations initially examine the case for single channel 40Gbit/s transmission using the return-to-zero (RZ), chirped-return-to-zero (CRZ) and non-return-to-zero (NRZ) modulation formats. This is then expanded to incorporate 16 wavelengths and the effect of channel spacing is explored. Finally conclusions based on the results are made with regards to upgrading a system to 40Gbit/s.

In the final chapter, a summary of the main elements of the thesis are given and the possible future work that can stem from this research is discussed.

1.5 • Original Contributions

The original contributions to research found in this thesis are:

- Error free experimental demonstration of demultiplexing from 40Gbit/s to 10Gbit/s using an electro-optic modulator with the aid of a dispersion imbalanced loop mirror, described in chapter 5.
- The experimental suitability of the DILM enhanced EOM OTDD for demultiplexing data over a distance of 200km SMF and DCF span, shown in chapter 5.
- The simulation of single channel transmission at 40Gbit/s using NRZ, RZ and CRZ data over a SMF and DCF fibre map with 100km amplifier separation, in section 6.6.
- The simulation of 16 channel WDM transmission at 40Gbit/s using NRZ, RZ and CRZ data over a SMF and DCF fibre map with incomplete dispersion slope compensation with a 100km amplifier separation in section 6.7
- The effect of increasing and decreasing the channel separation for 16 channel WDM transmission at 40Gbit/s using NRZ, RZ and CRZ data over a SMF and DCF fibre map with 100km amplifier separation, shown in section 6.8

Chapter 2

Propagation of Light in Fibres

2.1 • Introduction

In 1970 a fibre with a waveguide structure with and a loss of around 20dB/km was fabricated [1], and the ability to transmit light along a relatively low loss medium was realised. Another component, along with the fibre medium, required for the optical transmission of data system is a suitable optical data source. The invention of the Laser in 1958 and the realisation of the first laser in 1960 provided an intense, coherent, monochromatic source although the unclad fibre medium at that time had a loss of around 1000dB/km. In 1966 K. C. Kao and G. A. Hockham's paper on dielectric-fibre surface waveguides for optical frequencies surmised that a dielectric fibre with a refractive index higher than its surrounding region is a form a dielectric waveguide which represents a possible medium for the guided transmission of energy at optical frequencies [2]. Today standard single mode fibre has an attenuation of approximately 0.2dB/km at a wavelength of 1550nm.

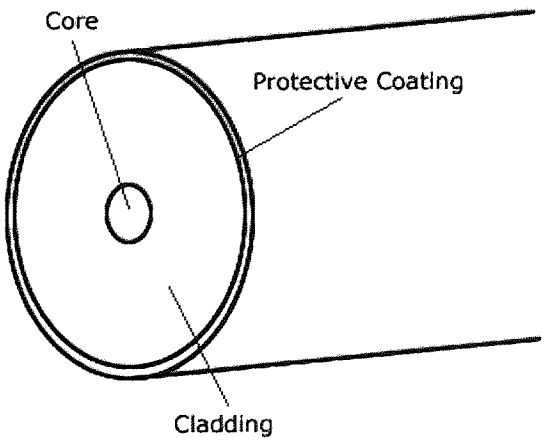

Figure 2.1: Cross section of an optical fibre depicting the core (n_2) cladding (n_2) and protective plastic coating (not to scale)

The waveguide in optical fibre is made of two materials of differing refractive indexes, a central core with a greater refractive index of that of the outer cladding (Fig. 2.1). Total internal refraction of the light is attainable due to this stepwise modulation of the refractive index across the diameter of the fibre cross section. As the refractive index of the core is greater than that of cladding, the incident ray is refracted away from the normal if the incident angle does not exceed the critical angle. In this situation the fibre acts as a waveguide. Most modern fibre in communication systems utilises silica as the main medium for the core and the cladding, owing to silica's low attenuation, and utilises this step index method. Fibres utilising a spherical refractive index step are not the only fibre available, other geometries such as graded index fibre and the elliptical core of some polarisation maintaining fibre are available but will not be considered here. Step index fibre can characterised by two parameters, Δ, sit the relative core-cladding index difference defined by;

$$\Delta = \frac{n_1 - n_2}{n_1}, \tag{2.1}$$

where n_1 and n_2 are the refractive indices of the core and cladding respectively. The second is the normalized frequency V is given by;

$$V = k_0 a\left(n_1^2 - n_2^2\right)^{\frac{1}{2}}, \tag{2.2}$$

where a is the core radius, $k_0 = 2\pi/\lambda$ is the wavenumber and λ is the wavelength of light. The V parameter defines the number of modes that can propagate through the fibre. For fibre that supports only one propagation mode, V is less than 2.405. Notice how the number of propagating modes is not only dependent on core area but is also reliant on the wavelength of the light, therefore SMF is only single mode at specific wavelengths.

The attenuation of signal power due to the characteristics of fibre is one of the most important linear effects to account for in the design of an optical communication system. Attenuation reduces the average power reaching the receiver, decreasing the optical signal to noise ratio and is also one of the factors that can limit the maximum amplifier separation. The attenuation coefficient α is given by;

$$\alpha = -\frac{1}{L}\ln\frac{P_{out}}{P_{in}}, \tag{2.3}$$

where P_{in} and P_{out} are the input and output powers respectively and L is the fibre length in km. The common procedure is to express the attenuation in the units of db/km by using;

$$\alpha = -\frac{10}{L}\log\frac{P_{out}}{P_{in}}. \qquad (2.4)$$

The attenuation profile for conventional single mode silica fibre is shown in Fig. 2.2. There are two main causes of loss in optical fibre, absorption and scattering losses.

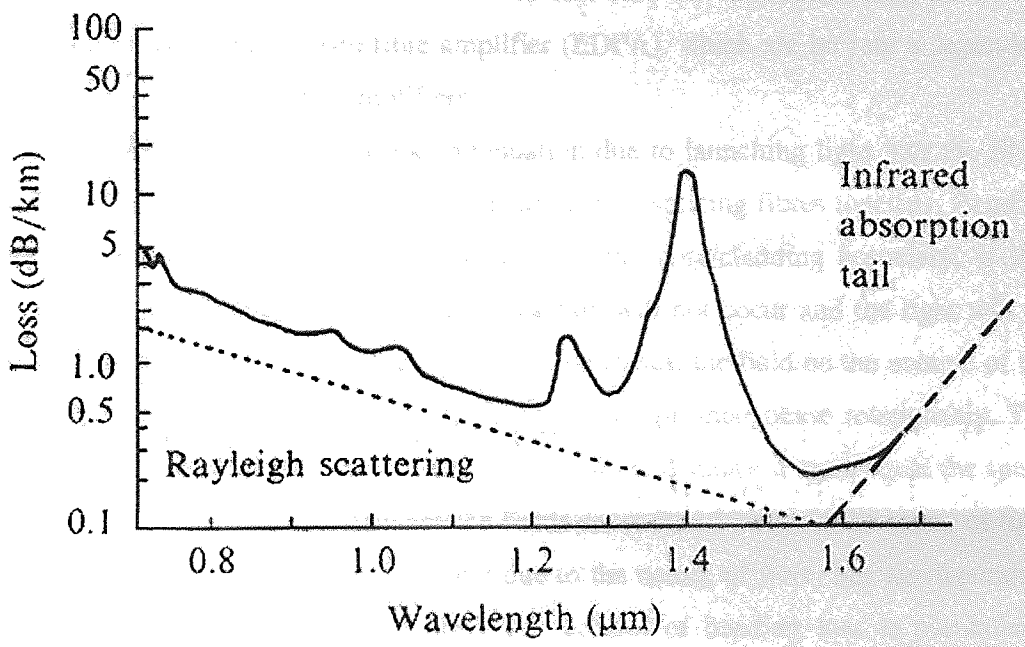

Figure 2.2: Attenuation profile for conventional single mode fibre showing the two low operating windows and highlighting the effects of Rayleigh scattering and Infrared absorption. Adapted from Miya et al (1979) [3] taken from [4]

Loss in a fibre due to absorption is derived from three constituent parts, absorption by atomic atomics defects in the glass composition, extrinsic absorption by impurity atoms and absorption by that of the intrinsic constitution of the material. Impurity absorption varies depending on the impurity. The absorption for metals is due to electrons absorbing photons, although these types of impurities are small. The largest impurity absorption is due to the OH ion that is difficult to avoid during fibre construction due to the water in the atmosphere. This has a strong absorption at 2.7μm and there are harmonics resulting from this peak at 0.95μm, 1.25μm and 1.39μm. The other main cause of loss is the scattering that arises from local fluctuations in density,

known as Rayleigh scattering. Rayleigh scattering follows a λ^{-4} dependence, dramatically increasing with decreasing wavelength.

The scattering and absorption characteristics are both incorporated in Fig. 2.2 and this loss profile, shown in Fig 2.2, and from this the three traditional operating windows can be identified for optical transmission. The first is at 850nm where the loss is ~10dB/km and was selected due to sources and detectors. The second window is at 1300nm, which is both the zero dispersion wavelength for conventional single mode fibre and a low loss region. Finally, the third window at 1550nm is now the most common and is used because it has the lowest loss of ~0.2dB/km and allows the utilisation of the erbium doped fibre amplifier (EDFA), which are bit rate independent as opposed to semiconductor amplifiers.

Other extrinsic losses can occur like attenuation due to launching light into the fibre, bending/compressing the fibre and loss incurred from splicing fibres together. Bending fibre changes the angle of the ray incident on the core/cladding boundary, if this exceeds the critical angle, total internal refraction will not occur and the light will be refracted out of the core. As well as the refraction losses, the field on the outside of the bend must travel faster than that of the inside to sustain their phase relationship. The velocity increases with the radial distance and at some distance it must equal the speed of light, when it exceeds this distance the fields are radiated away as the speed of light cannot be exceeded. These losses are not due to the nature of fibre, but are dependent on the physical properties of the fibre. The control of bending loss is particularly useful in situations where additional loss is required in a system or component.

The interaction a medium has with light is dependent on the optical frequency of the electromagnetic wave, resulting in different frequencies travelling at different velocities. This effect causes a pulse composed of various frequencies to disperse as it propagates along a fibre. Narrow bandwidth lasers, such as semiconductor DFB lasers, can be utilised in order to reduce dispersion, but even these are not of one true wavelength and still suffer from its effects. The two main causes of this dispersion in single mode optical fibre are dispersion caused by the material and dispersion caused by the waveguide. Material dispersion is due to the variation of the core material as a function of wavelength, which results in a wavelength dependence of the group velocity. Waveguide dispersion occurs as not all light propagating along the fibre is confined to the core and the light travelling in the cladding will travel at a different

velocity, this is known as waveguide dispersion. It is clear that by altering dimensions such as the core area, cladding area and the refractive index of the material will affect this interaction and can be used to control the resultant dispersion in an optical fibre. Dispersion causes a large problem in a communication system and has to be managed carefully. As optical communications represents bits with pulses of light, when a bit stream propagates along a fibre, dispersion will cause the pulses to spread. After propagating a sufficient distance, the pulses will broaden sufficiently so that they overlap with those in the adjacent bit slots, rendering the two bits undistinguishable by the receiver.

Conventional single mode fibre, which is the most common fibre installed in current commercial systems, has the dispersion profile described in Fig 2.3.

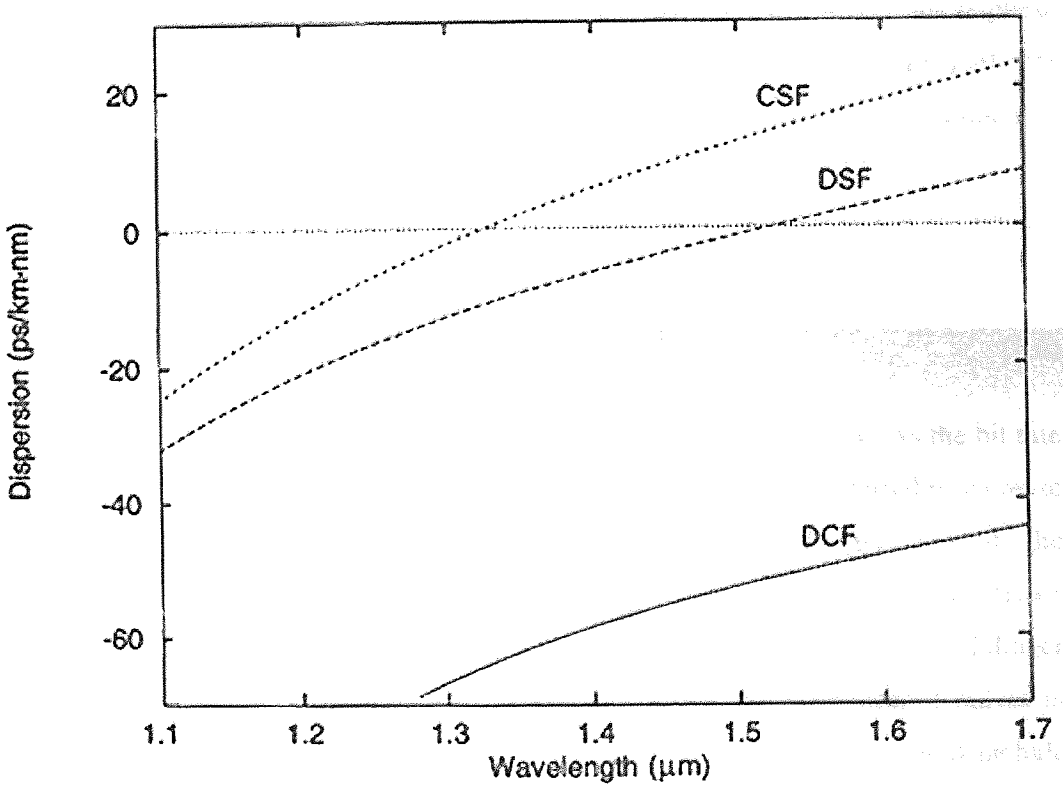

Figure 2.3: The dispersion profile for three types of fibre, showing dispersion against wavelength for conventional single-mode fibre (CSF), dispersion shifted fibre (DSF) and dispersion compensating fibre (DCF). Taken from [5]

The dispersion parameter D is measured in ps/(nm.km) and is described by the following equation;

$$D = \frac{d\beta_1}{d\lambda} \approx -\frac{\lambda}{c}\frac{d^2 n}{d\lambda^2}. \qquad (2.5)$$

Fig 2.3 shows that, for CSF, the zero-dispersion wavelength is around 1300nm but in order to take advantages of erbium doped fibre amplifiers, system wavelengths have shifted from the zero-dispersion wavelength, to 1550nm where the dispersion is approximately 17ps/(nm.km). 1550nm is in the anomalous-dispersion regime, where $D > 0$ and the higher frequency components (lower wavelengths) travel faster than the lower frequency components (higher wavelengths). The opposite occurs in the normal dispersion regime where $D < 0$. To operate at 1550nm in conventional single-mode fibre, the negative effects of dispersion must be counteracted.

For systems, these linear effects were initially of main concern and fibre nonlinearities were overlooked. These nonlinear phenomena can be split into two categories. Kerr nonlinearities comprise of effects such as self phase modulation (SPM), cross phase modulation (XPM) and four wave mixing (FWM). The other category are nonlinear effect that stem from atomic/molecular/material scattering, such as stimulated Brillouin scattering (SBS), stimulated Raman scattering (SRS) and core electrostriction. The Kerr-effect gives rise to an intensity dependent refractive index n given by;

$$n(z,t) = n_0 + n_2 \frac{P(z,t)}{A_{eff}}, \qquad (2.6)$$

where n_0 is the linear refractive index and n_2 is the nonlinear coefficient. As the bit rate and transmission distance increase, these nonlinear interactions also started to increase and it was no longer suitable to ignore these nonlinear effects. In order to study the propagation of pulses in optical fibre it is necessary to derive a model that describes the linear and nonlinear processes. Initially in this chapter, the nonlinear Schrödinger equation (NLSE) will be derived in order to understand the propagation of pulses in single mode fibre. The derivation of the NLSE will not be thorough but will include the important elements. The NLSE will then be used to analyse the effects of group velocity dispersion (GVD) in a linear dispersive medium and self phase modulation (SPM) in the nonlinear regime. The combined effects of GVD and SPM in relation to optical solitons will be considered for both the lossless and lossy case and finally the problems generated by soliton transmission in a communications system are examined.

The basic wave equation used to describe the propagation of an electromagnetic field in a cylindrical waveguide can be derived from Maxwell's equations [6];

$$\nabla^2\mathbf{E}-\frac{1}{c^2}\frac{\partial^2\mathbf{E}}{\partial t^2}=\mu_0\frac{\partial^2\mathbf{P}_L}{\partial t^2}+\mu_0\frac{\partial^2\mathbf{P}_{NL}}{\partial t^2}, \tag{2.7}$$

where c is the velocity of light, μ_0 is the permeability of free space. Since SiO_2 is a symmetric molecule, only the first, $\chi^{(1)}$ and third, $\chi^{(3)}$ order susceptibilities are considered for the induced polarisation, $\mathbf{P}(\mathbf{z},t)$ giving;

$$\mathbf{P}(\mathbf{z},t)=\mathbf{P}_L(\mathbf{z},t)+\mathbf{P}_{NL}(\mathbf{z},t). \tag{2.8}$$

We assume the nonlinear polarisation $\mathbf{P}_{NL}$ is only a small perturbation to the linear polarisation $\mathbf{P}_L$ and that the polarisation of the optical field is constant throughout propagation, as to validate a scalar approach. Also it is assumed that the optical field is quasi-monochromatic i.e., ω_0 is the central frequency, $\Delta\omega/\omega_0 << 1$ where $\Delta\omega$ is the spectral width. The electric field $\mathbf{E}(\mathbf{r},t)$ is a slowly varying function depending on $\mathbf{r}$, the direction of propagation and t, time given by;

$$\mathbf{E}(\mathbf{r},t)=\frac{1}{2}\hat{x}\left[\overline{E}(\mathbf{r},t)\exp(-i\omega t)+c.c.\right], \tag{2.9}$$

where $\hat{x}$ is the polarisation unit vector of the light and *c.c.* is the complex conjugate. Similar equations can be derived for the slowly varying nonlinear and linear polarisation components.

In order to continue deriving the generalised NLSE, a number of assumptions must be stipulated. Firstly we shall assume that the nonlinear response is instantaneous, which in effect neglects the vibrations to the third order susceptibility. This assumption is valid for pulses over 1ps but it must be included for pulses shorter than 100fs [7]. Also the nonlinear contribution to the dielectric constant, is taken as a constant in order to take the Fourier transform of;

$$\tilde{E}(\mathbf{r},\omega-\omega_0)=\int_{-\infty}^{\infty}\mathbf{E}(\mathbf{r},t)\exp[i(\omega-\omega_0)t]dt, \tag{2.10}$$

that satisfies;

$$\nabla^2\tilde{E}+\varepsilon(\omega)k_0^2\tilde{E}=0, \tag{2.11}$$

where $k_0 = 2\pi/\lambda$ is the propagation constant and;

$$\varepsilon(\omega) = 1 + \tilde{\chi}^{(1)}_{xx}(\omega) + \varepsilon_{NL}, \tag{2.12}$$

is the dielectric constant. The dielectric constant can used to define the intensity dependent refractive index $\tilde{n}$;

$$\tilde{n}(\omega) = n(\omega) + n_2|E|^2, \tag{2.13}$$

where n_2 is the coefficient of nonlinearity (not cladding index) given by;

$$n_2 = \frac{3}{8n}\mathrm{Re}\left(\chi^{(3)}_{xxxx}\right). \tag{2.14}$$

It is now convenient to use a separation of variables to take the form;

$$\tilde{E}(\mathbf{r}, \omega - \omega_0) = F(x, y)\tilde{A}(Z, \omega - \omega_0)\exp(i\beta_0 Z), \tag{2.15}$$

where $\tilde{A}(Z, \omega - \omega_0)$ is a slowly varying function of Z and β_0 is the wave number. In single mode fibre $F(x, y)$ is a Bessel function within the core and decays exponentially outside the core. The Fourier transform $\tilde{A}(Z, \omega - \omega_0)$ of the slowly varying amplitude $A(Z, t)$ can be written as;

$$\frac{\partial \tilde{A}}{\partial Z} = i[\beta(\omega) + \Delta\beta - \beta_0]\tilde{A}, \tag{2.16}$$

where $\Delta\beta$ is evaluated from a modal distribution $F(x, y)$ [8] and the perturbation in the refractive index due to nonlinearity and loss Δn given by;

$$\Delta n = n_2|E|^2 + \frac{i\alpha}{2k_0}. \tag{2.17}$$

The inverse Fourier transform provides the propagation equation and for this it is useful to expand $\beta(\omega)$ in a Taylor series about the carrier frequency ω_0 to give;

$$\beta(\omega) = \beta_0 + (\omega - \omega_0)\beta_1 + \frac{1}{2}(\omega - \omega_0)^2\beta_2 + \frac{1}{6}(\omega - \omega_0)^3\beta_3 + \cdots, \tag{2.18}$$

$$\beta_n = \left(\frac{\partial^n \beta}{\partial \omega^n}\right)\omega = \omega_0. \tag{2.19}$$

In the Taylor expansion, β_0 is the propagation constant, β_1 is the inverse group velocity, β_2 is the group velocity dispersion and β_3 is the third order dispersion. Substituting for β and $\Delta\beta$ whilst taking the inverse Fourier transform replacing $\omega - \omega_0$ by the operator $i(\partial/\partial t)$ gives;

$$\frac{\partial A}{\partial Z}+\beta_1\frac{\partial A}{\partial t}+\frac{i}{2}\beta_2\frac{\partial^2 A}{\partial t^2}+\frac{\alpha}{2}A=i\gamma|A|^2A, \tag{2.20}$$

where the nonlinearity coefficient is defined by;

$$\gamma=\frac{n_2\omega_0}{cA_{eff}}. \tag{2.21}$$

A_{eff} is the effective core area determined from the modal distribution $F(x,y)$ for the fundamental fibre mode. It is clear to see that the nonlinearity coefficient is inversely proportional to the effective area and thus depends on fibre parameters such as core diameter and the index difference between the fibre core and cladding. Therefore fibre manufacturers can tailor the nonlinearity of fibre for any application by modifying these parameters. For conventional single mode fibre the effective area is generally around $80\mu m^2$ providing a nonlinearity coefficient of approximately $1.3W^{-1}\,km^{-1}$.

It is useful to try and modify equation 2.20 by utilising a frame of reference moving with the pulse at the group velocity, v_g, by making the transformation;

$$T=t-\frac{Z}{v_g}=t-\beta_1 Z. \tag{2.22}$$

Equation 2.20 becomes;

$$i\frac{\partial A}{\partial Z}+\frac{i}{2}\alpha A-\frac{1}{2}\beta_2\frac{\partial^2 A}{\partial T^2}+\gamma|A|^2A=0. \tag{2.23}$$

This equation is known as the generalised nonlinear Schrödinger equation (GNLSE) and is a very good description for the propagation of pulses through single mode optical fibre when ignoring polarisation mode dispersion, and propagating in a single polarisation state [9]. The second term in the GNLSE designates the loss, the third term represents the group velocity dispersion and the final term governs the Kerr nonlinearity. In the case when there is no fibre loss, the equation is referred to as the nonlinear Schrödinger equation (NLSE). The equation can also be expanded to take account of higher order dispersion by including more terms from the Taylor expansion (2.18), as higher order dispersion becomes important when operating near the zero dispersion point (λ_0) where $\beta_2=0$.

Depending on the peak power or the initial width of an input pulse either the dispersive or nonlinear term in the GNLSE can dominate and effect the propagation along a fibre. It becomes useful to introduce two lengths scales, the dispersion length, L_D and the nonlinear length, L_{NL} that provide the length over which dispersive and nonlinear

effects become important for propagation over a fibre of length L. The first length scale, the dispersion length, is given by;

$$L_D = \frac{T_0^2}{|\beta_2|}, \tag{2.24}$$

and the second length scale, the nonlinear length, is given by;

$$L_{NL} = \frac{1}{\gamma P_0}, \tag{2.25}$$

where T_0 is the half width of the pulse (1/e pulse width), P_0 is the peak pulse power and γ is the nonlinearity coefficient. The pulse width more commonly used is the full pulse width at half the maximum intensity, T_{FWHM}, although this parameter is dependent on the pulse shape (equation 2.34).

Four different propagation regimes can be obtained by analysing the relationship between the length scales and the propagation length, there are as follows

i) $L << L_D, L << L_{NL}$: Neither dispersive nor nonlinear effects are important during pulse propagation.

ii) $L \geq L_D, L << L_{NL}$: GVD governs the pulse evolution and nonlinearity has a negligible effect.

iii) $L << L_D, L \geq L_{NL}$: Nonlinearity dominates pulse evolution and dispersion is irrelevant.

iv) $L \geq L_D, L \geq L_{NL}$: Both dispersive and nonlinear effects influence the pulse evolution.

The first regime is not important in the study of long distance communications as only broad pulses with low power propagating for short distances would be valid. This leaves us with the remaining three regimes and each one will be investigated in order that the effects of GVD, SPM and the existence of solitons can be studied.

2.3 • Group Velocity Dispersion

Using the length scales of the dispersion length L_D and the nonlinear length L_{NL} for pulse propagation along a fibre, we will consider the case where $L_D \geq L_{NL}$ and $L << L_{NL}$. This is the propagation regime where the group velocity dispersion dominates. The nonlinear Schrödinger equation derived in 2.2 still governs the propagation of

pulses in optical fibres although as GVD is dominating, we can ignore the nonlinear effects and reduce the nonlinear coefficient to zero, $\gamma = 0$. Also loss does not influence the behaviour of dispersion and can be substituted by the normalised amplitude U resulting in;

$$A(Z,T) = \sqrt{P_0}\exp\left(-\frac{\alpha z}{2}\right)U(Z,T), \tag{2.26}$$

$U(Z,T)$ then satisfies the partial differential equation;

$$i\frac{\partial U}{\partial Z} = \frac{1}{2}\beta_2\frac{\partial^2 U}{\partial T^2}. \tag{2.27}$$

Equation 2.27, above, can be solved using the Fourier method. $\tilde{U}(Z,\omega)$ is the Fourier transform of $U(Z,T)$ and is defined by;

$$U(Z,T) = \frac{1}{2\pi}\int_{-\infty}^{\infty}\tilde{U}(Z,\omega)\exp(-i\omega T)d\omega, \tag{2.28}$$

this then satisfies the ordinary differential equation;

$$i\frac{\partial \tilde{U}}{\partial Z} = -\frac{1}{2}\beta_2\omega^2\tilde{U}, \tag{2.29}$$

which, when integrated, has the solution;

$$\tilde{U}(Z,\omega) = \tilde{U}(0,\omega)\exp\left(\frac{i}{2}\beta_2\omega^2 Z\right), \tag{2.30}$$

where $\tilde{U}(0,\omega)$ is the Fourier transform of the pulse at $Z = 0$. This is given by;

$$\tilde{U}(0,\omega) = \int_{-\infty}^{\infty}U(0,T)\exp(i\omega T)dT. \tag{2.31}$$

Equation 2.31 illustrates that the pulse spectrum is unaffected by GVD as it propagates along the fibre but each of the spectral components receives a phase change proportional to the square of the frequency and the distance travelled. It is these phase changes that cause the alteration of the pulse profile as it propagates. Note also the dependence of the phase change on β_2 indicating that behaviour is different in the normal and anomalous regimes.

Substituting equations $\tilde{U}(Z,\omega)$ into $U(Z,T)$ provides the solution;

$$U(Z,T) = \frac{1}{2\pi}\int_{-\infty}^{\infty}\tilde{U}(0,\omega)\exp\left(\frac{i}{2}\beta_2\omega^2 Z - i\omega T\right)d\omega. \tag{2.32}$$

It will prove valuable to gain an understanding of how GVD affects a pulse as it propagates along a fibre. As a simple illustration, the case for a Gaussian input pulse will be considered here. The field of the Gaussian pulse is given by;

$$U(0,T)=\exp\left(-\frac{T^2}{2T_0^2}\right). \tag{2.33}$$

It is common practise to measure the take the pulse width as the full width at half the maximum intensity. For a Gaussian pulse the parameter T_0 is related to the FWHM by;

$$T_{FWHM}=2(\ln 2)^{1/2}T_0\approx 1.665T_0. \tag{2.34}$$

After propagating along a distance Z in fibre with a GVD of β_2, the amplitude of the pulse is described by;

$$U(Z,T)=\left(\frac{T_0}{(T_0^2-i\beta_2 Z)}\right)^{1/2}\exp\left(\frac{T^2}{2(T_0^2-i\beta_2 Z)}\right). \tag{2.35}$$

It can be seen that the Gaussian profile of the pulse is unchanged by GVD but the pulse width increases with Z. Consequently the pulse width becomes;

$$T_1=T_0\left[1+(Z/L_D)^2\right]^{1/2}. \tag{2.36}$$

As the increase in pulse width is inversely proportional to the dispersion length (which is proportional to launch pulse width squared), for a given fibre length shorter pulses broaden more rapidly than broader pulses. This is because the optical spectrum occupied by a shorter pulse is greater than that of a broader pulse and as the different spectral components travel with different velocities through fibre, there is a wider range of velocities for the shorter pulse than that of the broader pulse. L_D is also inversely proportional to the modulus of β_2 therefore, if the fibre has a greater dispersion the rate of broadening increases, even though the sign of the dispersion has no effect. The pulse will only preserve its width if all spectral components arrive together. Any time delay in the arrival of the different spectral components at Z results in pulse broadening.

In addition to the effect of pulse broadening, GVD also induces a frequency shift across the pulse during propagation. This instantaneous frequency change across the pulse is referred to as chirp. This can be seen by separating the equation for pulse amplitude after a distance Z into an amplitude and a phase term to give;

$$U(Z,T)=|U(Z,T)|\exp[i\phi(Z,T)], \tag{2.37}$$

where the phase can be found as [5];

$$\phi(Z,T) = -\frac{\mathrm{sgn}(\beta_2)(Z/L_D)}{1+(Z/L_D)^2}\frac{T^2}{T_0^2} + \frac{1}{2}\tan^{-1}\left(\frac{Z}{L_D}\right). \qquad (2.38)$$

As there is a time dependence to the phase $\phi(Z,T)$ signifying that at any point along the fibre the instantaneous frequency differs across the pulse from the central frequency ω_0 by;

$$\delta\omega = -\frac{\partial\phi}{\partial T} = 2\frac{\mathrm{sgn}(\beta_2)(Z/L_D)}{1+(Z/L_D)^2}\frac{T}{T_0^2}. \qquad (2.39)$$

As the above equation illustrates, unlike GVD induced broadening, the sign of β_2 does affect the linear frequency change across the pulse. Therefore, it can be deduced that in the normal dispersion regime, where β_2 is positive, $\delta\omega$ is negative at the leading edge of the pulse (where $T<0$) and increases linearly across the pulse. The opposite effect can be seen in the anomalous dispersion regime.

Only the case of the unchirped Gaussian input pulse has so far been considered. The Gaussian pulse shape can be used to approximate the pulse shape emitted by most lasers, although another pulse profile of some interest is that of the hyperbolic-secant (*sech*) squared as this is the shape of the fundamental soliton. If in a dispersion only system and a $sech^2(t)$ input pulse is used, the qualitative features of the dispersion induced broadening are almost indistinguishable to those of the Gaussian input pulse model. Oscillations can develop in the trailing edges of pulses when the input pulse has a steeper edged profile, like that of the super Gaussian, although the profile is still similar to that conventional Gaussian. Also due to their broader spectrum, steeper edged pulses will encounter a more rapid dispersion induced broadening.

The final circumstance is that of a chirped input pulse. When the input pulse has a linear chirp, the rate of the dispersion induced broadening is not only dependent on the sign of β_2, but also on the input chirp. If the input pulse chirp is of the same sign as that of the dispersion induced chirp then the pulse experiences broadening at a greater rate than that of an input pulse without chirp. In the opposite case, when the input pulse chirp is of an opposite sign to that of the dispersion induced chirp, the propagating pulse will compress until the effect of the dispersion induced chirp cancels the input chirp to give a transform limited pulse. Eventually the dispersion induced broadening will dominate over the initial chirp and the pulse will broaden at the same rate as that of an unchirped pulse.

So far we have only considered dispersion induced broadening due to the lowest order GVD term proportional to β_2 in the Taylor expansion (2.20) and we have ignored the higher order terms. When operating close to λ_0, i.e. near to where β_2 is equal to zero, and when considering wavelength division multiplexing, it becomes necessary to incorporate third order dispersion, β_3. Including third order dispersion expands the equation (2.26) by adding an addition term. The impact of including this term leads to an asymmetric and oscillatory temporal pulse profile [11].

The dispersion is commonly expressed as the group delay dispersion, D, as opposed to that of group velocity parameter, β_2, as the former is in the more useful units of $ps/(nm.km)$. Their difference is because the group delay dispersion is proportional to the second derivative of the refractive index with respect to wavelength as opposed to frequency. The two parameters are related by;

$$D = -\frac{2\pi c}{\lambda^2}\beta_2 \approx -\frac{\lambda}{c}\frac{d^2 n}{d\lambda^2}. \tag{2.40}$$

As it can be seen from the above equation, D has an opposite sign to β_2. This means that β_2 is negative in the anomalous dispersion regime and positive in the normal dispersion regime and whereas D is negative in the normal dispersion regime and positive in the anomalous dispersion regime.

2.4 • Self-Phase Modulation

The phase of an optical signal is dependent on the refractive index on intensity. As the intensity is time dependent for data, then the phase will also be time dependent. Since the optical frequency is equal to the rate of change of phase with time, the frequency spectrum of the signal will alter as it propagates. This is self phase modulation (SPM). In order to analyse SPM we must consider the regime where the pulse evolution is dominated by nonlinearity and GVD is negligible, $L << L_D$ but $L \geq L_{NL}$. It is clear therefore that eligible input pulses are those with a large peak power, to increase nonlinearity, and those with a wide pulse width, to reduce the effects GVD. To investigate this mathematically, we can set β_2 to 0 in equation (2.20) giving;

$$\frac{\partial U}{\partial Z} = \frac{i}{L_{NL}}\exp(-\alpha Z)|U|^2 U, \tag{2.41}$$

where α is the fibre loss coefficient which is typically around 0.2dB/km in SMF. The loss coefficient is an important parameter when considering Kerr nonlinearity as when a pulse is attenuated, the size of the nonlinear refractive index is also reduced. Remembering that the nonlinear length is given by $L_{NL} = (\gamma P_0)^{-1}$, the equation can then be solved to provide;

$$U(Z,T) = U(0,T)\exp[i\phi_{NL}(Z,T)], \tag{2.42}$$

where $U(0,T)$ is the input pulse amplitude ($Z = 0$) and the nonlinear phase shift, ϕ_{NL}, is given by;

$$\phi_{NL}(Z,T) = |U(0,T)|^2 \left(\frac{Z_{eff}}{L_{NL}}\right), \tag{2.43}$$

with;

$$Z_{eff} = \frac{1}{\alpha}[1 - \exp(-\alpha Z)]. \tag{2.44}$$

The above equations show that SPM induces a phase shift on the pulse that is proportion to the intensity $|U(0,T)|^2$ also observe that this nonlinear phase shift increases with the propagation distance Z. Z_{eff} is the effective length scale of the nonlinearity in a system encountering losses. This length is shorter than that of Z and matches the distance over which the same phase shift would occur without loss.

Self-phase modulation induces a difference in the instantaneous frequency across the pulse from its central value. This chirp can be given by;

$$\delta\omega = -\frac{\partial\phi_{NL}}{\partial T} = -\frac{\partial|U(0,T)|^2}{\partial T}\frac{Z_{eff}}{L_{NL}}, \tag{2.45}$$

and with a Gaussian input pulse (m=1) the SPM-induced chirp can be found to be;

$$\delta\omega = \frac{2T}{T_0^2}\frac{Z_{eff}}{L_{NL}}\exp\left(-\frac{T^2}{T_0^2}\right). \tag{2.46}$$

This equation illustrates that the chirp brought about by SPM increases in magnitude as the propagation distance increases, with new frequencies being created as the pulse propagates. The magnitude of the frequency chirp, like GVD induced broadening, depends on the gradient of the leading and trailing pulse edges. If the edges are steep, like that of a super Gaussian, there is little change in intensity across the pulse, especially across the central region. This results in a linear phase shift across the centre of the pulse [12]. Equation (2.43) shows that the nonlinear phase shift is dependent on

L_{NL} (which is inversely proportional to P_0), therefore the maximum phase shift occurs at the centre of the pulse ($T = 0$), as this is where there is the most intensity. Since U is normalised such that $|U(0,0)| = 1$, the maximum phase shift is;

$$\phi_{\max} = \frac{Z_{eff}}{L_{NL}} = \gamma P_0 Z_{eff} . \tag{2.47}$$

2.5 • Optical Solitons

Hasegawa and Tapert first suggested the use of solitons for optical communications in 1973 [13], but experiments were not performed due to the lack of suitable sources and low loss fibres. This is now no longer the case and many experiments have been carried out using optical solitons over transoceanic distances [14, 15].

Optical solitons are formed when there is a balance between linear and nonlinear effects, therefore in order to examine their behaviour we must consider the regime where both linear and nonlinear effects prevail. This is the final regime where $L \geq L_D$, $L \geq L_{NL}$, and both GVD and SPM have a significant effect on propagation. When considering continuous wave (CW) transmission in this regime the sign of the dispersion is important. If in the normal regime where β_2 is positive, there is a stable CW solution whereas in the anomalous regime where β_2 is negative the CW solution is unstable. This instability is known as modulation instability since it leads to spontaneous modulation of the steady state [16]. In optical fibres modulation instability manifests itself as a fragmentation of the CW radiation and into a train of ultrashort pulses. This can cause problems in NRZ systems where a long train of ones is in essence CW radiation, and due to modulation instability most NRZ systems operate in the normal regime. When considering pulse propagation it becomes more interesting, as when propagating in the anomalous dispersion regime the contrary effects of GVD and SPM can lead to the formation of optical solitons.

Assuming the case without fibre loss, $\alpha = 0$, the NLSE becomes;

$$i\frac{\partial A}{\partial Z} = \frac{1}{2}\beta_2 \frac{\partial^2 A}{\partial T^2} - \gamma |A|^2 A , \tag{2.48}$$

we can take β_2 as -1 as we are only considering the anomalous regime and normalise the equation using;

$$u = N\frac{A}{\sqrt{P_0}}, \xi = \frac{Z}{L_D}, \tau = \frac{T}{\tau_0}, \tag{2.49}$$

where P_0 is the peak power of the pulse, τ_0 is the width of the incident pulse and N is defined as;

$$N^2 = \frac{L_D}{L_{NL}} = \frac{\gamma P_0 \tau_0^2}{|\beta_2|}. \tag{2.50}$$

This gives;

$$i\frac{\partial u}{\partial \xi} + \frac{1}{2}\frac{\partial^2 u}{\partial \tau^2} + |u|^2 u = 0. \tag{2.51}$$

Note that if describing the normal dispersion regime the second term would be negative.

The NLSE can be solved using a method known as the inverse scattering method. This method was derived by Gardner et al. [17] and used by Zakharov and Shabat to solve the NLSE [18]. This inverse scattering method is beyond the scope of this thesis, but it is similar to the inverse Fourier transform method used to solve linear partial differential equations [19]. The result gained from using this method is;

$$u(\xi,\tau) = 2\eta_1 \sec h(2\eta_1\tau)\exp(2i\eta_1^2\xi), \tag{2.52}$$

where the eigenvalue η_1 determines the amplitude of the soliton and is also related to the amplitude and phase. The canonical form of the fundamental soliton can be obtained by normalising such that $2\eta_1 = 1$;

$$u(\xi,\tau) = \sec h(\tau)\exp(i\xi/2). \tag{2.53}$$

Therefore if a hyperbolic secant pulse designed so that the peak power and pulse width results in $N = 1$ or;

$$P_0 = \frac{|\beta_2|}{\gamma\tau_0^2}, \tag{2.54}$$

is launched inside a ideal lossless fibre with only Kerr nonlinearity and without higher order dispersion effect, it will propagate indefinitely without undergoing distortions with no changes in its pulse shape or width. The pulse also acquires a phase shift $\xi/2$ during propagation, although this phase is not dependent on time so the pulse does not acquire a chirp, resulting in a stable pulse spectrum.

As well as the fundamental soliton, there are also other soliton solutions for the NLSE and of particular interest are those higher order solitons whose initial form is given by;

$$u(0,\tau) = N \sec h(\tau), \tag{2.55}$$

where the soliton order is denoted by N. The peak power required to launch the Nth-order soliton is N^2 times that of that for the fundamental soliton. Although first order solitons do not change shape during propagation, those higher order solitons undergo a periodic evolution where the pulse splits and then merges back into its original form. The periodic behaviour is a characteristic of higher order solitons and the period is defined by the term Z_0;

$$Z_0 = \frac{\pi}{2} L_D = \frac{\pi}{2} \frac{T_0^2}{|\beta_2|}. \tag{2.56}$$

Unlike the fundamental soliton where the chirps induced by GVD (sign dependent on β_2) and SPM (constant sign) balance each other exactly, with higher order solitons there is an initial mismatch. Due to the high power the nonlinear length is shorter than that of the dispersion length so initially SPM dominates but over a distance GVD increases, opposing and then overtaking SPM, which creates the oscillatory evolution. Another important property of optical solitons is that they are very stable, even when the pulse shape or power is not ideally matched. The soliton will try and adjust itself during propagation and try to attain the conditions required for a fundamental soliton. During this transition the pulse can shed energy in the form of dispersive waves known as continuum radiation [20, 21]. Obviously this is an additional form of loss and noise and is detrimental to the performance therefore it is necessary to minimise any occurrences of energy shedding [21]. It is clear that solitons have characteristics that are desirable in a communications system, their shape remains constant, they are stable against perturbations, they have a stable spectrum and the interplay GVD and SPM eliminates their detrimental effects.

2.5.1 • Solitons and Fibre Loss

The above argument for solitons in fibre only holds when fibre losses are nonexistent, and in reality fibre losses cannot be disregarded so easily. It is easy to comprehend that loss during propagation will reduce the peak power of the soliton and as a result, induce broadening as there will be insufficient power to generate enough SPM to counteract the GVD. There are two ways to work against this unbalance, either by increasing the SPM, by compensating for the loss [22-24], or by exponentially

decreasing the effects of GVD during propagation [25-27]. In a communication system, the effects of loss are counteracted by periodically introducing amplifiers into a span of fibre that produce enough gain to offset the loss incurred during propagation. It has been shown that as long as the peak pulse power averaged over the propagation length is equal to that of the fundamental soliton power the stable propagation is still possible [22]. The preference is to do this all optically as this removes the problems incurred using bit rate dependent semiconductor based amplifiers that require time to recover after amplification. Their replacement is the now ubiquitous erbium doped fibre amplifier (EDFA) but also newer systems are looking re-introducing Raman based amplification to extend the amplifier spacing. Periodic amplification using EDFAs and semiconductor amplifiers are known as lumped amplification whereas continuous amplification, like Raman amplification, is known as distributed amplification. Distributed amplification is commonly Raman although work has been done using the distributed EDFA [28-30].

For this example we will be considering the lumped amplifier case [31, 32] where each EDFA is taken as a discrete amplifier and the amplifier length is much less than the span between amplifiers. Also that the loss is distributed across the span with the pulse power decreases exponentially between amplifiers and the gain of the amplifier equals that loss. We also assume that the dispersion along the length of the fibre remains constant. Adding a loss term to the initial soliton based NLSE gives;

$$i\frac{\partial u}{dz}+\frac{1}{2}\frac{\partial^2 u}{\partial\tau^2}+|u|^2u=-i\Gamma u\,, \tag{2.57}$$

where;

$$\Gamma=\frac{\alpha L_D}{2}=\frac{\alpha T_0^2}{2|\beta_2|}, \tag{2.58}$$

is the normalised loss. We have already seen that when Γ is ignored that the equation has steady and periodic solutions. Using the transformation $u(z,\tau)=a(z)v(z,\tau)$, equation 2.57 gives;

$$i\frac{\partial v}{dz}+\frac{1}{2}\frac{\partial^2 v}{\partial\tau^2}+a^2(z)|v|^2v=0\,, \tag{2.59}$$

where $a(z)$is a periodic function of z_a, where $z_a=L_a/L_D$ is the amplifier span, L_a, normalised to the dispersion length. In each period $a(z)$decreases exponentially due to fibre attenuation, and then is amplified to the initial value, a_0, giving;

$$a(z) \equiv a_0 \exp(-\Gamma z/2). \tag{2.60}$$

The concept of the path-averaged soliton is that if the amplifier span is short compared to the soliton period then the solitons evolve little over a short distance as compared with L_D. Over one soliton period, the variations in $a^2(z)$ are rapid and its effect can be averaged out, therefore the average or fundamental soliton $a^2(z)$ is set to 1;

$$\left\langle a^2(z) \right\rangle = \frac{1}{z_a} \int_0^{z_a} a(z) dz = 1, \tag{2.61}$$

resulting in;

$$a^2(0) = a_0^2 = \frac{2\Gamma z_a}{1 - \exp(-2\Gamma z_a)} = \frac{G \ln G}{G - 1}, \tag{2.62}$$

where $G = \exp(2\Gamma z_a)$. This shows that soliton evolution in the case for lumped amplifiers is the same as the lossless case provided that the amplifiers are the spaced so that $L_a << L_D$ and also that the peak launched power is a factor a_0^2 larger than the fundamental case, i.e.;

$$P_0 = a_0^2 \frac{|\beta_2|}{\gamma \tau_0^2}. \tag{2.63}$$

2.6 • Soliton Interactions

So far we have only been looking at the case where an individual pulse is propagating. As the goal in communications is to increase system bandwidth it becomes necessary to decrease the spacing between neighbouring bits in order to increase the bit rate, B. Therefore, we need to examine how close two solitons can come without affecting one another. Soliton to soliton interactions are nonlinear in origin and can take place between solitons of the same or different wavelengths. Taking two solitons with the same phase and amplitude, when they are temporally close, the tail of the leading pulse can overlap with the head of the second pulse. This creates some constructive interference that in turn leads to the refractive index increasing, causing a frequency shift in the leading pulse and slowing it down, whilst the trailing pulse speeds up. This brings the pulses closer together, increasing the overlap and escalating the nonlinear interaction. Eventually after a number of dispersion lengths the pulses collapse and form one pulse, but as the components of the new pulse are travelling at different

velocities they separate out and with the leading pulse now trailing. The same system of events happens again periodically with each new leading pulse. This can be analysed using numerical simulations [33] and the inverse scattering method [34, 35], with the inverse scattering method providing additional insight into the effect of pulse with different amplitudes and phases.

The amplitude of two solitons launched into an optical fibre can be described by the equation [30];

$$u(0,\tau) = \text{sech}(\tau - q_0) + r\,\text{sech}[r(\tau + q_0)]e^{i\theta}, \tag{2.64}$$

where q_o is related to the bit rate by;

$$B = \frac{1}{T_B} = \frac{1}{2q_0 T_0} \quad \therefore \quad q_0 = \frac{T_B}{2T_0}, \tag{2.65}$$

where T_B is the bit separation, r is the relative amplitude and θ is the relative phase of the two input pulses. As discussed earlier, the inverse scattering method includes varying phase and amplitude but in this instance we will simplify matters, only considering solitons that are in phase ($\theta = 0$), have equal amplitude ($r = 1$) and have a large separation compared to pulse width ($T_B >> 2T_0$). The period of soliton collapse and separation is given by;

$$Z_P = Z_0 \exp(q_0) = \frac{\pi L_D}{2} \exp(q_0). \tag{2.66}$$

For the lossless and phase matching case, the point at which the pulses collapse is equal to half this period and, as this situation is undesirable, the system length should be shorter than half the collapse period. Also the collapse period is proportional to the dispersion length, so in order to extend the collapse period, the dispersion for the system should be low.

It is possible to alternate the phase between neighbouring solitons in order to prevent soliton collapse [36, 37]. When the solitons are not in phase with each other the solitons separate even for relatively small values of θ [38]. Even thought the solitons are not colliding this can cause recovery problems at the receiver. If the soliton has drifted from its designated bit-slot and into a neighbouring slot, errors will be introduced. It is true that in a real system not every bit-slot adjacent to a soliton will be occupied, but this introduces more problems due to the uneven balance of forces on the soliton.

For the cases when the amplitude is uneven but the phase is equal, the problems are greatly reduced. The interaction is still periodic but there is no collapse [39, 40] as the intensity difference results in a difference between the phase developments for the two solitons, cancelling the attractive and repulsive forces.

With WDM soliton systems, multiple soliton bit streams are transmitted over the same fibre at different frequencies. The process increases in complexity, as now there is the possibility of solitons with different carrier frequencies colliding because of their different group velocities [41]. As the two solitons at different velocities approach each other they stimulate a frequency shift Δf, with a maximum frequency shift of;

$$\Delta f_{\max} = \frac{1}{\left(3\pi^2 T_0^2 f_{ch}\right)}, \tag{2.67}$$

where f_{ch} is the channel separation. This frequency shift induces an increase or decrease in the velocity of the soliton as a solitons velocity is subject to its frequency. After the collision each soliton regains its initial frequency but undergoes a temporal shift given by;

$$\Delta t = \frac{1}{\left(\pi^2 T_0^2 f_{ch}^2\right)}. \tag{2.68}$$

For a stream of ones this poses no problem, as all the bits would be shifted by the same amount. For a bit stream, where ones and zeros occur randomly, if two solitons of different frequencies met the transaction would be as above, although some solitons in the bit stream may 'collide' with a zero, resulting in no temporal shift. The outcome would be both channels would suffer from timing jitter.

2.6.1 • Soliton Interactions and Amplification

The situation of soliton interaction must be examined further when combined with the stipulations of the guiding centre soliton that, in one period solitons evolve little over the dispersion length and that the amplifier spacing should be much shorter than the dispersion length, $L_a << L_D$. This condition can be linked to the width T_0 by introducing equation 2.24 for the dispersion length, resulting in;

$$T_0 >> \sqrt{|\beta_2| L_A}. \tag{2.69}$$

We can investigate the effects on the bit rate of a soliton communications system as in equation 2.65 we related bit rate to bit slot and bit slot to q_0, which represents the

factor by which the bit slot is larger than the soliton width. Therefore we can rewrite equation 2.69 to give;

$$B^2 L_A >> \left(4q_0^2|\beta_2|\right)^{-1}. \tag{2.70}$$

It is obvious therefore, that the use of amplifiers in a soliton system can limit the bit rate and the amplifier spacing.

2.6.2 • Signal to Noise Ratio

Introducing amplifiers into a system not only reduces the permissible bit rate and amplifier spacing but it also introduces noise in the form of spontaneous emission into a system. ASE builds up over transmission as it is amplified each time is passes through another amplifier and after several spans, a significant noise level can build up, closing the received data eye. In order to maintain error free transmission a high signal to noise ration (SNR) must be maintained during propagation. There are other forms of noise that can reduce the SNR at the receiver including thermal and shot noise, although the most dominant is the beating of the signal and ASE [42].

The SNR is used to quantify the relative size of the signal level compared to the noise level and is generally given by the mean-square signal current divided by the mean-square noise current detected at the receiver;

$$SNR = \frac{\left\langle i_s^2 \right\rangle}{\left\langle i_n^2 \right\rangle}, \tag{2.71}$$

where i_s and i_n are the detector currents due to the signal and noise respectively. If a detector with 100% quantum efficiency is placed directly after the amplifier the signal current is given by;

$$\left\langle i_s^2 \right\rangle = \left(P_0 R\right)^2, \tag{2.72}$$

where $R = q/hv$ is the responsivity of the detector, P_0 is the power output from the amplifier, q is the charge on an electron, h is Planck's constant and v is the signal frequency. The current due to the noise of the beating of the signal and the ASE is given by;

$$\left\langle i_n^2 \right\rangle = 4F_0 P_0 R^2, \tag{2.73}$$

and F_0 is the noise power of the ASE given by;

$$F_0 = (G-1)\mu h\nu \Delta f \ , \tag{2.74}$$

where G is the gain of the amplifier, μ is the population-inversion (or spontaneous-emission) factor and Δf is the bandwidth. For a chain of N_a amplifiers the SNR can be found by substituting these into equation 2.71;

$$SNR = \frac{(P_0 R)^2}{4N_a F_0 P_0 R^2} = \frac{P_0}{4N_a (G-1)\mu h\nu \Delta f} \ , \tag{2.75}$$

This shows that if the signal power is increased, there is an understandable increase in SNR. With solitons this cannot be increase as the soliton peak power is determined by the pulse width and dispersion, this does however mean that there is a limit on how low the fibre dispersion can be. An important observation is the behaviour of the SNR when the gain is changed. If the gain is decreased the SNR will increase, but in order to transmit over the same system length it is obvious that the number of amplifiers must be increased to compensate for the transmission loss. As gain is exponential with distance and the number of amplifiers is linear, the reduction in gain is greater than the increase in the number of amplifiers resulting in an increase in SNR.

2.7 • Timing Jitter

2.7.1 • Gordon-Haus Jitter

In order to transmit solitons long distances to compensate for the attenuation induced by fibre and other components, amplifiers must be included in the system. In all optical systems it commonly known that EDFAs introduce noise into a system due to their amplified spontaneous emission, decreasing the signal to noise ratio (section 2.6.2). Another effect that is not so easily realised is the ASE-induced timing jitter known as Gordon-Haus jitter that affects soliton based systems.

We have already shown that solitons are robust to external perturbations; but it is this resilience, the solitons ability to re-adjust itself that leads to this jitter. Some of the ASE noise originating from the EDFA is absorbed by the soliton as it passes through the amplifier causing a random change to the solitons frequency. As the speed at which a soliton propagates though a fibre is dependent on the frequency, then this small random change in frequency causes a relative change to the solitons speed. The change in velocity translates into a shift from the expected arrival time at the receiver, and as

each bit in the bit stream is affected randomly, they all arrive at slightly different instances, resulting in timing jitter. This interaction between soliton and noise is small for one amplifier, but the effect cascades for a string of amplifiers resulting in a significant temporal shift at the end. It is these random arrival fluctuations that are referred to as Gordon-Haus timing jitter [43-45]. In order to design system parameters effectively it becomes necessary to try and quantify the magnitude of the jitter generated when propagating through a number of amplifiers.

Assuming all amplifiers are equal and deliver the same variance in frequency $\langle \delta\omega^2 \rangle$, then the variance after N amplifiers can be assumed to be;

$$\langle \Delta\omega_N^2 \rangle = N \langle \delta\omega^2 \rangle . \tag{2.76}$$

The change in group delay on a pulse in one amplifier span, length L_a, with dispersion β_2 is defined as;

$$\Delta t_g = \beta_2 L_a \delta\omega , \tag{2.77}$$

and, as the jitter is random, we establish the variance of the group delay as;

$$\langle \delta t_1^2 \rangle = \beta_2^2 L_a^2 \langle \delta\omega^2 \rangle . \tag{2.78}$$

Extending this to include all the delays after N amplifiers all with an equal span length, L_a, we obtain the total variance;

$$\langle \delta t_N^2 \rangle = \beta_2^2 L_{amp}^2 \sum_{i=1}^{N} (N-i)^2 \langle \delta\omega^2 \rangle . \tag{2.79}$$

For a large number of amplifiers, we can approximate;

$$\sum_{i=1}^{N} (N-i)^2 \approx \frac{1}{3} N^3 . \tag{2.80}$$

The variance in frequency is given by [45];

$$\langle \delta\omega^2 \rangle = \frac{2\pi n_2 N_{sp} hc(G-1)}{3 t_0 \beta_2 \lambda^2 A_{eff} a_0^2} , \tag{2.81}$$

where n_2 is the nonlinear coefficient, N_{sp} is the spontaneous emission noise factor for the amplifier, h is Planck's constant, c is the speed of light in a vacuum, G is the amplifier gain and a_0 is the soliton amplitude define in equation 2.62. This then provides us with the variance for N amplifiers;

$$\langle \delta t_N^2 \rangle = \frac{2\pi n_2 N_{sp} |\beta_2^2| hc(G-1) L^3}{9 t_0 \lambda^2 L_a A_{eff} a_0^2} , \tag{2.82}$$

where the total fibre length, $L = NL_a$. The r.m.s. jitter after N amplifiers is obtained by taking the square root of equation 2.72. Due to the L^3 term, it is plain that the Gordon-Haus jitter will pose an increasingly bigger problem as the system length increases and will eventually limit the maximum soliton system length. In order to increase this length, in may look like increasing the amplifier spacing is a suitable alternative, although this would result in an increase in gain. The best way is to reduce the system dispersion, although reduced dispersion introduces higher order dispersive effects and also affects the soliton power, restricting our ability to adjust this value.

To determine the maximum system limit we must calculate the amount of jitter required for a pulse to arrive outside its time window, $2t_w$, at the receiver. Assuming Gaussian statistics, in order to an attain an acceptable error-free bit-error rate of 10^{-9} or less requires;

$$\left\langle \delta t_N^2 \right\rangle \leq \left(\frac{t_w}{6.1} \right)^2 . \tag{2.83}$$

We can now obtain the maximum system length;

$$L_{\max}^3 \leq 0.1372 \frac{T_{FWHM} t_w^2 A_{eff} L_a a_0^2}{n_2 N_{sp} D_2 h (G-1)} . \tag{2.84}$$

This equation is missing an explicit link to the system data rate R, but it is clear that the data rate will affect the magnitude of the timing window as well as the permissible pulse width and therefore have an affect on the jitter limited maximum system length. In order to include the data rate, we make the assumptions that;

$$\kappa_F = RT_{FWHM} \quad \text{and} \quad \kappa_w = Rt_w , \tag{2.85}$$

where the inverse mark to space ratio is given by κ_F and the size of the timing window for a given bit rate is κ_w. The maximum possible system length can now be written as;

$$L_{\max}^3 = \frac{0.5158}{R} \left[\frac{\kappa_F \kappa_w^2 A_{eff} L_a a_0^2}{n_2 N_{sp} D_2 h [\exp(\alpha L_a) - 1]} \right]^{1/3} , \tag{2.86}$$

where the gain has been taken as $G = \exp(\alpha L_a)$. This shows that the maximum system length is inversely proportional to the data rate. The arguments for changing the amplifier span remain the same, although it is now more apparent that the gain is dependent on amplifier spacing.

2.7.2 • Core Electrostriction

Electrostriction is another source of timing jitter in soliton systems. Confinement of the soliton in the core generates acoustic waves that travel to the cladding and back to the core through electrostriction. As this wave travels, it causes density variations in the refractive index that in turn lead to changes in the refractive index and hence changes in the velocity of the soliton. As this index changes last for around 2ns, this effect not only interacts with the soliton creating the wave but also with following solitons as, at 40Gbit/s, the bit slot is only 0.025ns wide. If the bit stream were all ones each bit would create and experience the same uniform time shift from the acoustic wave, but as data contains both ones and zeros, the shift on a soliton would depend on the value of the preceding bits, leading to the randomness of the jitter. As this jitter is deterministic, it is possible to employ coding algorithms to control this effect [46] and it is also possible to reduce the strength of the acoustic interaction by using fibre with a low dispersion [47, 48].

2.8 • Soliton Jitter Control

It has become clear the timing jitter is a large problem in soliton-based systems and it eventually limits the transmission performance. A number of soliton control methods have been demonstrated in order enhance the system performance. These range from the simple introduction of integrating filters into the system or by employing modulation techniques to transmitted date. A number of these schemes will be discussed here.

2.8.1 • Frequency Filtering

The main benefit of using filters in soliton transmission is that they significantly reduce the effects of Gordon-Haus jitter [49]. Filters make use of the fact that the spectrum of the soliton is much narrower than that of the spontaneous emission from the EDFA. As stated in section 2.7, timing jitter originates from the soliton absorbing some of the energy from the ASE, altering the frequency of the soliton and causing it to change its speed. Introducing filters introduces additional loss into the system,

although increasing the gain of the amplifier can compensate for this. The bandwidth of the filter is selected so that the soliton may pass, but most of the ASE is rejected, in effect restricting the central frequency of the pulse to within the pass band of the filter. When filters are introduced into the transmission line, the mean square jitter (equation 2.72) is reduced by a factor f;

$$\left\langle T_0^2(Z)\right\rangle_{filtered} = \left\langle T_0^2(Z)\right\rangle_{unfiltered} f(4\delta Z), \tag{2.87}$$

where δ is the excess gain required to overcome the loss of the filter and we are assuming that the loss is distributed over the entire link. The function f is given by;

$$f(x) = \frac{3}{2x^3}\left[2x - 3 + 4\exp(-x) - \exp(-2x)\right]. \tag{2.88}$$

When $x >> 1$, $f(x) \sim 3x^{-2}$ and as x is linked to Z, this effectively means the function f varies with Z^{-2}. The end result is that by introducing filters the limit imposed by Gordon-Haus jitter has increased or the system length or data rate can be increased.
One negative effect of adding a filter into a system is that the filter may cause clipping the wings of the soliton. As solitons compensate for any change in shape by shedding energy, extra gain at the amplifier is necessary to compensate for this additional loss and to restore the initial soliton balance. There is a limit to the strength of the filter. The stronger the filter, the more loss it will induce and the more gain will be required to offset this loss and, as Gordon-Haus jitter increases with gain, eventually the filter will result in greater timing jitter. Another problem is that increasing the gain of the amplifiers to compensate for the inclusion of filters reduces the signal to noise ratio at the receiver.

2.8.2 • Amplitude Modulation

Solitons can be controlled in the time domain by using amplitude modulators. Amplitude modulators are commonly used at the transmitted end of a system as a way of encoding a light pulses; attenuating a pulse symbolizes a zero and allowing pulses to propagate to represent a one. Using an amplitude modulator periodically such that it's peak transmission occurs at the centre of the pulse arrival time window, if the soliton is not at the anticipated point, it is moved back to the correct position. This is because the part of the soliton in the centre of the time window is undergoing less attenuation than the other parts of the soliton, so in the same was as using filters moves the soliton in

the frequency domain, amplitude modulators do so in the time domain. This time domain movement will also counteract any of the soliton-soliton interaction that have caused a pulse to move out of its bit slot by moving them back into their correct position. Unlike filters, amplitude modulators will not compensate for the change in velocity due to a soliton propagating through the amplifier so if modulators were used mid-span the solitons would still move out of the bit slots due to their different propagation speeds.

A problem using amplifiers is that, as with installing all physical components, it must be durable and have a long lifetime if it is to be installed mid span, especially in long haul submarine systems. Amplitude modulators will also require a sinusoidal clock frequency to modulate them, and this frequency needs to follow the variations of propagation time due to thermal events, therefore it needs to be generated locally from the incoming bit pattern. Adding clock recovery for every modulator adds greater complexity and expense to the system. Amplitude modulators, like all electronic devices, are not bit rate independent and will need to be replaced if the bit rate was to be increased. If amplitude modulators are not used frequently enough and the soliton has moved closer to the midpoint of the next timing window, then the modulator will push the soliton into the next time window instead of the correct window. Finally amplitude modulators add additional loss into the system, resulting in the same increasing gain problems as the frequency filters.

2.8.3 • Sliding Frequency Filters

The Sliding filter scenario incorporates filters in the same way as the fixed-filter solution although the central frequency of filter gradually evolves over the transmission line. Both the fixed-frequency filter and amplitude modulators reduce the SNR at the receiver, because the increase in gain used to offset their loss increases the noise in the vacant zero bit slots. With sliding filters the soliton frequency moves with that of the filters and when the solitons spectra has move by more than it own width the build up of ASE is filtered out. As we are inducing a frequency shift on the solitons, their velocity will increase but as this affects all solitons in the same manner, the spacing between solitons remains the same. Sliding filters also have the added

benefit of reducing soliton interactions enabling higher data rates [50, 51] and depending on the pattern of the sliding filter trail then this can be reduced further [52]. The shape of the filters has also provoked interest [53-55], in particular optical filters that have a flat pass band as they reduce the loss incurred. Also Butterworth filters can have narrower pass band without requiring as much gain as conventional Fabry-Perot filters. One problem with sliding filter schemes is that setting up the system can be difficult due to the precise frequency control requirements, so physically the filter profile must remain stable.

2.8.4 • Phase Modulation

Like amplitude modulators, phase modulators can be used mid span to control and suppress Gordon-Haus jitter [56-58]. The phase imposed on the soliton is distributed over the soliton due to their particle like nature, resulting in a change in carrier frequency. This frequency change can be used to guide the soliton back into its correct bit slot by over correcting for the timing jitter. This enables phase modulators to compensate for both frequency and positional changes.

In practical terms, phase modulators do not need to be used at every amplifier as they can create large chirps and compensate for large amounts of timing and frequency shifts. Unlike amplitude modulators, phase modulators do not require large amount of gain to offset their insertion loss but like amplitude modulators they must be placed frequently enough so that the soliton is near to its own bit slot rather than the neighbouring one in order to avoid guiding the soliton into the wrong slot. Implementations of phase modulator schemes generally use either a conventional modulator to apply the phase shift or a nonlinear process like cross phase modulation with a stream of clock pulses [58]. As with the earlier control methods described, introducing phase modulators into a system generates additional cost and complexity. Unlike the earlier methods there is the possibility of providing phase modulation control all optically using XPM and all optical clock recovery resulting in bit rate transparent guiding.

2.9 • Summary

In this chapter, the generalised nonlinear Schrödinger wave equations was presented and two length scales, known as the dispersion length and the nonlinear length, were introduced. This led to four regimes; where GVD dominates, Nonlinearity dominates, where neither affects propagation and where both influence pulse evolution. By propagating a pulse in the anomalous dispersive region and with sufficient intensity, Solitons can be generated. These pulses are highly adaptable and will attempt to maintain their shape, which ultimately leads to their downfall. When propagating though spans with periodic EDFA, Solitons absorb some of the ASE noise that originates from the amplifier. The solitons now contains components of another frequency and, as the speed at which the light propagates through fibre is dependent on its frequency, the soliton speeds up or slows down. The randomness of this absorption leads to differing frequencies for sequential solitons, and results in timing jitter at the receiver. Schemes exist for the compensation of Gordon-Haus timing jitter, but they are complex and add to the component cost of a system.

When designing a new system that is to utilise solitons, parameters such as the amplifier gain, amplifier span, pulse width and fibre specification, like dispersion and core area, should all chosen to enhance the soliton propagation. Low dispersion reduces Gordon-Haus jitter but increases third order dispersion, the average soliton require a large pulse width but this increases soliton-soliton interactions [59]. Another restriction arises because the amplifier length must be much shorter than the dispersion length, this means that either the pulses need to be broad, placing a restriction on the maximum bit rate, or the dispersion must be low. Reducing the amplifier span decreases the required gain for each amplifier and reduces the SNR although this also requires that there are more amplifiers over the system length, increasing the system cost. If in the future the system was to be upgraded to a higher bit rate, the system may no longer be able to support solitons as the fibre and amplifier separation were designed for solitons at a lower bit rate.

Installed terrestrial or submarine networks may not be able to utilise the solitons resistance to GVD. As the amplifier spans will be fixed, they may be too distant to support solitons. Also the high local dispersions would require huge launch powers to generate enough SPM to counteract the GVD, and this power level may not be

attainable at a repeater due to amplifier saturation levels. It also may not be possible to employ the periodic solitons timing jitter control methods such as sliding frequency filters that need to be introduced along the transmission span. Due to the limitations solitons place on system parameters, the solitons intolerance to upgrades and the remote possibility that they could be used in currently installed systems, solitons are deemed as an inoperable commercial solution.

Chapter 3

Dispersion Management and Wavelength Division Multiplexing

3.1 • Introduction

With the advent of the erbium doped fibre amplifier (EDFA), the primary wavelength band for optical communication systems moved from 1300nm to 1550nm, no longer at the zero dispersion wavelength for most of the installed standard single-mode fibre. Loss was no longer the limiting factor in optical communications and transmission performance became limited by chromatic dispersion and nonlinearity. The opinion was that soliton transmission had found an elegantly way to neutralise these effects by playing them off against each another, unfortunately soliton transmission created additional problems. Due to the nature of solitons, launched pulse powers have limited flexibility in order to keep the balance between GVD and SPM and they are susceptible to Gordon-Haus timing jitter owing to their broad spectrum. Complex methods involving modulators and filters were employed as a means of controlling jitter (section 2.8) although these solutions are costly, complex and reduce the probability of system reliability. In the mid nineties results of soliton and RZ transmission using dispersion compensation started to emerge [60-62], provoking research into dispersion managed soliton (DMS) systems [63-66].

Before research was progressing the understanding of the DMS, wavelength division multiplexing (WDM) using non-return to zero (NRZ) data was showing the feasibility of transmitting multiple wavelengths over a single fibre [67]. WDM took advantage of both the EDFA and dispersion management, yet these newer technologies were not ideally suited for the broadcast of multiple frequencies. Dispersion maps were equalised for single wavelengths, and as the compensating fibres did not provide unity slope compensation, the disparity between the dispersion seen by wavelengths increased over distance resulting in a greater chromatic dispersion penalty with respect to single channel systems. Likewise, the small signal gain spectra for the EDFA is wavelength dependent whereas the link loss is not [68], leading to large variations in

the signal to noise ratio for cascaded EDFAs. Not only are there linear discrepancies to overcome, but also launching multiple wavelengths presents new penalties in the form of deleterious inter-channel nonlinear and parametric interactions such as FWM and XPM. Depending on the signal power, these interactions can reduce the OSNR and generate additional frequencies, depleting power from the signal wavelength. These additional processes will be described in more detail in section 3.7.

Finally there is the use of the DMS within WDM systems. Do the system specifications necessary for optimising DMS transmission correlate with those necessary for WDM transmission? As the benefits of the single channel DMS power enhancement allow increased peak power for transmission, this in turn aggravates the deleterious inter-channel effects. If a balance is to be found, does it still fall within the classification of the DMS and is it practically realisable?

3.2 • The Dispersion Map

The idea behind a dispersion-managed system is to adopt a periodic map of non-uniform dispersion along the length of the transmission path. This non-uniform dispersion is often constructed by using segments of differing fibres with alternating normal and anomalous dispersion, although newer types of fibre are available that have a dispersion map written in the fibre continuously along its length. Generating low path-averaged dispersion was not initially intended for pseudo-soliton propagation but was used in low-powered, linear transmission in order to operate at 1550nm over SMF [69]. In linear systems, the dispersion map was used to escape the limitations imposed by the dispersion length whereas for systems operating in the nonlinear regime, careful balancing of the fibre dispersions can be used for generating soliton-like propagation.

An example of a dispersion map, based on the parameters of the SMF, DCF fibre map used in the recirculating loop (Section 4.5.2), is given in Fig. 3.1. The main aim of the dispersion map is to reduce the path average dispersion of the system. The value of the local dispersion can be manipulated in order to optimise propagation although there are no theoretical limitations on how to achieve this; therefore dispersion maps can be comprised from fibres of varying lengths and uneven dispersions. Typically the values of the local dispersion in each of the fibres sections that form the dispersion map are greater than that of the path average dispersion, producing propagation dominated by

linear dispersion within the high local dispersion steps whilst a nonlinearity, that is much weaker than for conventional solitons, supports the pulse on average.

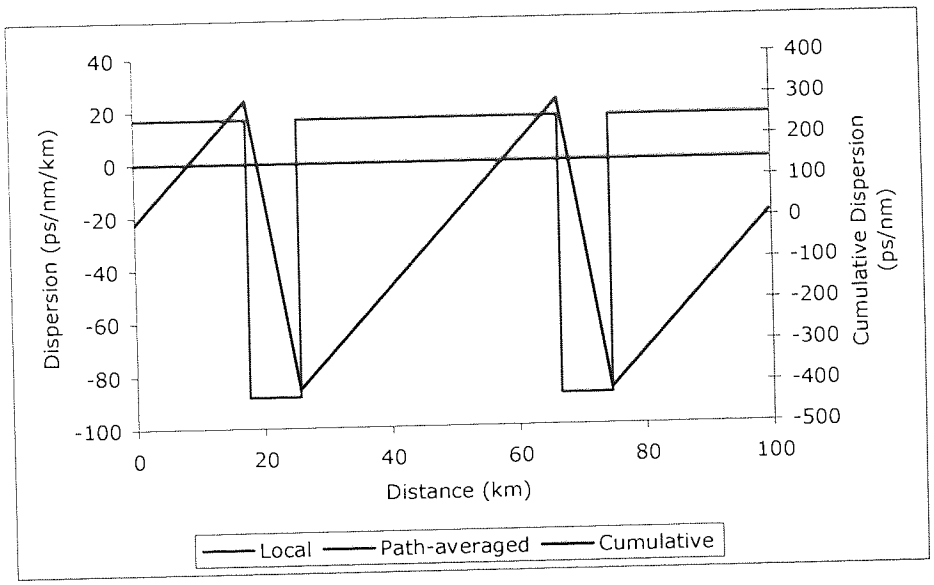

Figure 3.1: The local, path-averaged and cumulative dispersion for a 100km fibre dispersion map comprising SMF and DCF used in recirculating loop experiments

Fig 3.1 describes a non-symmetric dispersion map, although for DMS applications it is the norm to have a symmetric dispersion map with an initial half step of anomalous dispersion fibre, but it is worth noting that it is equally valid to have a symmetric dispersion map where propagation in the initial half step is in the normal dispersion regime [70]. In standard fibre systems introducing short periodic lengths of dispersion compensating fibre can create a dispersion map but, as mentioned earlier, an equally valid method is to compensate the SMF dispersion by using other fibres such as reverse dispersion fibre (RDF) but in larger quantities. Speciality fibres, such as Vascade fibre by Corning, have been designed specifically for generating an optimum dispersion map and have both normal and anomalous dispersion. Considerable work goes into the design and optimisation of the dispersion map and the interplay of the effects such as to use high or low local dispersion.

Theoretically there is no limitation on how to optimise a dispersion map, with simulation tools possessing the ability to tailor any of the fibres parameters, yet in reality such fibre may not exist. Experimentally research has shown that 40Gbit/s over 2700km is possible whilst implementing a multiple dispersion management fibre map [71], namely a dispersion map containing multiple fibre types and in this instance a

2km NZDSF, 50km SMF and 10km DCF fibre map. Again this is acceptable in the laboratory where introducing an additional short length of fibre to balance the map is uncomplicated, although in the field this may not be possible. Mid-span modifications to a commercial system would require accessing existing fibre and the introduction of an additional length of compensating fibre, resulting in an increased propagation distance whilst the physical repeater distance remains unchanged. Also, the periodic nature of the dispersion map would need to be preserved yet sequential terrestrial fibre spans may not be equal, requiring the introduction of additional span and compensating fibres, increasing the loss between amplifiers. If the amplifiers can no longer provide the gain required to offset the new span losses, transmission performance will be compromised. Therefore the dispersion-managed soliton may not be the best upgrade solution for a commercial system.

3.3 • Dispersion Managed Solitons

Since the discovery of the dispersion map it has been found that stable soliton like transmission using periodic dispersion compensation is possible, although the pulse propagation is significantly altered for that of a conventional soliton. This may seem strange, as solitons cannot form in the normal dispersion regime and propagation leads to large pulse broadening and chirping. If the map period is small compared to the nonlinear length, nonlinear effects are small and the pulse behaves in a linear manner affected by the chirp induced by dispersion. Looking at lengths longer than the nonlinear length, where the dispersion map is repeated many times, the effects of SPM can be balanced by dispersion creating a form of soliton [72]. Consider a hyperbolic secant pulse being launched into the two-step symmetric dispersion map akin to that shown in Fig. 3.1 with an initial half-length of anomalous dispersion fibre, a full length of normal dispersion fibre and a final half-length of anomalous dispersion fibre. Due to the high local dispersion as the pulse propagates along the first half step it becomes chirped and the pulse width increases with the higher frequencies leading. As the pulse enters the normal dispersion fibre it experiences a chirp of the opposite sign, slowing the higher frequencies and speeding up the lower frequencies. Half way through the normal fibre, the cumulative chirp, the FWHM and the pulse bandwidth are all at their minimum values for this step. From this point on and until the end of the fibre step, the

normal dispersion induced chirp is dominant and the pulse begins to broaden again until it enters the final half step of anomalous fibre where the pulse is re-compressed and the pulse bandwidth returns to it's maximum. So in summary in one map period the pulse width has two minima, at the two chirp free points in the middle of each step, and the pulse bandwidth oscillates around the map period, with one minimum per map. It is worth noting that the average pulse bandwidth is larger in anomalous fibre than it is in normal fibre resulting in a net anomalous chirp even when the average dispersion is zero [73].

A useful definition for defining this type of dispersion map, i.e. with unequal lengths of positive and negative dispersion fibre, is known as the map strength, S [74], and is defined as;

$$S = \frac{L_n \beta_n - L_a \beta_a}{T_{FWHM}^2}, \tag{3.1}$$

where L_n, L_a are the normal and anomalous lengths, β_n, β_a are the normal and anomalous dispersions and T_{FWHM} is the pulse width at the full width half maximum. This equation can be simplified if the sections of anomalous and normal dispersion fibre are equal;

$$S = \frac{L\Delta\beta}{T_{FWHM}^2}, \tag{3.2}$$

where $\Delta\beta$ is the dispersion difference and L is the total map length. The map strength is a useful indicator to the amount of pulse spreading that will occur in the dispersion map. Large map strengths can be gained by either large local dispersion or small pulse widths and vice versa for small map strengths. As the map strength is inversely proportional to the square of the pulse width, the launched pulse width greatly effects propagation.

For optimum DMS transmission, the chirp free point must be at the midpoint of the fibre sections and it is also beneficial to launch from this chirp free point, rather than chirping the initial pulse [75]. These optima will not be attainable for WDM transmission over a fibre map without full slope compensation. Consequently, each wavelength suffering from residual dispersion at the end of each map period will see a chirp free position offset from the optima. This chirp free point movement is cumulative and increases after each span, unless residual dispersion compensation is provided over each map period, and will eventually destroy the balance of dispersion

and nonlinearity. This effect must be considered when employing dispersion-managed solitons for WDM systems.

3.4 • Power Enhancement

Conventional solitons are generated using the balance between the linear, dispersion, and the nonlinear, SPM. Due to the power dependent nature of fibre nonlinearity, for a given dispersion, only pulses of a specific power will generate the correct amount of SPM. As mentioned in chapter 2, even solitons with larger than optimum launch powers will adapt and shed energy until the ideal soliton is formed, putting a limit on maximum optical signal to noise ratio (OSNR) available at the receiver. The evolution of the DM soliton over one map period is unlike the soliton in that, for a symmetric dispersion map launched at the chirp free point, the peak power reduces and then increases as described in 3.3. Consider a DMS launched with the same peak power as the fundamental soliton; as the peak power decreases, the nonlinear effects also reduce until the peak power start to increase, the cycle is then repeated. On average across this cycle, the effective nonlinearity seen by a DMS is less than that seen by a fundamental soliton. Therefore the launched pulse energy of the DMS can be increased to match the average nonlinearity seen by the fundamental soliton, resulting in an effective power enhancement over the soliton when recovered at the chirp free point.

In 1997, Yu et al noticed a dependence on the energy enhancement generated by DMS transmission with the map strength [79], albeit an earlier version of map strength, as the version used was a factor of two different from equation 3.1, although for our purpose, we shall use S as previously described. Just as with conventional solitons, DM solitons require sufficient power to propagate within a given dispersion map [76];

$$E_{sol} = E_0\left\{1+0.7\left[\frac{(\beta_1-\beta_{ave})l_1-(\beta_2-\beta_{ave})l_2}{T_{FWHM}^2}\right]^2\right\}, \tag{3.3}$$

where E_{sol} and E_0 are the energies of the DM soliton and first order soliton, β_1, β_2 and β_{ave} are the dispersion of the first and second fibres and their average dispersion, and finally l_1 and l_2 are the fibre lengths. This can be reduced further for dispersion maps with a small strength, $S < 2$, [77];

$$E_{sol} = E_0\left(1+0.7S^2\right). \tag{3.4}$$

Although if the map strength is large, $S > 4$ the energy enhancement is also dependent on the normalised average dispersion, the approximate energy enhancement can be found in [78];

$$E_{sol} = \frac{a}{SD}\left(S - b\sqrt{(S-b)^2 + cSD}\right), \tag{3.5}$$

where $a = 0.2$, $b = 3.7$, c = 180 and D is the normalised average dispersion.

The closer the map strength is to zero the greater the energy enhancement, allowing for a pulse with greater energy and hence greater recovered OSNR, to be transmitted whilst the power on average remains the same. For dispersion maps with higher map strengths beyond 10, the energy enhancement saturates since the pulse energy cannot exceed the energy of a soliton in the anomalous segment [78]. This is another benefit of the dispersion-managed soliton.

3.5 • Dense Dispersion Management

In order to maintain the high local dispersion to prevent Gordon-Haus timing jitter, the pulses will experience broadening and overlapping, generating the intra-channel nonlinear effects. Reducing the dispersion lowers the map strength, but this reduces the energy enhancement. At higher bit rates, where pulse widths are small, the inverse relationship between pulse width and map strength results in large map strengths. These large map strengths can be reduced by introducing multiple periods of a short dispersion map between the amplifiers, i.e. $Z_p << Z_a$. This technique is known as dense dispersion management (DDM) and has produced a number of impressive transmission and simulation results [80-82]. When DMS are used with DDM systems, these are known as dense dispersion managed solitons (DDMS).

Figure 3.2 shows the dispersion maps used for the DDMS transmission over 7000km at 160Gbit/s simulated in [80]. The DDM span is characterised by the multiple short lengths of alternating anomalous and normal dispersion fibre between amplifier spans. All three fibre maps have the same map strength of S ~ 1.6, and this has been maintained for shorter periods by increasing the dispersion of the fibre. The pulse used for DDMS transmission had a minimum pulse width of 1.5ps and the amplifiers had a separation of 50km. All three dispersion maps performed similarly and estimated Q's were greater than 6 over 7000km. Although when PMD was considered for these high bit rates, the transmission distance was reduced to just over 2000km.

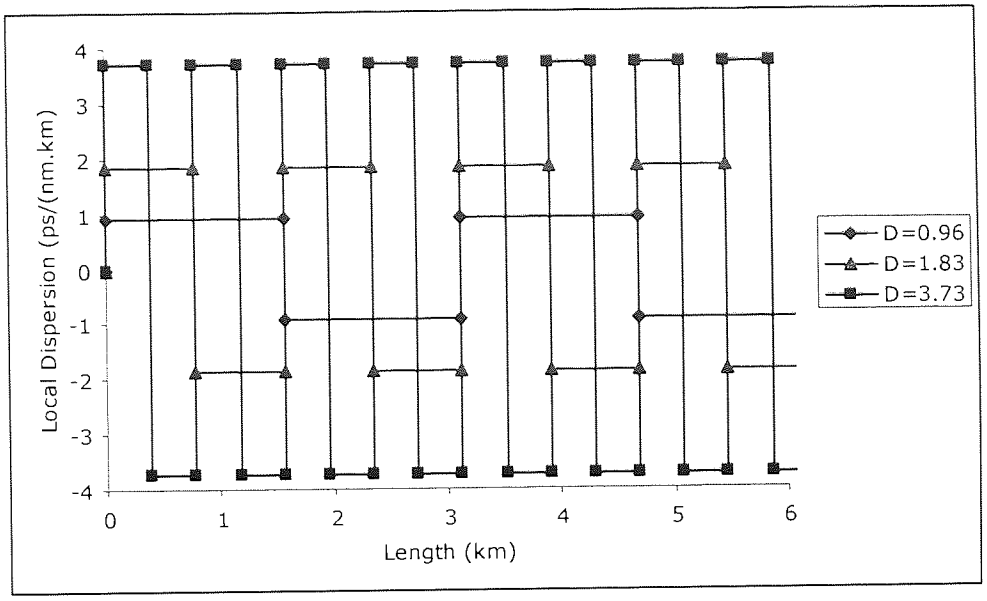

Figure 3.2: The three dense dispersion maps used for trans-oceanic DDMS transmission at 160Gbit/s in [80]

One problem with DDM is the map sustains higher peak powers for a longer time than the longer step length DM equivalent. In time division multiplexed (TDM) environments these high map strengths provide minimal pulse breathing and intrachannel effects, whereas in wavelength division multiplexed (WDM) systems high powers lead to unwanted inter-channel effects.

3.6 • Quasi-Linear Transmission

Unlike in soliton transmission where the regime is fixed for a stable solution, Quasi-linear transmission is a term for describing a regime where fast variations of the channel waveform with cumulative dispersion allow averaging of the intra-channel effects generated by fibre nonlinearity [83]. Quasi-linear is not a term solely applicable to dispersion management, although dispersion mapping is still important as it can alleviate some of these intra channel effects.

The increase gained in system launch power by the DMS over that of the fundamental soliton will in turn increase the SNR at the receiver, although if the map strength is small, with limited pulse breathing across the fibre map, a large peak power is sustained. High peak power is beneficial in terms of SNR at the receiver, although

along the span, negative nonlinear interaction can occur degrading the SNR. In the linear regime, when increasing launch power there is a linear gain in SNR, whilst in the nonlinear regime, the greater power instigates greater nonlinear interactions decreasing the SNR with increasing power. The quasi-linear regime exists where the power level is such that the nonlinear interactions degrade the SNR yet they do not counteract the improvement in SNR gained by increasing power.

The results of propagating data at 40Gbit/s with pulse duration of 4ps over six repetitions of a dispersion map comprising of 100km of SMF with β = -21.0ps^2/km and 21.25km of DCF with β = 99.0ps^2/km, is shown in Fig. 3.3.

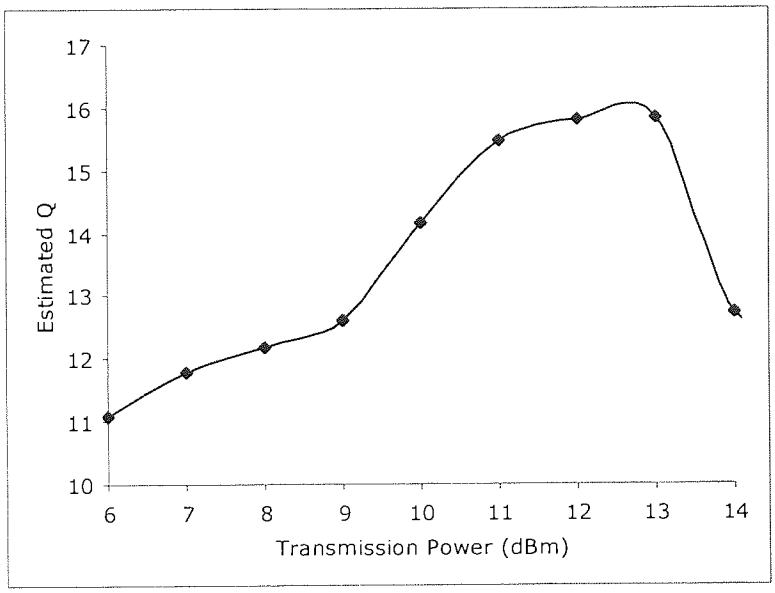

Figure 3.3: Estimated Q verses transmission power (dBm) for a single channel RZ transmission over a SMF and DCF dispersion map

The operating conditions do not support DMS transmission as the large map strength of 1051 signifies a linear system. Initially the estimated Q increases linearly with power until 11dBm as the increase in transmission power increases the SNR, opening the eye and providing a larger Q. The quasi-linear region exists between 11dBm and 12dBm as the linear increase has declined due to the introduction of nonlinear interactions yet there is still an increase in Q as the nonlinear interaction do not complete counteract the gains made by increasing the power. Between 12dBm and 13dBm there is a marginal decrease in the Q as the nonlinearities begin dominate and

reduce the opening of the eye. This then leads to the nonlinear regime where the Q falls off more rapidly due to the total domination of the nonlinear interactions.

At bit rates above and including 40Gbit/s the bit period between pulses is less than 25ps, significantly reducing the systems tolerance to pulse broadening compared with that of a 10Gbit/s system. Unless the map strength for the pulse is small such that the pulse width does not oscillate significantly, the pulses will extend into the neighbouring bit slots. Transmission in this regime is often referred to as "pulse overlap" transmission. When these pulses overlap, an intrachannel XPM-induced pulse-to-pulse interaction that is dependent on the bit stream occurs [84, 85]. This intrachannel cross phase modulation (IXPM) takes the form of a frequency shift on each pulse, and as the data is random, it results in timing jitter through dispersion. The degree of IXPM is dependent on the degree of pulse overlap [84]. For systems that do not overlap, i.e. classical soliton systems, the intrachannel interaction is very small, when there is a partial overlap the interaction is strong, but when pulses overlap nearly completely the interaction is also very small. Therefore, in order to reduce this nonlinear interaction, lower peak powers should be launched whilst operating in the partial overlap regime or strongly and weekly dispersion-managed maps should be used. This reduced interaction aided the successful transmission over a dispersion map with large map strength for RZ pulses at high bit-rates [86].

Another effect is intrachannel four-wave mixing (IFWM) [84, 85] that again, occurs in strongly dispersion-managed systems experiencing overlapping pulses. As the pulses overlap the high local dispersion results in the blue spectral components speeding up (if $D > 0$) and overlapping with the red spectral components of another pulse. When the two pulses overlap, the four-wave mixing (FWM) effect occurs due to the differing frequencies of the two fields and results in the generation of another field at their central frequency in the middle of the bit slot. If there is no data within that bit-slot then ghost pulse is generated, if there is a one, then the IFWM-generated field leads to amplitude jitter. This effect, like IXPM, can be reduced by the correct choice of operating regime with lower peak power of the greatly dispersed pulses producing less interaction than that of the partially overlapped higher peak-powered pulses.

3.7 • Wavelength Division Multiplexing

3.7.1 • Introduction

So far we have only been considering the single channel case for dispersion managed transmission and wavelength division multiplexing has only been mentioned in passing. It is perhaps the most commonly used method used to increase system bandwidth at lower data rates and has produced transmission at speed above 10Tbit/s, albeit over short distances [87]. WDM entails propagating multiple signals at different wavelengths along the same length of fibre with each frequency being modulation by different data patterns. WDM complicates the scenarios by introducing an additional dimension whereby not only one channel must achieve optimal performance, but multiple channels. Introducing additional frequencies presents additional effects and problems to be overcome in the system. Nonlinear and parametric interchannel interactions such as XPM (section 3.7.2) and FWM (section 3.7.3) are generated, invalidating TDM optimisations. In fact for WDM DDM soliton transmission at 40Gbit/s, quasi-linear transmission has provided better results than soliton transmission, even though the soliton format provided greater single channel results [88].

3.7.2 • Cross-Phase Modulation

When two or more wavelengths propagate concurrently along a fibre, they interact with each other through fibre nonlinearity. Cross-phase modulation is one of a number of effects, for instance stimulated Raman scattering (SRS) [89], which occur when two signals are transmitted with different carrier frequencies. Unlike Raman scattering, cross phase modulation does not generate additional waves, cross phase modulation can couple the two fields without energy transfer. XPM occurs in fibre because of the intensity dependent refractive index, which is not only reliant on the intensity of a single beam but also on the intensity of other signals. These intensity fluctuations do not solely affect one channel, but the intensity dependent fluctuations from one channel can modulate the phase of another.

Assuming two linearly polarised signals propagating at different wavelengths, one with amplitude A_1, copolarised with the second signal with amplitude A_2, can be written as [90, 91];

$$\frac{\partial A_1}{\partial z}+\frac{i\beta_2}{2}\frac{\partial^2 A_1}{\partial t^2}+\frac{\alpha}{2}A_2=i\gamma\left(\left|A_1\right|^2+2\left|A_2\right|^2\right)A_1, \tag{3.6}$$

where α is the fibre attenuation, γ is the nonlinear parameter. The phase shift induced during propagation on channel 1 by channel 2 due to XPM is;

$$\phi_1=2\gamma P_2\Delta z, \tag{3.7}$$

where P_2 is the power of channel 2. Deviation from copolarisation of the two propagating channels causes a decrease in the strength of the XPM interaction [92], with linear polarisation enduring the worst-case distortions.

In [93], an expression for the XPM efficiency, η_{XPM} was derived which is independent of the channel power and polarisation;

$$\eta_{XPM}=\frac{\alpha^2}{\omega^2 d_{sp}^2+\alpha^2}\left[1+\frac{4\sin^2\left(\omega d_{sp}L/2\right)\exp(-\alpha L)}{(1-\exp(-\alpha L))^2}\right], \tag{3.8}$$

where ω is the modulation frequency, and d_{sp} is the walk-off parameter, given by;

$$d_{sp}=\frac{1}{v_g(s)-v_g(p)}=\int_{\lambda_p}^{\lambda_s}D(\lambda)d\lambda. \tag{3.9}$$

This efficiency factor does not take into account the intensity distortions that are generated by XPM. The result of equation 3.8 for two channels modulated at 40GHz can be seen in Fig. 3.4. The fibre parameters were taken from the simulations in chapter 6, with the SMF having a dispersion of 17ps/(nm.km) at 1550nm, a length of 100km and loss coefficient of 0.2dB/km. The DCF had a dispersion of -80ps/(nm.km), a length of 21.25km and loss of 0.35dB/km. Due to it's lower local dispersion, the SMF has a greater efficiency region than the DCF, with an efficiency of 0.12 for a channel separation of 100GHz. For both cases maximum efficiency occurs when the two signals are overlapped, i.e. d_{sp} = 0. Similar to SPM, XPM induces modulation instability via the phase modulation, which is clearly causes signal degradation during WDM transmission. For NRZ WDM systems XPM increases when a long string of ones occur in the bit pattern, owing to the increased cross-wavelength interaction time [94]. Even with dispersion managed RZ transmission that reduces interchannel distortion in WDM transmission, the system has to be designed to reduce the XPM, which also results in timing jitter as well as amplitude jitter [90].

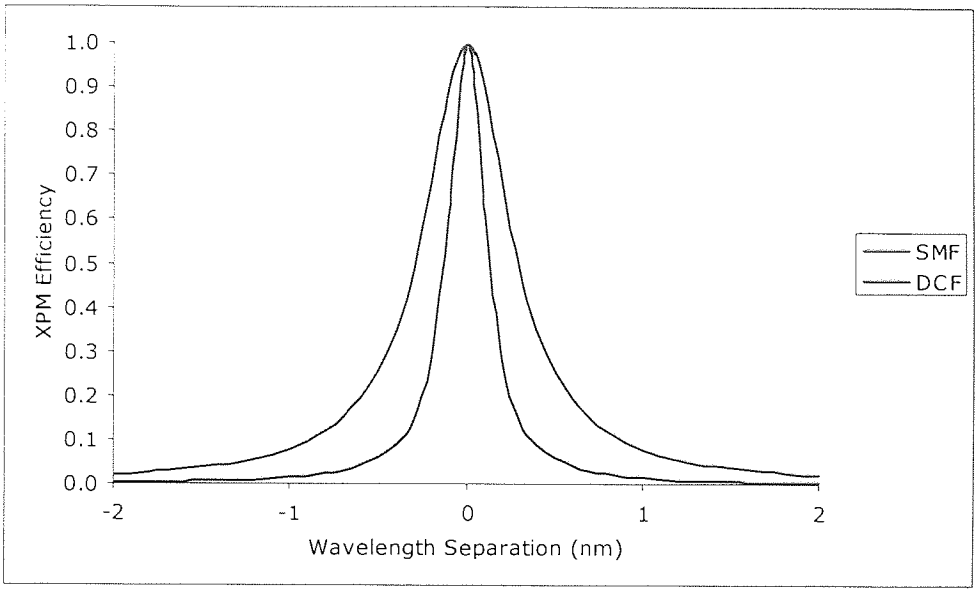

Figure 3.4: The XPM efficiency, η_{XPM}, against wavelength separation for 100km of SMF and 21.25km of DCF at 40GHz

3.7.3 • Four Wave Mixing

Four-wave mixing (FWM) is a third order parametric process [95] and therefore, the phase matching necessary for FWM requires a specific choice of frequencies and refractive indices. In WDM systems, the beating of the different wavelengths induces phase modulation of the channels and results in additional energy being generated. Consider three frequencies, f_i, f_j and f_k copropagating along an optical fibre; a new wave at frequency f_{ikj} is generated when [96];

$$f_{ijk} = f_i + f_j - f_k . \tag{3.10}$$

If the channels are not evenly spaced, the additional signal will form into an unwanted signal but as most systems operate with equally spaced channels the new frequency will coincide with an existing channel. The form of this interaction will depend on the bit pattern, with the power adding to the one or the zero, either way, it results in eye closure.

The power generated at the new frequency depends on the FWM efficiency η_F, and is given by [97, 98];

$$P_F = |A_F(L)|^2 = \eta (d_F \gamma L)^2 P_i P_j P_k e^{-\alpha L}, \tag{3.11}$$

where P_i, P_j and P_k are the power of the three copropagating frequencies, L is the fibre length, α is the fibre attenuation, γ is the nonlinear coefficient and d_F is the degeneracy factor and results in $d_F = 1$ when $i = j$ and $d_F = 2$ when $i \neq j$.

Assuming the original channels are all copolarised, the FWM efficiency, η_{FWM}, is given as;

$$\eta_{FWM} = \left| \frac{1 - \exp[-(\alpha + \Delta k)L]}{(\alpha + i\Delta k)L} \right|^2, \tag{3.12}$$

which is dependent on the channel spacing through the phase mismatch governed by Δk;

$$\Delta k = \beta_F + \beta_k - \beta_i - \beta_j \approx \beta_2(\omega_i - \omega_k)(\omega_j - \omega_k). \tag{3.13}$$

Another way of writing the FWM efficiency is given by [99];

$$\eta_{FWM} = \frac{\alpha^2}{\alpha^2 + \Delta\beta^2}\left[1 + 4\frac{\exp(-\alpha L)\sin^2(\Delta\beta L/2)}{[1 - \exp(-\alpha L)]^2}\right]. \tag{3.14}$$

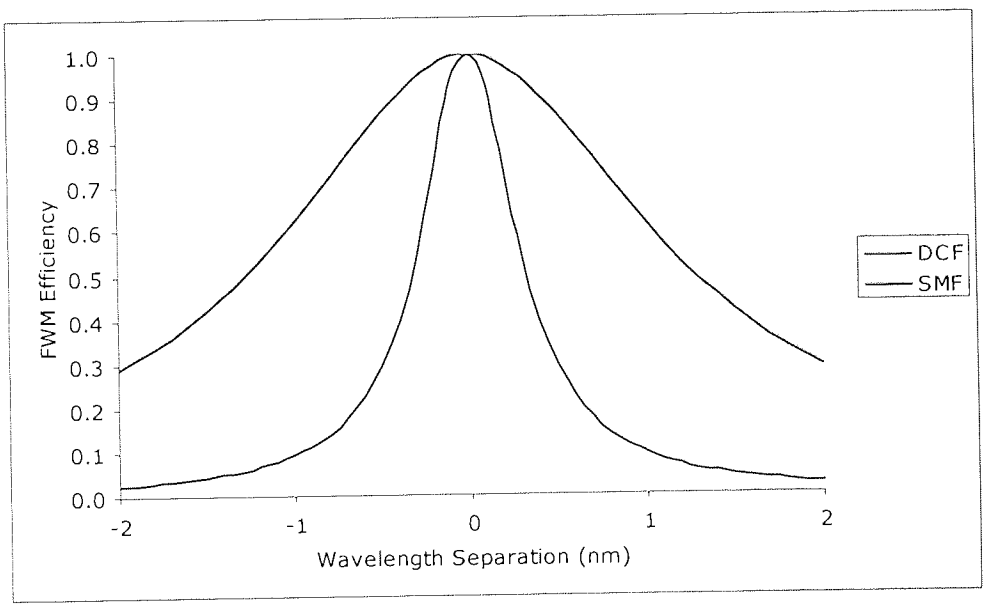

Figure 3.5: The FWM efficiency, η_{FWM}, against wavelength separation for two signals propagating in a 100km length of SMF and 21.25km length of DCF

Fig. 3.5 was obtained by using the fibre parameters listed above in 3.7.2 and using the efficiency given in equation 3.14. The most efficient FWM mixing occurs when the signal are phase matched, i.e. $\Delta\beta = 0$. As with the XPM efficiency, FWM efficiency is much greater in the lower dispersion SMF than the DCF, although unlike XPM, it is

not dependent on the frequency of modulation. The SMF had an efficiency of 0.5 for a separation of 1.3nm whereas this DCF had a separation of 0.3nm for the same efficiency. The most effective way to minimise FWM is to use high local dispersion fibre to minimise the phase matching, although at high bit rates this can lead to the intrachannel interactions mentioned earlier.

3.8 • DMS vs. WDM

The DMS provides an attractive solution to the problems generated by the conventional soliton. In the previous chapter, the use of the conventional soliton as a transmission format for systems was rejected due to their high dependence on system parameters. The DMS is slightly more system friendly in that it avoids the jitter inherent in solitons, yet it still has a strong dependence on the system parameters. Map strength is the defining term for a DMS, and to maintain a low value for this parameter, the pulses must be large for long spans with high dispersion, or they must be narrow for short spans with low dispersion. TDM of the DMS approach provides an increase of the bit rate but a reduction in the bit slot. In order to sustain the same map strength whilst reducing the pulse duration to fit in the narrower bit slot, either the dispersion or the dispersion map period needs to be reduced. This is seen in the high bit rate systems that adopt the DDMS approach where they utilise multiple periods of a short dispersion map between amplifiers.

From a practical point of view, these requirements present problems. An installed system based on long amplifier spans and SMF would require large pulses to satisfy the restrictions of the small map strength, only allowing slower system bit rates. The DMS approach is more suitable for a system based around short spans utilising DSF. Whilst the DDMS approach provides the ability to transmit high speed OTDM data, it may not be suitable for installed systems where PMD is high, as the small bit window cannot tolerate this dispersion and dramatically reduces the DDMS transmission performance [80]. The DDMS approach also generates additional problems with regards to system maintenance. If a span is broken or requires modification, this could alter the periodicity nature of the dispersion map, and could destroy the soliton.

WDM offers the ability to upgrade the information capacity of a network by introducing additional channels. This is at the expense of the introduction of additional

nonlinear effects such as XPM and FWM although there is a number of ways that these can be reduced. The effects are dependent on phase matching between the channels, if highly dispersive fibres are used this reduces their efficiency. This efficiency can also be reduced by increasing the wavelength separation between channels. Also, as high launch powers are not required to generate the nonlinearities for the DMS, launching with lower powers would reduce these nonlinear interactions.

For systems using high local dispersion and long amplifier spans, WDM interactions are small due to the high mixing of the frequency components and the high span loss. For systems using low dispersion fibre with shorter amplifier spans, WDM interactions are higher, but the full impact of their negative effects can be avoided by operating in the quasi-linear regime. The issue of PMD is largely avoided as the bit window has not increased. Therefore by adopting a WDM based approach, little restrictions are placed on the fibre in the installed system.

Comparing OTDM and WDM from a practical standpoint, the introduction of additional channels increases the complexity at the multiplexer and demultiplexer for both cases. Also they both require additional gain from the installed amplifiers to maintain the same energy per pulse after upgrading. OTDM places restrictions on the time domain window whereas WDM places restrictions on the available frequency bandwidth per channel.

DDMS WDM is almost an oxymoron. For a DDMS to propagate it requires a short dispersion map that periodically returns to the chirp free point and also requires narrow pulses to obtain the high powers required for the nonlinearity. In WDM, this periodic return to the chirp free point would increase the amount of time phase matching occurs along the span, and increase the efficiency of the negative WDM nonlinear effects. Narrower pulses not only have the higher peak powers that generate more inter-channel effects, but they also increase the optical bandwidth, reducing the separation between energy of each channel and increasing the efficiency of the nonlinear effects. To overcome the inter-symbol interference generated from the overlapping spectrums, the channels could be spaced further apart, although this is at the expense of spectral efficiency. However a regular DMS WDM system could be possible using speciality fibred such as NZDSF where the dispersion map was tailored to reduce the phase matching, yet have low enough dispersion to allow the DMS to propagate. One restriction on the NZDSF is that it must provide full slope compensation so that the

chirp free point is maintained, or else the DMS will only be sustained on the channel with the required path averaged dispersion.

3.8 • Chapter Summary

To summarise this chapter we introduced the concept of dispersion mapping, by which the fibre span comprises of both anomalous and normally dispersive fibres. This dispersion map can be organised either symmetrically or asymmetrically although in the case of dispersion managed solitons, a symmetric dispersion map with and initial half step of anomalous fibre is normally used. Map strength is the parameter that is used to quantify dispersion maps, and soliton like propagation occurs when these strengths approach one. This DMS avoids the problem of timing jitter associated with conventional solitons due to the low path averaged dispersion of the fibre map. The DDMS is used in high speed TDM systems where a restriction is placed on the bit window, but it maintains the map strength for DMS by utilising multiple repetitions of short fibre map between amplifier spans and maintaining the low path-averaged dispersion.

Due to the breathing nature of the DMS pulse width across a span, the average peak power remains the same as a conventional soliton, yet the peak power at chirp free points is enhanced, providing a greater SNR at the receiver than conventional solitons. The DMS naturally enhances the SNR at the receiver due to this power enhancement, yet not all systems may be able to utilise this due to the restriction the DMS places on system parameters. For systems unable to sustain DMS, improvements in SNR are made by increasing the launch power. Unfortunately SPM is no longer beneficial, and the increase in launch power increases nonlinear effects that generate errors at the receiver. Initial a linear increase in SNR is gained for the increase in launch power until the power is sufficient to generate nonlinear interactions, which at first are not sufficient to counteract the gain in SNR although when the powers are sufficient the nose they introduce counteract that of the SNR gain from increasing power. The region where nonlinear effects exist, but do not dominate is known as the quasi-linear regime. The nonlinear WDM effects of XPM and FWM were introduced and it was shown that both are dependent on the phase matching of signal components, although the efficiency is dependent on the modulation frequency for XPM, but not for FWM. The

efficiency of these interactions can be reduced by increase the separation of channels (which reduces the spectral efficiency) or by increasing the local dispersion.

With regards to systems, WDM is preferred to DMS for existing systems due to the heavy restrictions that DMS place on a system and its unsuitability for future upgrades, although the DDMS and even WDM DMS are suitable for new high speed TDM based systems.

Chapter 4

Laboratory Transmission Techniques

4.1 • Introduction

The ability to perform transmission experiments in the laboratory has many advantages over field tests as optimisation of component location and other effect can be performed quickly. Increasing focus is being placed on the quality of source components for communication experiments, as the evolution of high bit-rate systems generates a demand for sources that can maintain wavelength accuracy, a high extinction ratio, variable chirp control and stable high output powers. Employing poor quality source components limits the quality of the received data before transmission begins and most defects, such as source jitter and amplitude instability, will be amplified during the transmission process, instigating greater eye closure. There are three main methods for generating a modulated communications source, directly gain switching a DFB laser, lasers with integrated modulators for instance electro-absorption modulator lasers (EML) and continuous wave (CW) lasers utilising external modulators. Directly modulating a laser reduces the component count and cost, sources with inbuilt modulators reduce component count, but with an increase in cost and external modulation bestows flexibility but at the most cost.

In this chapter we shall be examining the necessary components required for laboratory based testing of an optical fibre communications system. The performance of a number of optical sources starting with the gain switched DFB and the use of light injection to suppress the jitter. We then look at externally modulating a signal using electro-optic and electro-absorption modulators. The PriTel pulse source is then examined, as this will be the main source for later work, and the operation of its OTDM is given. The main element for simulating a transmission system is the recirculating loop, and the principle of its operation is given. The method used for measuring the loops dispersion is explained and the main polarisation effects seen in

fibre are briefly discussed. Finally the process used for the estimation of errors based on the quality of the received eye is presented.

4.2 • Gain Switched DFB Lasers and Jitter Suppression

Distributed feedback (DFB) lasers emit radiation in a single longitudinal mode, or single frequency, by means of a diffraction grating coupled to the active region of the length of a semiconductor laser cavity. The longitudinal mode is defined by the parameters of the grating and the other modes are reflected back by the grating to prevent lasing, in general, this provides suppression in the order of 40dB [100]. Directly modulating the output of a semiconductor DFB laser by modulating the input current is an attractive proposition due to the low cost, the high output powers available and the ease of use. Unfortunately, one of the side effects associated with current modulation is a carrier density modulation, consequently generating a frequency chirp that can limit the transmission distance. Inexpensive diodes have been widely used for very short reach (VSR) applications although for systems aiming for longer transmission ranges, DFBs with good sidemode rejection and low chirp operation are required. [101-107]. Further to the unwanted frequency chirp, semiconductor lasers also exhibit relaxation oscillations. When the gain of a semiconductor laser is switched from below threshold to inversion the output power overshoots and then reaches a steady state through damped relaxation oscillations. These distortions are clearly unwanted, as they will affect the desired launch pulse dimensions.

Another outcome ensuing current modulation of a semiconductor laser is timing jitter induced by random fluctuations of photon density within the cavity at threshold. The resultant jitter arises from inconsistencies between the electrical frequency and the optical pulse time intervals, closing the received eye. One technique for suppressing this jitter is by imbuing the cavity with additional photons from either an additional source or from reflections coupled back into the cavity. Light injection via continuous wave light or light reflected back into the cavity has been reported on a number of occasions [108-110] and has proved successful. It is important to recognise that this timing jitter is different to the SPM induced Gordon-Haus timing jitter (2.7.1), and Gordon-Haus timing jitter will only exacerbate this effect.

Fig. 4.1 displays the layout of the equipment necessary for testing the suitability of mode locking a gain switched DFB laser.

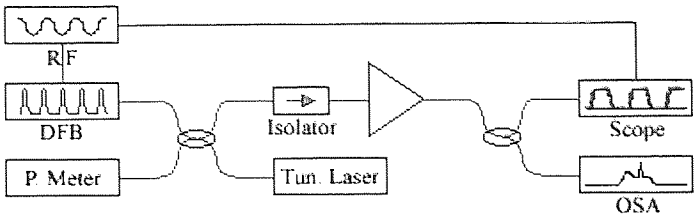

Figure 4.1: Schematic diagram show the apparatus necessary for gain switching of a distributed feedback laser using external light injection from a CW source.

A 1.0GHz electrical sinewave generated by a frequency synthesizer was combined with an adjustable DC bias to enable gain switching of the DFB laser source, which operated at a wavelength of 1546nm. In order to minimise fluctuations from the source and EDFA were temperature stabilised and a constant current, of 80mA and 18mA, was provided for both the EDFA and the DFB respectively. The output of the DFB was split into a calibrated 50/50 coupler whilst the tuneable CW laser, monitored by a power meter, injected light back into the DFB cavity from the opposing direction. The respective output from the seeded DFB was then isolated and amplified to provide gain for the optical spectrum analyser (OSA) and sampling scope and also to prevent any additional back reflections or ASE re-entering the laser cavity. In order to prevent attenuation of frequency components, and thus broaden the pulse on the sampling scope, the 30GHz input of the scope was fitted with a 32GHz photodiode. It was necessary for the CW source to have a variable output power and wavelength in order to establish the optimum parameters for mode locking. The reason being, if the wavelength is close to the source wavelength and little output power is required to inject a sufficient number of photons into the core, then the source could be replaced with a lower cost grating.

Fig. 4.2 shows the result attained for the rising and falling edge jitter for the gain switched DFB against the wavelength and power from the CW light seeded into the DFB cavity. To optimise the jitter reduction for the rising edge of the pulse, a wavelength downshift of 0.5nm and a power input to the cavity of –4.0dBm provided a jitter at the FWHM of 1.5ps, whilst for the falling edge, the conditions for the optimum jitter of 2.6ps matched the DFB wavelength but necessitated an increase in power to

-2dBm, the maximum power provided by the tuneable laser. Clearly in order to optimise both the rising and falling jitter, a input source with a 3dB bandwidth greater than 0.5nm and a output power greater than 1dB would be necessary to overcome the losses of the coupler and cover the wavelength regions that provide the best possible jitter reduction. A reflection-based device would not be suitable due to the high powers necessary and the large bandwidth. Looking at the average of both results, a wavelength of 1546nm at –4.0dbm would provide rising and falling jitter of 3.0ps and 3.1ps respectively. This would enable good jitter reduction when using a narrow bandwidth reflector for seeding, but the source would undergo 6dBm of loss through the coupler plus additional attenuation due to the mirror or grating based device before being reflected back to the cavity, requiring an average output power much greater that 2dBm from the source.

In order to provide a suitable long distance communications source from a DFB, a DFB with a higher output power is necessary to take advantage of cheaper reflection based jitter reduction. Furthermore the pulses from these sources will also need to be compressed in order to be suitable for high speed transmission purposes. This could be done by using both linear and non-linear compression, which could be achieved by the use of a number of methods such as compression using optical loop mirrors [111], dispersion-decreasing fibre [112] and highly nonlinear fibre [113]. Clearly the financial savings gained by gain switching a DFB are removed by the necessity for a higher-powered DFB and the additional components necessary for jitter reduction and pulse compression.

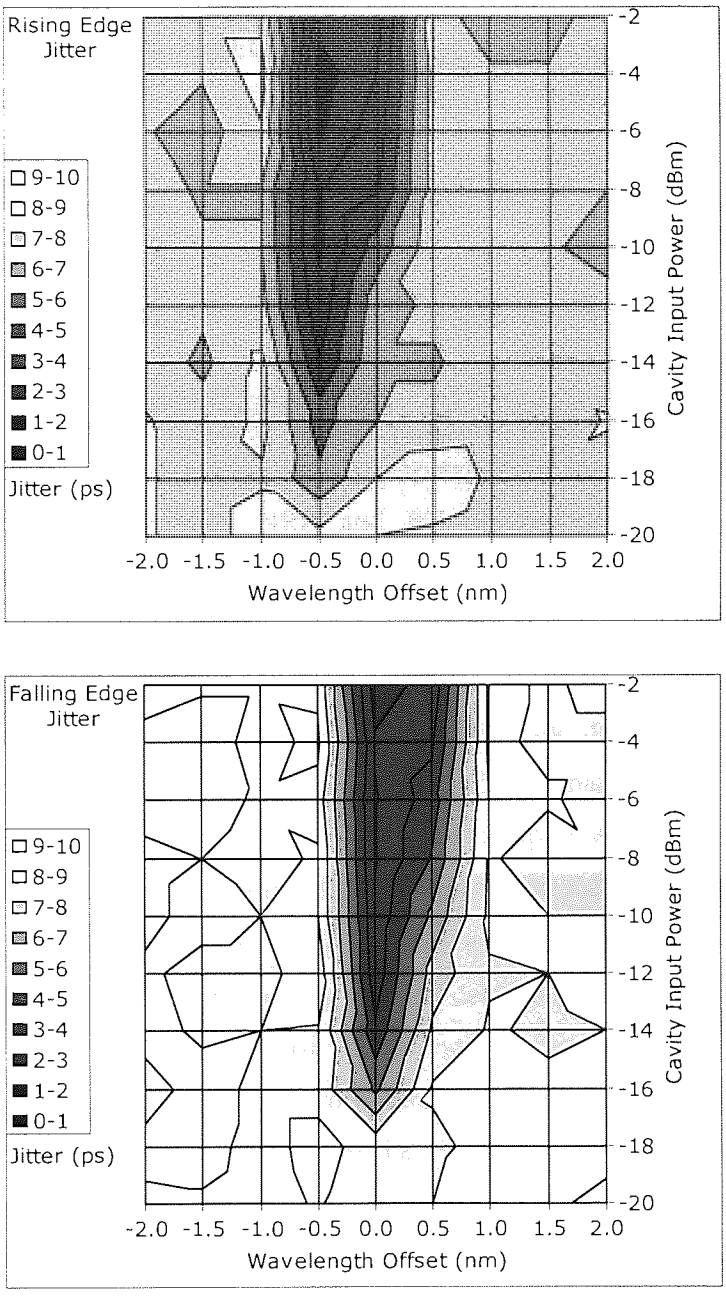

Figure 4.2: Rising and falling edge jitter (ps) against CW seeding source cavity input power (dBm) and wavelength offset (nm) from the DFB central frequency. Map of jitter show greatest jitter (light yellow) through to least jitter (blue)

With the use of an external modulator, DFBs or semiconductor lasers can be used in CW mode, providing greater wavelength and amplitude stability by removing the need for gain switching and modulated externally. Modulators increase the flexibility of the source, which can be freed to be wavelength tuned without drastically affecting the output data, unfortunately optical modulators are polarisation sensitive and have a high insertion loss. By utilising one modulator, NRZ data can be accomplished and for optical RZ data two modulators are necessary, although one can attain electrical RZ by using a single modulator and applying a modulated electrical signal rather than using a sine wave. Utilising external modulators also expands the range of possible modulation formats from the conventional NRZ and RZ, increasing the range of source possibilities. By biasing an additional modulator after the RZ data, driving it at half the clock frequency across the null bias position on the transfer curve yields an alternating optical phase modulation format known as carrier-suppressed RZ (CSRZ) [114, 115]. By including an additional phase modulator, driven by the data signal, after the RZ pulse source provides a chirped return-to-zero (CRZ) that has been popular for long distance transmission [116]. Duobinary is a more complex modulation scheme that utilises external phase modulation that has been proved in radio communications and was adapted for optical transmission [117]. This uses three output levels of output data, 1, 0 and –1, generated by adding one-bit delayed data to the current signal, distinguishing levels 1 and -1 by opposing phase rather than intensity.

Lithium Niobate is used in amplitude modulators due to its low loss in the infrared region and its high electrooptic coefficients, i.e. the proportionality between refractive index and electric field. The electrooptic effect is the change in refractive index of a material experiencing an applied electric field. The effect is linear, proportional to the electric field and only occurs in materials, like Lithium Niobate, that do not posses inversion symmetry. Unfortunately the electrooptic effect is polarisation dependent, [118] therefore the polarisation state of the input light must be carefully maintained in order to maximise performance from these devices.

In bulk layer devices, electroabsorption modulators (EAMs) operate on the principle of the Franz-Keldysh effect [119]; an electric field-induced wavelength shift and broadening of the absorption band edge. This is also known as the quantum confined

Stark effect in multi-quantum well structures [120]. For both cases, the response is highly nonlinear and is wavelength sensitive. When the device experiences no voltage the wavelength is longer than the absorption edge and suffers little attenuation, when reverse biased the absorption edge broadens inducing attenuation. EAMs also impose a chirp due to SPM. During the transition between one and zero, increasing and decreasing the power within the modulator, a simultaneous refractive index change occurs generating a phase shift across the pulse during the transition [118]. Fig. 4.3 shows the transmission profile for both the $LiNbO_3$ modulator used for data application and an EAM.

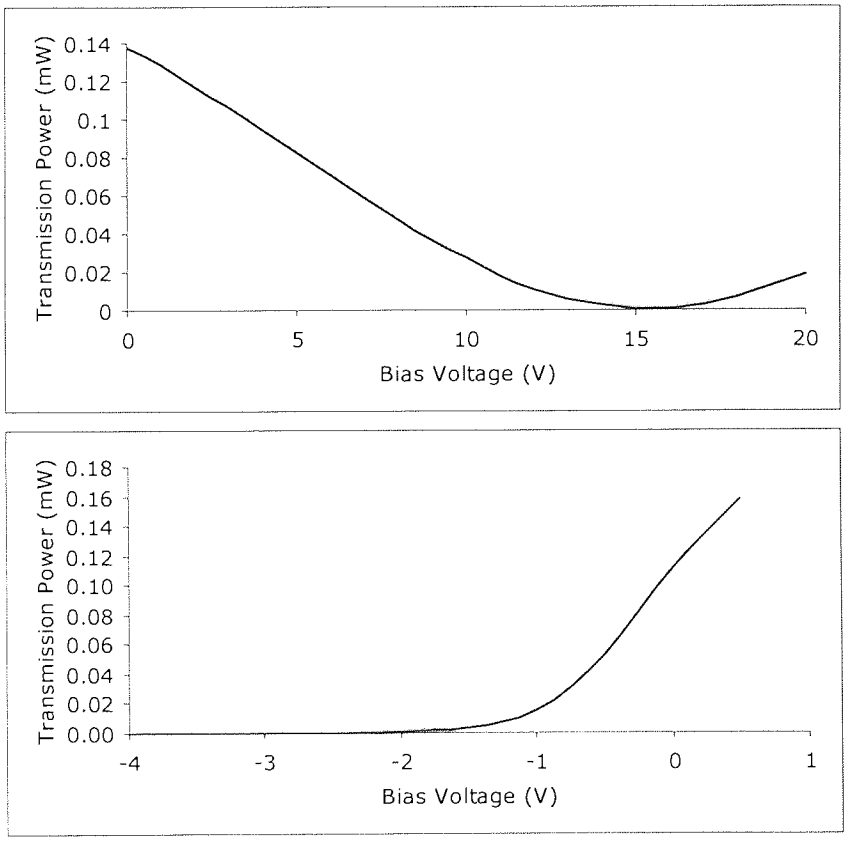

Figure 4.3: The transmission power (mW) against bias voltage for a $LiNbO_3$ EOM (top) and an EAM (bottom)

The EOM has a large linear region and would require a drive voltage of 12V/34dBm to provide an output with maximum extinction of around 21dB. The EAM has a nonlinear response with little variation in output power between -4 and -2 volts, also it necessitates a lower drive voltage of 4V/24dBm to generate a similar extinction.

With the advent of the commercial 40Gbit/s electro-absorption modulator (EAM) [120], direct external modulation has become a viable method for 40Gbit/s telecommunications data generation; unfortunately the devices are sensitive. In the research environment, where the data fabricated is pseudo-random in nature, the necessity to operate at a base rate of 40Gbit/s in order to investigate systems based on this data rate is not yet necessary, albeit for high data rates, this becomes useful. The commonly used method for increasing the system data rate is to utilise optical time division multiplexing (OTDM) [121, 122].

The main laser sourced used for transmission experiments was the PriTel fibre laser. As opposed to the conventional semiconductor lasers, this apparatus utilises a length of fibre for the main laser cavity with an EDFA providing the gain, coupled with a 20Ghz EAM to generate the pulses. Table 4.1 summarises the main parameters given by PriTel.

Wavelength Range	1542nm to 1560nm
Maximum Average Output Power	50mW
Pulse Duration	2ps to 10ps at 10GHz
Bandwidth	0.3nm to 1.3nm at 10GHz
Frequency	DC to 20GHz

Table 4.1: Summary of the PriTel fibre laser parameters

With regards to pulse duration and bandwidth, the PriTel fibre laser is not tuneable across the entire 2ps to 10ps range and will only lock in at a certain frequencies. Due to the nature of the fibre laser, altering the cavity length to enable this locking will also effect the round trip time and also the output wavelength. This can be seen in Fig. 4.4 and Fig 4.5 where an arbitrary output wavelength of 1550nm was chosen and the synchronisation control of the laser was adjusted to select different pulse durations whilst operating at 9.95328GHz. In order to resolve the duration of the PriTel, the 500GHz bandwidth Ando AQ7750 scope was used to perform the temporal measurements depicted in Fig 4.4. Also, the data acquisition was averaged eight times before capture and the amplitudes of the temporal measurement have been normalised in order to aid comparison. By tuning the synchronisation control, only five pulses

with a FWHM of 8.5ps, 9.5ps, 3.8ps, 2.9ps and 2.3ps and with respective bandwidths of 0.40nm, 0.51nm, 0.54nm, 0.72nm and 1.04nm were available.

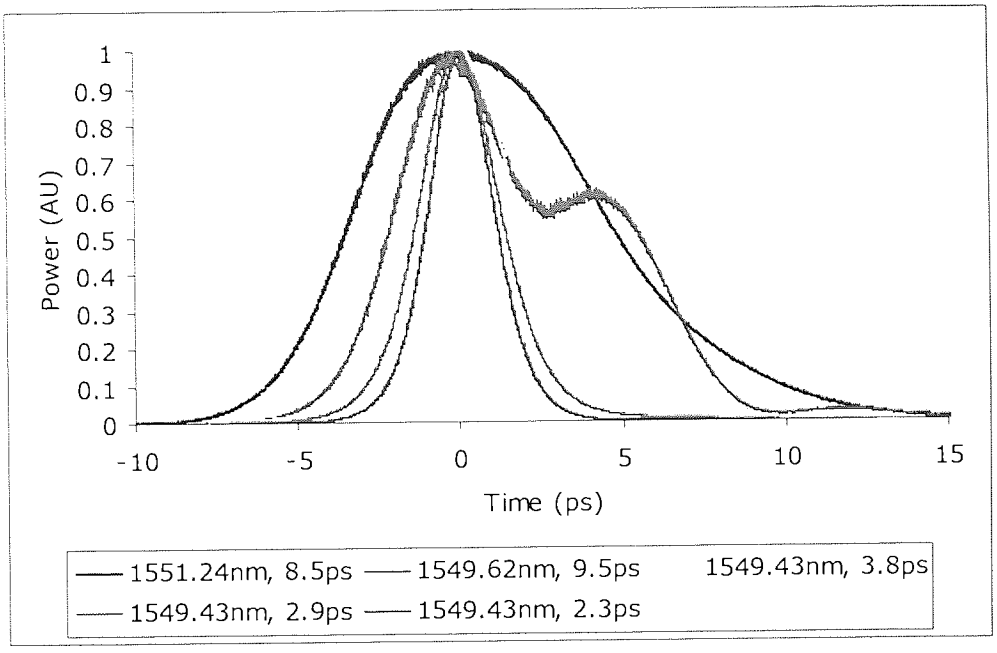

Figure 4.4: The temporal output of the PriTel fibre laser for the five available pulse durations at 1550nm.

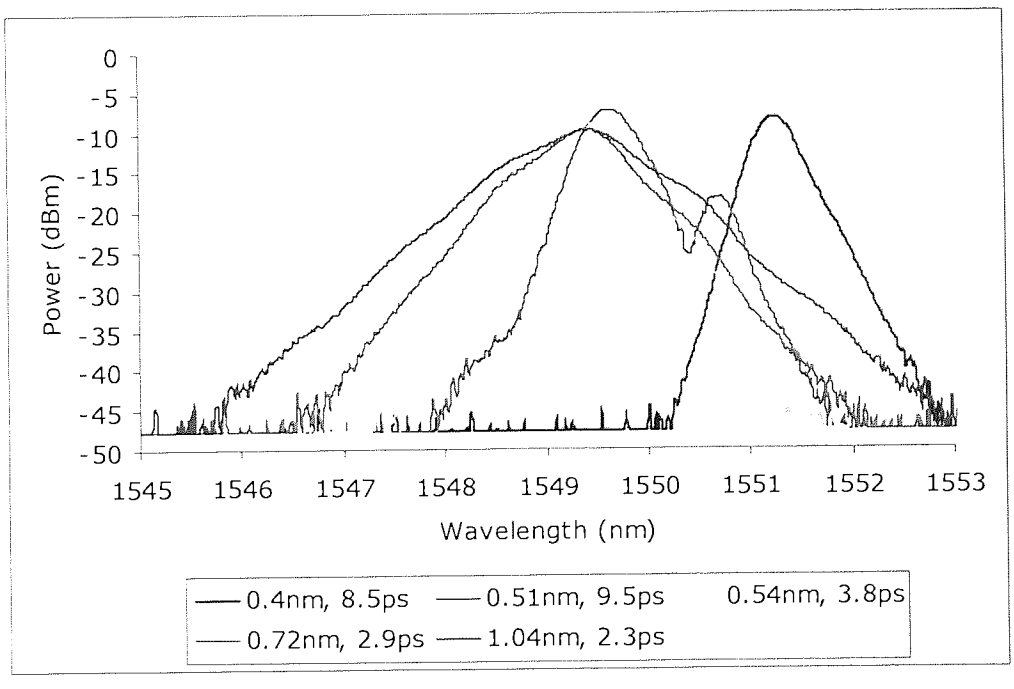

Figure 4.5: The bandwidth of the pulses output from the PriTel fibre laser at 1550nm

The narrower pulses of 2.3ps and 2.9ps closely fitted the Sech profile provided by the scope, the 3.8ps pulse more closely fitted a Gaussian profile whilst the two broadest pulses of 8.5ps and 9.5ps did not fit either profile. The 8.5ps and 3.8ps pulses are not symmetrical and their tails extend further on one side than the other whilst the 9.5ps pulse has a secondary hump on one side. In the optical domain, none of the spectra are symmetrical and the 9.5ps pulse had an uneven spectral output with the main peak at 1549.6nm and a secondary peak at 1550.8nm. When another arbitrary wavelength is chosen and the PriTel is driven at the same frequency, pulses with similar profiles are attainable.

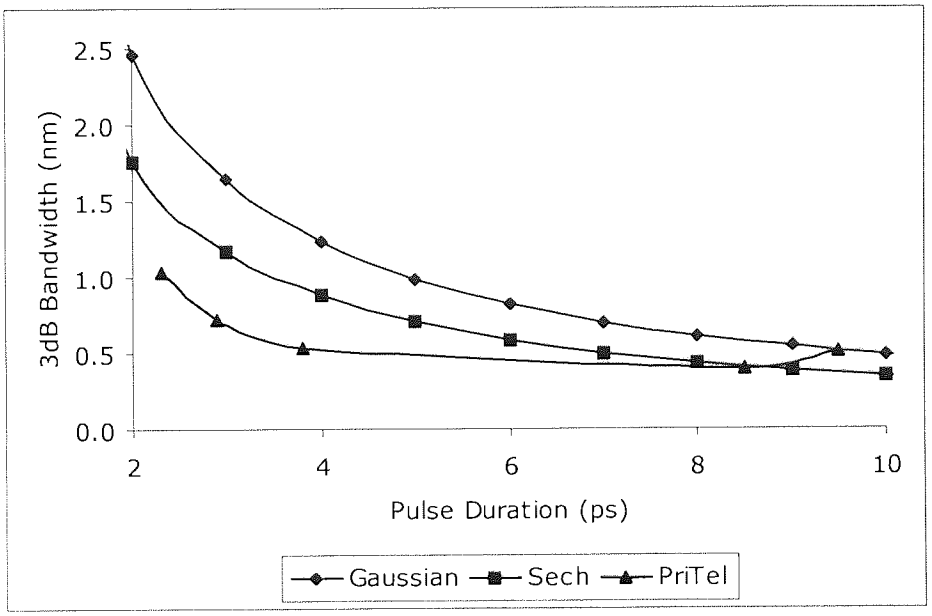

Figure 4.6: Pulse duration against 3dB spectral bandwidth for transform limited Gaussian and Sech pulse profiles and the PriTel fibre laser

Fig. 4.6 depicts the pulse duration against 3dB bandwidth of the PriTel fibre laser alongside the transform limited Gaussian and Sech pulse profiles, with the time bandwidth product (TBWP) of 0.44 and 0.315 used for the Gaussian and Sech pulses respectively. Clearly the output of the PriTel is chirped as none of the PriTel output pulses fit their expected TBWP profiles. Attempts were made to quantify the chirp of the PriTel with an Apex AP2440A Optical Complex Spectrum Analyser, although due to the instability of the sources spectrum, this measurement could not be taken. In fact, the output pulse profiles of the PriTel changes during daily operation, requiring resynchronisation that can result in different output parameters.

As the Ando scope and Apex spectrum analyser was only available on a short-term loan it was only used for characterising the output of the PriTel fibre laser. Due to the lower bandwidth of the 32GHz Agilent lightwave converter used during experiments, neither the asymmetry nor the double pulse like nature of the PriTel output was observed.

The experimental arrangement for the data application and OTDM of the PriTel pulses is shown in Fig. 4.7.

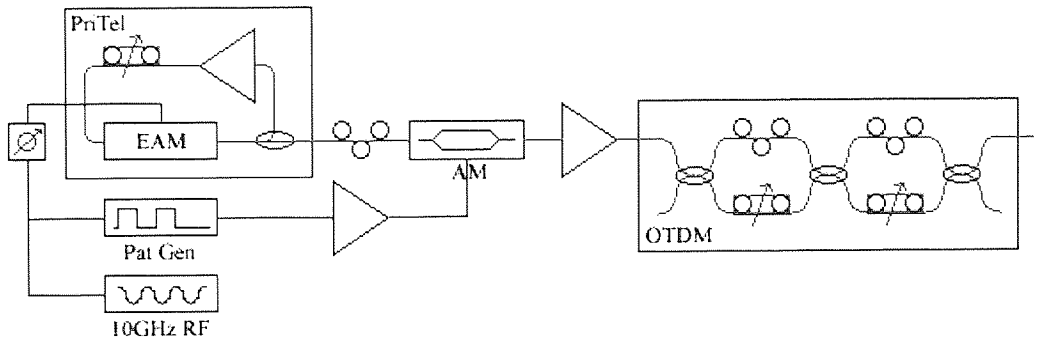

Figure 4.7: Diagram describing 40Gbit/s transmission apparatus. Comprising the 10Gbit/s PriTel fibre laser, external data modulation via an amplitude modulator (AM) and multiplexing up to 40Gbit/s using an optical time division multiplexer (OTDM)

A simplified version of the PriTel fibre laser is given to provide an idea of its operation rather than describing the operation in full as the full schematic is overly large, and includes complex polarisation maintaining control loops and additional monitoring outputs. The ring laser is modulated by a sinewave, generated by a CW RF synthesiser, at the 10Gbit FEC free frequency of 9.95328GHz via a 20GHz EAM. The resultant pulse stream provided by the major output has a repetition rate of 10Gbit/s, a pulse width of 3ps and an average power up to 50mW, depending on the gain provided within the laser cavity. The chirp on the output pulse stream also fluctuates depending on the setup characteristics of the PriTel, such as cavity length, and also due to the internal EAM. Powers greater than 0dBm coupled into the Lithium Niobate amplitude modulator could cause damage to the modulator, therefore a lower powered PriTel monitor output is propagated into the modulator, via a polarisation controller in order to avoid the polarisation dependent losses induced by the electro-optic effect. This modulator is driven by the amplified output of the Pattern generator, referenced to RF synthesiser, combined with a DC bias to provide the PRBS data. Misalignment of the

pulses from the PriTel with the switching window of the modulator results in spurious pulses; therefore an electrical phase shifter is used on the PriTel clock input to align the time windows of the modulator with the pulses from the PriTel.

Optical time division multiplexing (OTDM) the data from its base rate of 10Gbit/s to 40Gbit/s is attained by interleaving copies of the original 10Gbit/s data with the original in time. By utilising a Mach-Zehnder arrangement after the amplified output of the $LiNbO_3$ it is possible to delay propagation in one arm with respect to the other with the aid of a fibre delay line. Stretching the fibre in the fibre delay line causes an increase in fibre length, therefore increasing the transmission time for data propagating along that arm of the Mach-Zehnder, resulting in a propagation delay for that arm with respect to the other when the signals are recombined. Causing a delay of half the time window of 100ps is insufficient for adequate mixing as this would result in sequential bit repetition within the recombined 20Gbit/s PRBS data, instead a larger delay is used to avoid this. The entire process is repeated by the use of an additional Mach-Zehnder after the first, in order to double the resultant bit rate to 40Gbit/s. As depicted in Fig. 4.7, the Mach-Zehnders also have polarisation controllers in the opposite arm to the fibre delay lines in order to align the polarisation of the interleaved channels. This allows one 10Gbit/s ODM channel to propagate through both controllers; two channels to propagate through a single controller and the final channel to propagate through neither controller. By using an additional polarisation controller and a polariser on the output of the OTDM, the 4 x 10Gbit/s channels can be transmitted in the same polarisation state. The polariser can also be used to equalise the channel powers and compensate for any disparity in attenuation seen by each channel. Not only do the polarisation controllers provide the ability to align the channels to one polarisation, they can also be used to align the channels, sequentially, in orthogonal polarisations [121]. Using a polariser or polarisation beam splitter before the demultiplexer allows channels of one polarisation state to propagate to the demultiplexer and isolates channels in the orthogonal polarisation. This in turn halves the bit rate necessary for the demultiplexing electronics and doubles the bit windows at the receiver. This enables the uses of cheaper, slower bit-rate equipment or the doubling of the transmission bit-rate with respect to the demultiplexer. This is similar to the polarisation interleaving technique used in WDM systems where adjacent wavelengths are at orthogonal polarisations in order to increase spectral efficiency [123].

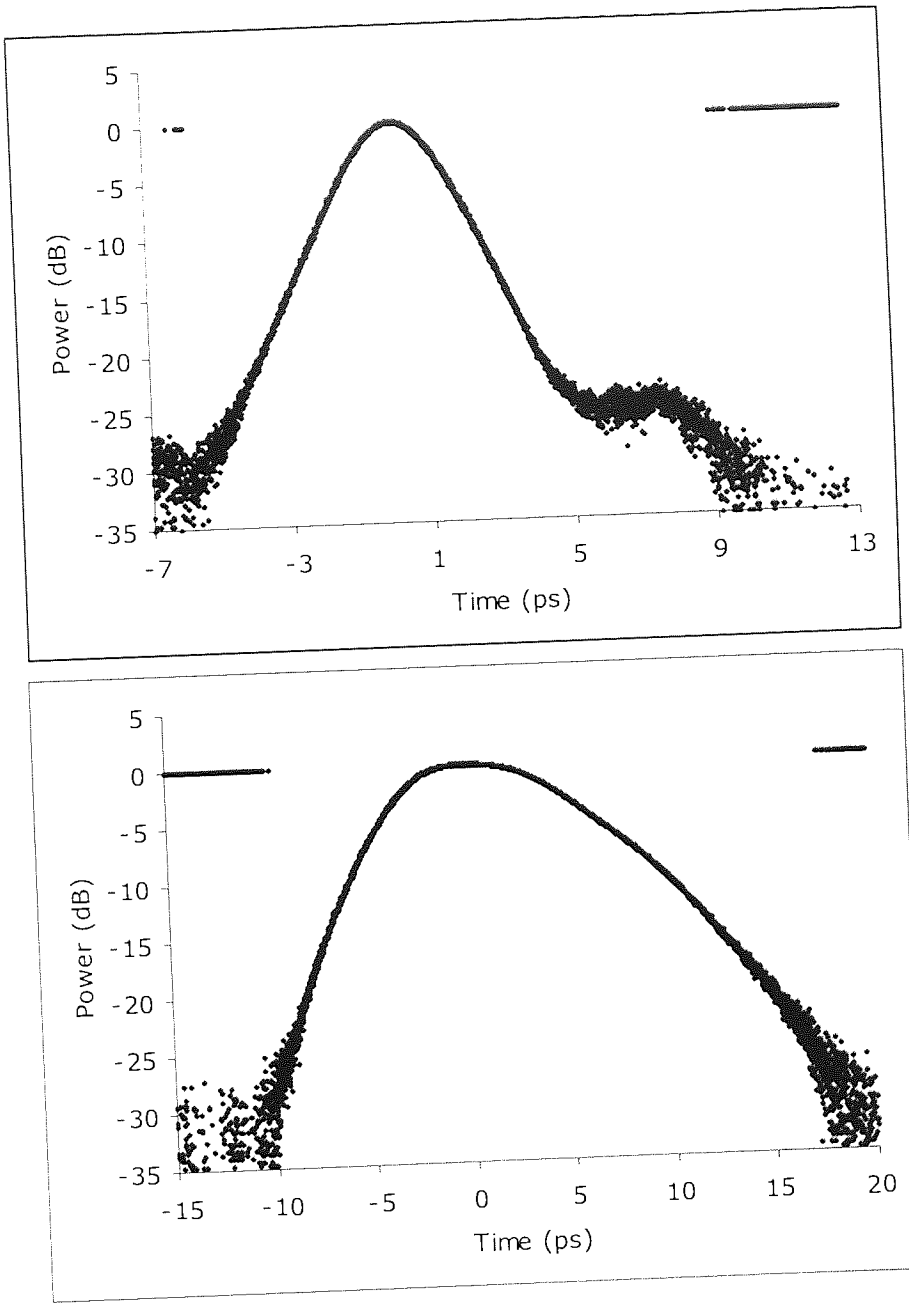

Figure 4.8: Normalised temporal output for the 2.3ps (top) and 8.5ps (bottom) pulses from the PriTel fibre laser. The amplitude has been converted to a log scale to highlight the pedestal of the pulses

As described above, the OTDM aligns copies of itself atop each other, separated in time. As these pulses overlap and the bit windows decrease, the importance of pulse shape and the pulse pedestal increases. Care must be taken to make sure that there is insufficient energy within the pedestal of adjacent pulses to prevent the pedestals mixing and being detecting in the wrong bit slot at the receiver. Fig 4.8 shows the

normalised output from the PriTel for the 2.3ps and 8.5ps pulses. The amplitudes have been converted into a log scale to emphasise the energy within the pulse tails. This conversion has resulted in spurious data points appearing at 0 as the Ando scope has recorded some of the lower input powers input in negative watts.

The conversion to a log scale has shown that the pulse is not as symmetrical as one would suspect by examining the pulse on a linear scale, as a pedestal is clearly visible on the right hand side of the 2.3ps pulse whereas the asymmetry of the 8.5ps pulse is clear in Fig. 4.8 and Fig. 4.4. As the 40Gbit/s bit window is 25ps, any notable pulse tails extending outside of this range will interact with an adjacent 1 or could be miss-detected as a 1 in an empty bit slot. For the 2ps pulse, the tail energy falls to a maximum of 27dB below the peak within the first 17ps of the pulse and beyond this point, the pulse energy falls below the detection level of the Ando scope. The output of the OTDM is shown in Fig 4.9.

For the 2ps pulse, there is no noticeable overlap between adjacent temporal channels. In order to emphasise the asymmetric pulse pedestals of the laser, the results in the upper graph have been converted into a log scale, although no overlap can be seen above the noise floor. There would be no noticeable overlap of the 2ps pulse at the receiver with that of the adjacent pulse providing that dispersion is fully compensated and the pulse returns to its original profile. However, the energy for solitary 8.5ps pulse falls below the detection threshold after 30ps, resulting in an overlap between the pulses when multiplexed to 40Gbit/s. Overlapping with an adjacent 1 would result in a total energy of 22dB below the peak power arising at the bit window boundary. This is less than 1/100 of the peak pulse energy and interaction would not be detectable at the receiver provided that this power is below or attenuated below the receiver threshold. As discussed in Chapter 3, interaction between overlapping pulses occurs during transmission due to dispersion generating inter-channel interactions. Due to the broader spectrum of the 2.3ps it would experience larger dispersive effects than that of the 8.5ps pulse and overlap between pulses would be larger. Depending on the severity of the interchannel effect and that of coherent mixing in the receiver, the less degrading of the two effects may have to be accepted.

The output from the OTDM can then be amplified to the correct launch power for transmission and then propagation can occur with the aid of a recirculating loop.

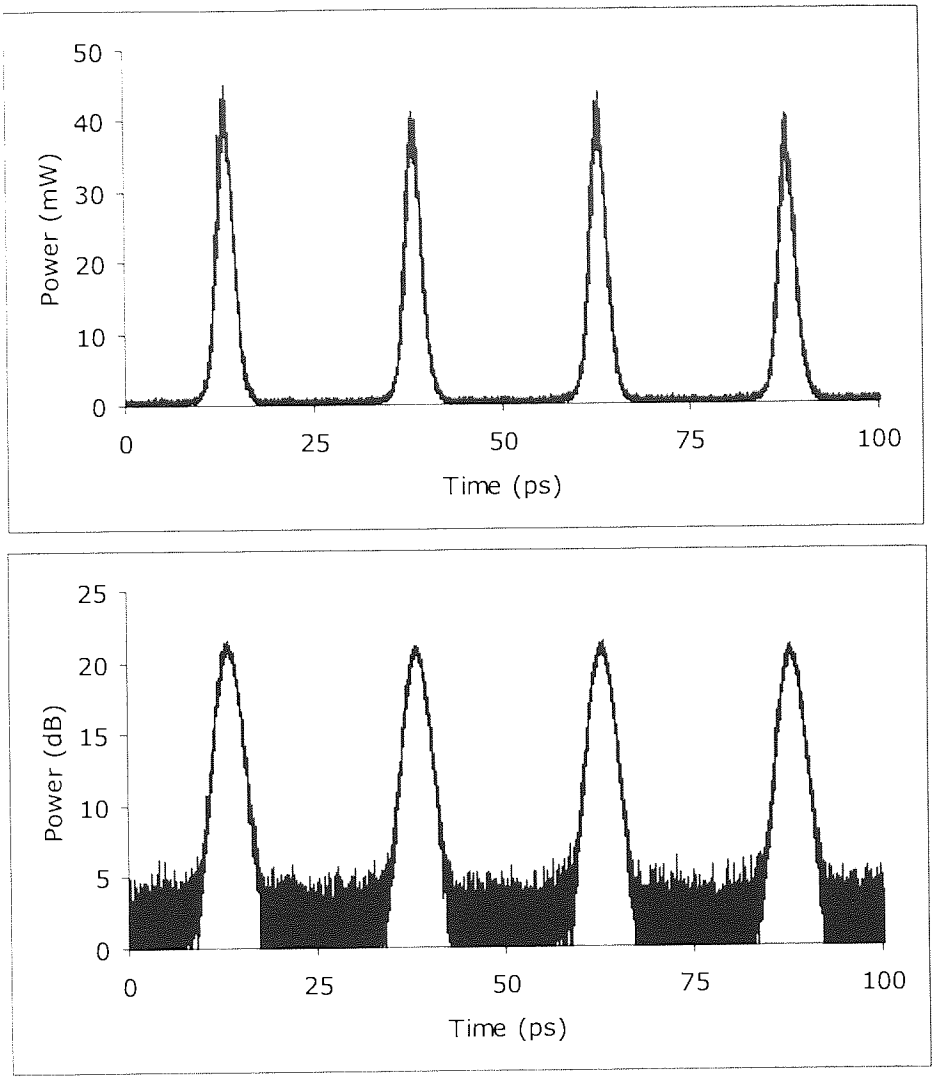

Figure 4.9: Time against power for the time division multiplexed PriTel fibre laser. The upper image shows the power in mW and the lower image depicts the power in dB

4.5 • Recirculating Loop

The typical optical communications link consists of two terminals, one housing a transmitter and the other containing a receiver, connected by repetitions of fibre and amplifiers. Typical terrestrial systems are required to transmit data over 400km in Europe and up to 1600km in the US whereas submarine systems extend up to 10,000km for trans-pacific links. With the long distances involved and the high costs of components, installing these systems is clearly a large financial burden to any organisation wishing to implement such a system. In order for research establishments,

who do not have access to network infrastructure, to investigate long-haul transmission, a compact and cheap solution that provides an alternative to installing a system must be found.

The recirculating loop takes advantage of the periodic nature of the dispersion map by forcing the data to propagate through the same fibre span and components multiple times. These repetitions can be built up to match the desired system length, and then the output can be analysed. As well as reducing costs, the recirculating loop has a number of advantages for the researcher. The loop transmission experiment can contain all the components found in transmission systems such as filters, amplifiers, regenerators and diagnostic equipment. Due to the relatively small number of components required in order to simulate a full system, these can be quickly changed and contrasted, providing a flexibility that is unattainable in the field.

4.5.1 • Recirculating Loop Control

In order to simplify the operation of the recirculating loop, we will first consider how the light propagates around the loop and then we shall examine how the data is extracted from the loop and measured. The modulated light enters the loop via the input and the data output from the loop is sent to be analysed by error detection equipment. Fig. 4.10 describes the physical setup of the basic recirculating loop control mechanism.

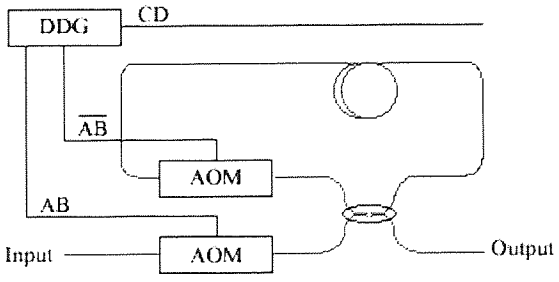

Figure 4.10: The basic components necessary for recirculating loop construction incorporating the 50/50 coupler, two acousto-optic modulators (AOM) and the digital delay generator (DDG). The logic outputs are highlighted above the DDG outputs.

Fundamentally, the recirculating loop consists of four components, two NEOS acousto-optic modulators (AOM): one at the loop input and one at the end of the fibre

loop, a 50/50 coupler, and a digital delay generator (DDG). In order to propagate around the loop, one loops length of data is generated and fills the loop and then the light is propagated a number of times around the loop. This propagation is controlled via a Stanford Research Systems 535 DDG, which has a delay resolution of 5ps, an RMS jitter of 50ps and supplied TTL outputs to the AOM and other equipment. The DDG was used to create five output triggers, T_0, A, B, C, D, and four control signals, AB, notAB, CD, and notCD. Fig. 4.11 displays the timing diagram formed by these signals and their relation to recirculating loop operation.

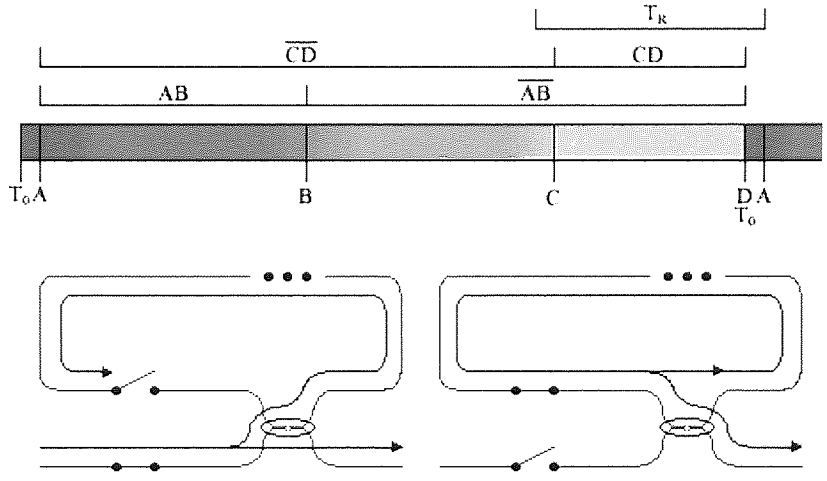

Figure 4.11: The digital delay generator logic and trigger outputs against time for recirculating loop control (top). Also diagrams showing the gate operation (bottom) for recirculating loop switching during the fill (left) and propagation (right) periods

To control the light propagating around the loop, there are two elementary timing periods, the fill time, AB, and the propagation time, notAB, and they are used to alternately attenuate the signal input to the loop AOM and input AOM respectively. During the fill time, the input AOM is activated and light is allowed to propagte through it, the 50/50 coupler and both into the loop and out into the error detection section. This period of time is greater than recirculation time, T_R, (approximated by T_R = L/cn or 4.89μs/km in SMF) to prevent large absences of light recirculating around the loop, which will be interpreted as 0's by the error detector. The light reaches the loop AOM and is attenuated until notAB, upon where the input AOM attenuates the input signal and the loop AOM allows the light to propagate through the coupler and

both back into the loop for an additional recirculation and to the error detection section. This time period is described by;

$$T_{BC} = (N-1)T_R + \frac{T_R}{10}, \tag{4.1}$$

where N is the number of recirculations required and T_R is the recirculation time. AOMs are used in for loop control rather than faster conventional communications modulators, such as LiNbO3 AM and EAMs due to their greater extinction ratio. AOMs operate by generating a standing wave pattern, via and acoustic wave, which acts like a grating and diffracts the beam. If modulators with lower extinction ratios are used, the light would not be attenuated to a level sufficient enough to prevent the light leaking through and being recirculated (and hence amplified). After the end of this period, the cycle is repeated again.

So far we have only concentrated on propagating around the recirculating loop and not yet explained how to obtain the error measurement we require. As we only wish to obtain results from the N^{th} and final recirculation of the loop, we setup a measurement time period at the end of our loop cycle, CD. This control signal is used to trigger the BERT and other test equipment so that they only analyse the data from the final recirculation. Period CD is set to $0.8T_R$ and combined with the extra $0.1T_R$ of period BC and of T_0A provides one full recirculation of data. The reasoning behind this timing sequence is so that guard bands are formed to protect the measurement period from triggering discrepancies and errors originating from the switching of the AOMs, typically around 200ns. If the measurement period overlaps two recirculation periods, the PRBS pattern will be inconsistent. Consequently, the pattern received by the BERT will not form the PRBS signal anticipated and, even though the data is uncorrupted and the received eye is open, errors will be reported.

One of the side effects of the recirculating loop arises from this method of data acquisition. As the measurement period is a fraction of the entire cycle, as the propagation distance increases the fraction of the overall time devoted to the measurement period diminishes. The result is that a longer period of real time is required to attain the 1×10^9 bits for an error free BER measurement in loop conditions than in a real system.

Although the components under test within the recirculating loop do not control the behaviour of the loop, they do exact an influence on the loop. All components specified for a system, such as filters, amplifiers and the fibre itself have profiles that

deviate from the specified profile due to deviations in manufacturing techniques. Conventional transmission systems employing multiples of the same elements, all with slight deviations from the mean, create an average approximating the profile specified at the end of the transmission span. In contrast, loop based experiments utilise the same element during each recirculation, amplifying the defects. Therefore, fluctuations from the ideal in a singular item used a multiple times will be magnified in the loop rather than single uses of multiple components equalising the spurious effects in conventional systems. This is particularly important with respect to the polarisation dependence of the loop as EDFAs frequently exhibit polarisation dependent gain (PDG) and other components have polarisation dependent losses (PDL), resulting in some polarisation states dominating over others. Using polarisation controllers within the loop can optimises transmission performance by matching the polarisation to that of the dominating state, although this is not conducive to accurate system portrayal. Alternatively a polarisation scrambler can be employed within the loop to maintain the randomness of the light. Increasing the loop length and including multiple fibre spans can alleviate this problem as multiples of the same elements are used, inducing averaging and increasing the propagation distance before the spurious effects generated by the components are seen.

There are other benefits to using a longer loop, such as the loop time becomes long compared to the amplifier recovery times, also there is a reduction in the attenuation induced by the loop equipment and performance statistics become more realistic [124]. On the other hand, shorter loops reduce expenditure by using fewer components, comparisons of experimental equipment can be realised more rapidly and the periodicity of research components of limited availability can be increased. Before deciding on the length of the recirculating loop to be used, the aims of the results gained from the experiment must be considered.

In communication systems, the loss of the fibre should equal the gain of the amplifiers, but in a loop environment the losses of the loop components must also be overcome. It is a straightforward process to measure the losses of components and fibres and the gain of the amplifiers, but it can be difficult to attain a quick measurement of the losses during transmission. Using a monitor tap from the output of the recirculating loop, input to a photodiode on an oscilloscope, allows monitoring of the intensity levels from the loop with respect to time. This can be used to balance the power within the

recirculating loop and can also be used as a quick reference to the number of recirculations undertaken.

4.5.2 • Loop Dispersion

The importance of fibre loss and the dispersion map has been covered in previous chapters and drastically affects the propagation results for recirculating loop experiments. One of the aims of recirculating loop experiments is to exploit the reduced number of components required for an experiment although all items within the loop should remain flexible in order to maximise transmission performance. Figure 4.12 shows the BERs of two 10Gbit/s single channel experiments with different wavelengths around a 99km SMF and DCF fibre loop.

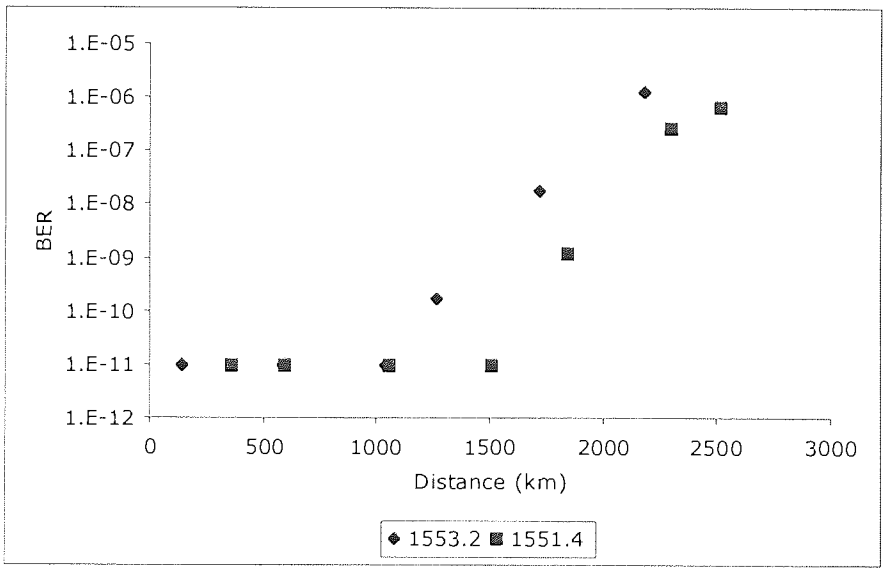

Figure 4.12: BER plotted against propagation distance (km) for two 10Gbit/s single channel recirculating loop experiments over a 99km SMF and DCF map for two wavelengths, 1553.2nm (diamonds) and 1551.4nm (squares)

The fibre map comprised of 16km SMF, 8km DCF, 42km SMF, 8km DCF and 25km SMF. The laser source for both experiments was the PriTel fibre laser tuned to 1553.2nm and 1551.4nm, externally modulated with a 2^{31-1} PRBS pattern as described in Fig. 4.11, albeit without the OTDM. The PriTel was tuned to wavelengths that provided stable operation and the launch power and amplification within the loop was kept constant for both experiments. It is clear that the 1551.4nm outperforms the

longer wavelength, and as all other experimental variables were kept constant, it must be due to the different dispersion each wavelength experiences. Therefore it is necessary to be able to identify the ideal operating wavelength for the loop dispersion. Fig 4.13 shows the apparatus necessary for measuring the dispersion of the recirculating loop. Essentially the layout is that same as the recirculating loop and includes the same components, 3dB coupler, EDFAs, transmission fibre and filters, but without the AOMs.

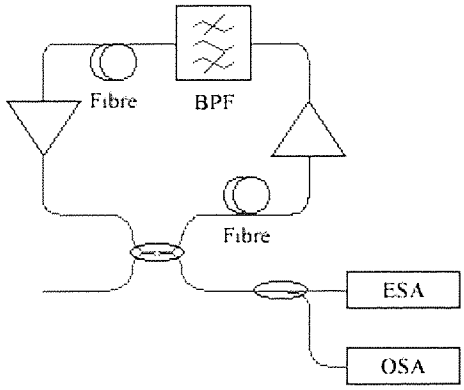

Figure 4.13: Example of the recirculating loop setup for dispersion measurement. Additional elements include the use of a band pass filter (BPF), electrical and optical spectrum analysers (ESA, OSA)

Setting the amplifiers to maximum would cause the loop to lase, with the loop performing the roll of fibre cavity. The output wavelength, controlled by varying the central frequency of the band pass filter, is monitored on the optical spectrum analyser (OSA) and the cavity modes are tracked on the electrical spectrum analyser (ESA). As the wavelength of the laser changes, the propagation time increases due to dispersion, this can be seen as a change in frequency of the harmonics. Monitoring the change of frequency, $\Delta\nu$, frequency, ν, and identifying the mode number, m, provides the change in round trip time $\Delta t = -m\Delta\nu/\nu^2$. Detecting the wavelength change, $\Delta\lambda$, and calculating the cavity length, $L = c/n\Delta\nu$ where n is the refractive index, provides the values necessary for identifying the dispersion, D (ps/(nm.km)). This method not only finds the average dispersion of the fibre, but also includes the dispersion of any component within the loop, although it is susceptible to temperature fluctuations that result in changes in round trip time. Obviously if there are any frequency specific components within the loop, such as gratings, they need to be removed before using this method.

There are a number of terms that are used to describe polarisation effects that occur within a transmission system. The state of polarisation (SOP) of the signal light evolves during propagation and also changes over time. The evolutionary change to the SOP occurs when the fibre experiences a physical change, such as splices, fixed bends or meeting a device. The temporal changes to the SOP occur when the fibre experiences a rise in temperature or a change in pressure. The attenuation exerted on a signal by a component may also have some small polarisation dependence. This polarisation dependent loss (PDL) can cause a problem with a recirculating loop, as the SOP changes after each recirculation and if a component has a high PDL, this unwanted attenuation cannot be optimally minimised.

Another polarisation effect in a recirculating loop utilising EDFAs is polarisation hold burning (PHB) [125]. This occurs when an EDFA is saturated in one polarisation state but not in the orthogonal state. The signal in the originally linearly polarised state will see less gain that the signal in the orthogonal state. This gain difference is small in an individual amplifier, typically around 0.07dB [126] although along a chain of amplifiers, this becomes sizable. PHB causes amplified spontaneous emission (ASE) noise to be built up faster along the polarisation state orthogonal to the signal than along the parallel axis, increasing the effective noise figure of amplifiers along the span [127]. The PHB effect can be minimised by scrambling or modulating the polarisation at the launch end at a rate faster than the EDFA response time of 1/130μs or 7 kHz [126,127].

In perfectly symmetrical optical fibre both orthogonal polarisations have the same group delay. Unfortunately fibres suffer from birefringence (a difference in phase and group velocity of the two modes) cause by intrinsic and extrinsic perturbations, such as imperfections or asymmetry generated during manufacture and also from physical effects on the fibre after production. Delays dependent on the SOP occur due to this randomness of the birefringent axes and it is from this that Polarisation Mode Dispersion (PMD) originates. As PMD is a vast subject, it is not considered in any depth in this thesis although its effect on systems must be considered. Environmental changes such as temperature fluctuations throughout the day or random stress on the

fibre cause the PMD to randomly vary, resulting in an effect that constantly varying. If a pulse was launched down a fibre with equal power on both axes, the PMD would affect each axis differently, resulting in a differential group delay (DGD) at the output, and could result in two pulses. In comparison to PMD, GVD suffers minor fluctuations and can be easily compensated whilst PMD is stochastic in nature. This effect is particularly important when investigating the upgrade of a system using older fibres, which would have suffered greater variations during manufacture than modern fibres, and have greater PMD as a consequence. Secondly, as the bit rate is increased, the system cannot tolerate as much temporal variation in the output due to the smaller bit period.

4.5.4 • Q Value Measurements

The main item of equipment used to quantify the quality of a system is the Bit Error Rate tester. This provides an analysis on each incoming bit and, depending on the voltage threshold, identifies whether it is of the correct value. Another method of quantifying the recovered data is by measuring the quality factor of the received eye diagram. The numerical indicator of this quality factor is termed the Q value. In the absence of a bit error rate analyser and by taking histograms of the eye, a sampling scope can be used to measure the Q value [128] given by,

$$Q = \left(\frac{|\mu_1 - \mu_0|}{\sigma_1 + \sigma_0} \right) \tag{4.1}$$

where $\mu_{1,0}$ is the mean values of the ones and zeros and $\sigma_{1,0}$ is their standard deviation. The Q factor is a unitless quantity expressed as a linear ratio or it can be expressed in decibels as $20 \log (Q)$. When measuring the ones and zeros to attain the Q value, a decision level to separate the two data levels must be decided before taking the histogram. This level can be difficult to determine due when the eye is nearly closed, therefore setting a decision level of 50% between the maximum one and zero level is used for these cases.

The Q factor can be linked to the BER, which is based upon Gaussian pdfs, [129] through the complementary error function given in Matlab as;

$$erfc(x) = \frac{2}{\sqrt{\pi}} \int_x^{\infty} e^{-\alpha^2} d\alpha \tag{4.2}$$

where providing the BER;

$$BER(q) = \frac{1}{2} erfc\left(\frac{q}{\sqrt{2}}\right) \tag{4.3}$$

This function leads to a BER definition based on the Q factor, yielding a BER of 1e-9 for a Q factor of 6. Using this method to predict BER performance can be hazardous. If the BER statistics deviate from the Gaussian, the BER prediction from the Q value would suffer discrepancies from the measurements taken from a BER tester. For example, electrical noise at the decision circuit is not exactly Gaussian in nature although the Gaussian approximation can lead to close estimates [130, 131]. In [132], it was shown that pattern dependence leads the Q factor to underestimate the quality of the data for long pseudorandom data patterns with large margins. Experimentally this effect can avoided by measuring Q values for a number of word lengths.

Ideally, Q values should not be used experimentally, although there is a use for them when taking stringent system measurements alongside conventional BER measurements. For a BER of 10^{-15} at 40Gbit/s, a time of almost 7 hours would be required to obtain enough bits; this duration is extended further when using a recirculating loop where BERs are only measured periodically. Over such a long period of time, experimental apparatus tend to wander or drift around their nominal level due to effects such as temperature or PMD. The solution to this was presented by Bergano et al [133], and involves extrapolating the Q factor from measured BERs at varying decision threshold voltages. The data is then fit to an ideal curve of BER as a function of the threshold voltage given by,

$$BER(V) = \frac{1}{4} erfc\left(\frac{|\mu_1 - V|}{\sigma_1\sqrt{2}}\right) + \frac{1}{4} erfc\left(\frac{|V - \mu_0|}{\sigma_0\sqrt{2}}\right). \tag{4.4}$$

Again, equation 4.4 is an estimation and assumes Gaussian noise statistics and is subject to the limitations of that assumption. As no system BERs are given in this thesis, this technique is given here for completeness.

Q values are frequently used in optical simulations, and discussion regarding these can be found in Chapter 6.

This chapter has described suitable laser sources and modulators for communication experiments up to bit rates of 40Gbit/s. The jitter suppressed DFB used is not suitable for 40Gbit/s operation as it has a frequency limit of 1GHz, and to OTDM this to 40Gbit/s would introduce too much loss in the source. Both EOM and EAMs were introduced with EAM providing a nonlinear response whereas EOMs have a large linear region. The EAM was also found to require lower power RF signal to provide similar extinction to the EOM. For modulating data at 10GHz, the narrower switching window of the EAM may alter the shape of input pulses and it also adds chirp that requires compensation, whereas the broad switching window and low chirp make the EOM ideal for data modulation. The PriTel fibre laser was characterised and provides very narrow pulses. This source was found to have poor stability and frequently requires resynchronisation. Parameters such as it chirp, spectral bandwidth and pulse duration also fluctuate over time. Variations of these parameters do not make it suitable for commercial systems where stability and reliability are paramount, although as a research tool, it narrow pulses are ideally suited for the investigation of solitons and dispersion managed solitons. It was explained how the timing of the recirculating loop and the triggering of components should be conducted, particular the importance of the use of guard bands to prevent errors whilst triggering equipment at the receiver. Finally, the calculation of Q based on the mean and standard distribution was found to be at best, an estimation, due to approximations made on the Gaussian distribution of errors.

Chapter 5

Optical Time Division Demultiplexing Techniques

5.1 • Introduction

In the previous chapter, optical time division multiplexing (OTDM) of the PriTel fibre laser was shown. In this chapter we shall be examining both electronic and optical methods of optically time division demultiplexing (OTDD). OTDM is capable of providing substantially higher transmission data rates than those achievable with electronic multiplexing. In the electrical domain, limitations on the speed of available electronics currently limit multiplexing to data rates of 40Gbit/s in equipment such as the Agilent technologies ParBERT. In the optical domain, where commercially available picosecond pulse sources such as the Calmar Optics and PriTel fibre lasers are obtainable, OTDM-based data transmission is limited by losses in the OTDM, and bit rates up to 320 Gbit/s has been demonstrated [134, 135]. The restrictions on an OTDM based system are placed on the demultiplexing end of the system rather than the multiplexing side. One factor preventing the commercial deployment of these systems is the relatively high cost of the components involved in the transmitter and receiver; in particular the demultiplexing process demands reliable high-speed components. One method of OTDD requires use of singular or cascaded optical modulators and EAMs have been successfully used to OTDD at speeds of 80Gb/s [136] and 160Gb/s [137]. In this chapter 4 x 10Gbit/s OTDD utilising an EAM is shown.

The solutions to the problem of OTDD do not exist solely in the electronic domain, optical interferometer based devices have been used successfully for OTDD [138, 139]. Many different types of interferometers exist, although the all use the principle of generating a phase shift to unbalance the symmetry of the interferometer and allow switching. With the aid of high powers within these switching devices, nonlinear effects such as self-phase modulation (SPM) (Chapter 2) and cross-phase modulation (XPM) (Chapter 3) can be generated and used to disrupt the symmetry to allow

switching. For network purposes, the use of a low cost, bit rate transparent OTDD is clearly appealing. In this chapter we shall examine the principles of the operation of the interferometer with regards to OTDD and experimentally examine the dispersion imbalanced loop mirror (DILM) for this purpose.

5.2 • Conventional OTDD Techniques

Single channel transmission experiments have been performed at Aston University since 1995 and a maximum distance of 16,000km was achieved using dispersion managed soliton techniques at 10 Gbit/s [140], and results of over 10,000km have been reported by other institutions [115]. This data rate has been increased to 40Gbit/s with the use of source explained in 4.4. Using dispersion managed soliton techniques error free transmission performance at 40Gbit/s was possible over 1200km with a SMF/DCF map [122] although this distance was increased by the Oki Electric Industry Company to over 2700km using a multiple dispersion managed profile [142].

A range of demultiplexing methods has been proposed and demonstrated [134,135,143,144] using both optical and electrical methods to demultiplex the incoming signal. The opto-electronic methods mainly utilise the nonlinear response of an EAM (Section 4.2.3) for demultiplexing from 40Gbit/s to 10Gbit/s [135, 143]. When driven at 10GHz, the EAM generates a switching window with a sub 25ps FWHM that allows one in every four pulses to pass and attenuates the other three channels. EAM-based OTDD have also proved successful for demultiplexing at higher bit rates 160Gbit/s, 80Gbit/s [145, 146]. The method adopted for 40Gbit/s can be increased to 80Gbit/s by either the use of polarisation multiplexing or a nonlinear filter [144].

The reason for demultiplexing down to a 10Gbit/s data rate is due to the limitations posed by the electronics on either end of the system, primarily the Bit Error Rate (BER) test set and it ancillary components. The bit error rate test set available comprised of an Anritsu MP1763B PRBS pulse pattern generator and the corresponding Anritsu MP1764B BER detector, both have an electrical bandwidth of 12GHz, suitable for FEC 10Gbit/s transmission analysis, but to slow for operation at 40Gbit/s. True 40Gbit/s BERTS are being investigated although current solutions by companies such as Agilent Technologies, Ando and Anritsu that involve multiplexing

up to 40GHz from 2.5GHz for the Agilent and 12GHz respectively. The aim of the 40Gbit/s to 10Gbit/s demultiplexer is to extract a 10GHz clock from the incoming signal to drive the Modulator and BER detector so that the BER can be measured on each of the four channels. Fig. 5.1 shows the 10GHz electrical output from a 10Gbit/s signal (left) and a 40Gbit/s (right) 2^{31-1} PRBS signal with an even mark to space ratio.

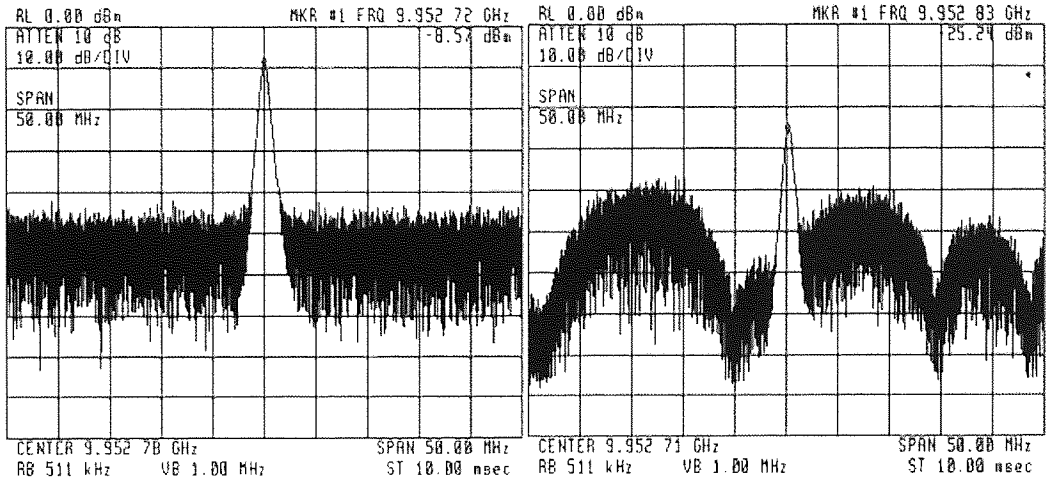

Figure 5.1: The 10GHz electrical output spectrum for a 10Gbit/s (left) and 40Gbit/s (right) 2^{31-1} PRBS back to back optical signal with equal mark to space ratio taken on a 40GHz electrical spectrum analyser

At 10Gbit/s, the 10GHz fundamental is 40dB greater than its sidebands, whereas at 40Gbit/s the 10GHz component is only a harmonic and is only 15dB greater than the surrounding frequency components. Not only does the clock recovery have to tolerate the smaller 10GHz frequency component, it also has to tolerate the phase wander of the incoming signal. Variations in temperature over time can increase or decrease the fibre length in a span, varying the propagation time and changing the frequency. The rate of change of this frequency results in the phase wander.

Fig. 5.2 describes the arrangement of the equipment necessary for a 4 x 10Gbit/s OTDM transmission experiment, including a simplified version of 40Gbit/s transmitter shown in Fig. 4.7 and the recirculating loop from Fig. 4.10. As the operation of the 40Gbit/s source and the recirculating loop has been previously mentioned, we will examine the OTDD.

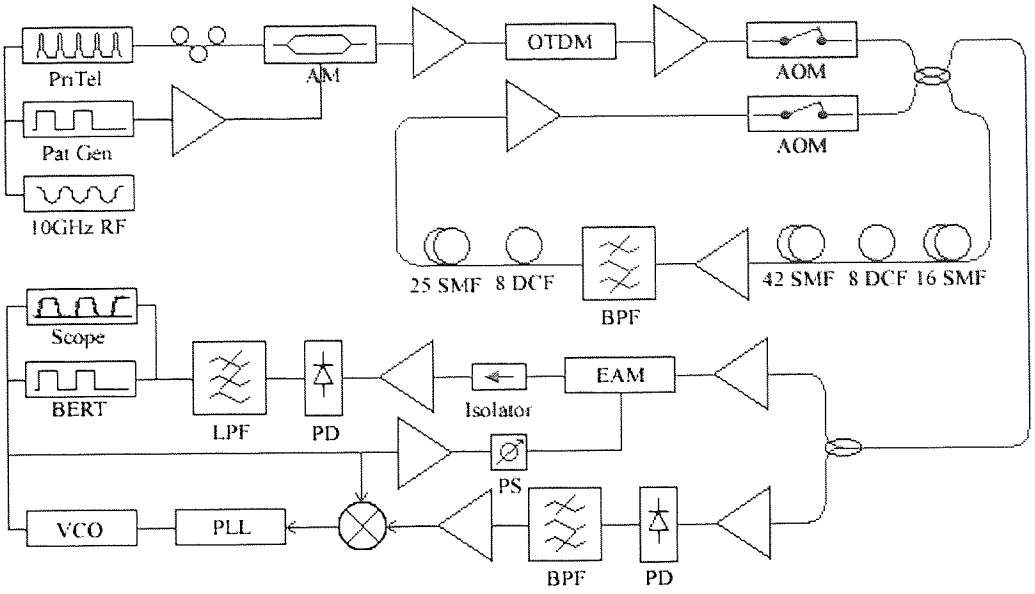

Figure 5.2: Schematic showing the experimental arrangement for a 40Gbit/s transmission system utilising a 40Gbit/s source, recirculating loop for propagation and a 12GHz BERT set for data generation and error detection. The fibre loop shows an SMF, DCF fibre map.

The OTDD is split into two subsections, clock recovery and error detection. The output of the recirculating loop is split via a 3dB coupler, providing a copy of the propagated signal to both subsections. The clock recovery circuitry is fundamentally a feedback design comprising of a 10GHz mixer, a 10GHz phase locked loop (PLL) and a 10GHz voltage controlled oscillator (VCO). The input to the clock recovery circuit is amplified to counteract the loss of the coupler before the input and to offset any remaining losses from the loop. The optical signal is then converted into an electrical signal by a photodiode, filtered via a Q filter and amplified by a 10GHz narrowband amplifier before it is mixed with the 10GHz output of the VCO. The resultant frequency from the mixer is sent into the phase locked loop, which drives the VCO. The frequency of the VCO is close to that of the data signal provided that the difference between the signals does not exceed the range of the PLL. The VCO produces a 10GHz clock output that is then fed back into the mixer and also to any of the error detection equipment that requires a 10GHz trigger. Unlike the transmitter, the clock recovery subsection is designed to isolate the 10GHz component, and as such narrow bandwidth amplification can be used. This provides greater gain for the 10GHz harmonic than the other frequency components, effectively attenuating unwanted signals and improving the contrast. Also, if the filter bandwidth is not broad enough to

encompass the range of the drifting 10GHz harmonic, it may isolate only sidebands, locking the phase lock loop to the central frequency of the filter, not the incoming signal.

On the error detection path from the 3dB coupler, the signal is amplified before propagating through the EAM. The modulator is driven by the recovered 25dBm ($4V_{p-p}$) 10GHz clock and positioned correctly by adjusting the DC bias, it produces a switching window sufficiently narrow enough to allow one of the 4 OTDM channels to pass whilst attenuating the remaining channels. Altering the phase of 10GHz recovered clock input to the modulator causes the switching window to move in time domain, allowing the selection of each of the 4 OTDM channels for error detection. The OTDD signal propagates through an isolator to prevent back reflections into the EAM and is amplified to offset the 7dB insertion loss of the EAM before being converted to an electrical signal by the 10GHz photodiode. A 5GHz low pass filter before the error detector removes the higher frequency components, opening the eye diagram. Not only this, when using directly modulated lasers the relaxation oscillations can be stripped by the filter, as their frequency is normally twice that of the bit rate, preventing eye closure.

Fig 5.3 gives examples of this broadening as it compares the 10Gbit/s eye after the EAM, viewed using a 32GHz photodiode, and the 10GHz electrical eye input to the BERT.

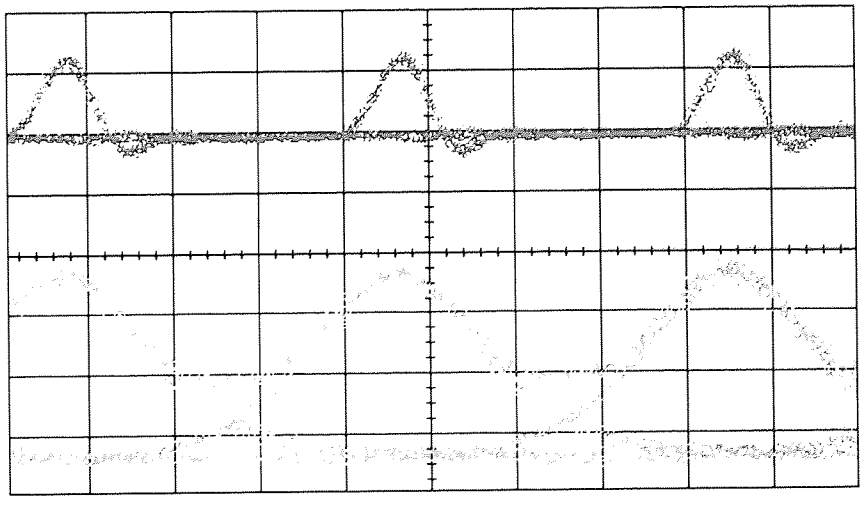

Figure 5.3: The recovered eye diagrams for a 10Gbit/s optical signal (top) and a 10GHz electrical signal (bottom) after demultiplexing from 40Gbit/s. The scale on the x-axis is 25ps/div

The electrical eye is a lot broader than that of the optical eye, partly due to the lower bandwidth of the 10GHz diode, but additional broadening occurs due to the presence of the 5GHz low pass filter. Due to the terminal damage sustained by the EAM in an experiment, 40Gbit/s BER measurements on the EAM based OTDM were not obtainable.

5.3 • Fibre Interferometers

Interferometers are one of numerous devices used in communications systems as the different designs demonstrate a number of interesting properties. When power levels inside these devices are large enough to generate nonlinear effects such as SPM and XPM they can be used for switching applications [147]. Fig. 5.4 exhibits two such interferometers, the nonlinear fibre loop mirror (left) and the Mach-Zehnder (right), both of which utilise nonlinear phase shifts for optical switching, albeit only a SPM induces phase shift for the Mach-Zehnder.

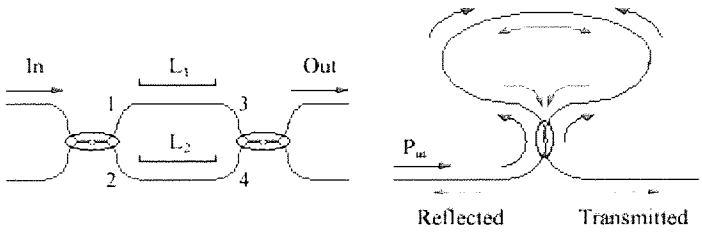

Figure 5.4: Schematic illustration of two types of fibre interferometers. The left diagram depicts a Mach-Zehnder interferometer with input and output ports. The right diagram shows a fibre loop mirror with input/reflected and the transmitted ports

5.3.1 • Mach-Zehnder Interferometers

The Mach-Zehnder interferometer consists of two couplers with the output ports of the first being connected to the input ports of the second coupler. When a signal propagates through port one of the coupler the signal is split and, if the path lengths are different, the two signals acquire different phase shifts before they mix at the coupler. As the two signals propagate over two separate paths, there is no XPM induced phase shift between the two couplers.

Consider a coupler with input ports 1, 2 and output ports 3, 4 and a coupling ratio α_1 can be described by [148];

$$A_3 = \sqrt{\alpha}A_1 + i\sqrt{1-\alpha}A_2, \tag{5.3}$$

$$A_4 = i\sqrt{1-\alpha}A_1 + \sqrt{\alpha}A_2. \tag{5.4}$$

Now we can expand the situation to consider the pair of couplers in Fig. 5.1 with coupling ratios α_1 and α_2 separated by lengths L_1 and L_2. When there is only light input to one arm of coupler one, the outputs can be described by;

$$A_1 = \sqrt{\alpha}_1 A_{in}, \tag{5.5}$$

$$A_2 = i\sqrt{1-\alpha_1}A_{in}, \tag{5.6}$$

then after propagating along the two different paths, the signals acquire linear and nonlinear phase shifts. We can then put the equations in the form of $A(z) = Ae^{i\phi}$;

$$A_3 = \sqrt{\alpha}_1 A_{in} \exp\left[i\beta_1 L_1 + i\alpha_1\gamma|A_{in}|^2 L_1\right], \tag{5.7}$$

$$A_4 = i\sqrt{1-\alpha}_1 A_{in} \exp\left[i\beta_2 L_2 + i(1-\alpha_1)\gamma|A_{in}|^2 L_2\right], \tag{5.8}$$

where the linear phase shift is, $\phi_L = \beta L$, the nonlinear phase shift due to SPM is, $\phi_{NL} = \gamma PL$ and the power is modulus squared of the electric field, $P = |A|^2$. The output field of one port from coupler two can be attained using the above equations as the inputs for the coupler equations;

$$A_{out} = \sqrt{\alpha_2}A_3 + i\sqrt{1-\alpha_2}A_4, \tag{5.9}$$

$$A_{out} = A_{in}e^{i\phi}\left[\sqrt{\alpha_1\alpha_2} + \sqrt{(1-\alpha_1)(1-\alpha_2)}\right]. \tag{5.10}$$

The power transmitted can then be converted from the electric field providing;

$$P_{out} = P_{in}[\alpha_1\alpha_2 + (1-\alpha_1)(1-\alpha_2) - 2[\alpha_1\alpha_2(1-\alpha_1)(1-\alpha_2)]^{1/2}\cos(\phi_L + \phi_{NL}), \tag{5.11}$$

where;

$$\phi_L = \beta_1 L_1 + \beta_2 L_2, \tag{5.12}$$

$$\phi_{NL} = \gamma P_{in}[\alpha_1 L_1 - (1-\alpha_1)L_2]. \tag{5.13}$$

Equation (5.13) can be simplified by using two 3dB couplers, i.e. $\alpha_1 = \alpha_2 = 0.5$;

$$P_{out} = \frac{P_{in}}{2}[1 - \cos(\phi_L + \phi_{NL})]. \tag{5.14}$$

For this case, the nonlinear phase shift is null if $L_1 = L_2$ also as the linear phase shift is frequency dependent, this device can be used as a filter. Also, it is clear that the output power is a sinusoidal function dependent on the total phase shift. Depending on this

phase shift, the output power will be switched from one output port to the other, with a phase shift of π switching all the output power from one port to the other [149].

The result of equation 5.14 can be seen in Fig. 5.5 where the Output Power (W) is plotted as a function of Input Power (W) for various arm lengths, where $\alpha_1 = \alpha_2 = 0.5$, $\gamma = 1.6W^{-1}km^{-1}$, $\beta_1 = 2.04e^{-11}ps^2/nm$, $\beta_2 = 2.04e^{-11}ps^2/nm$ and $L_1 = 1km$. L_2 was initially set for 1km and decreased by 0.2km.

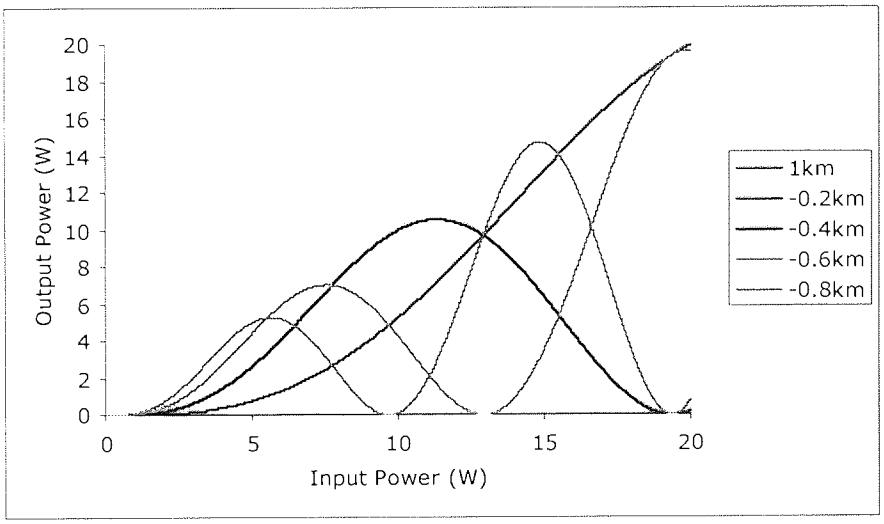

Figure 5.5: Output Power (W) against Input Power (W) for a Mach Zehnder interferometer with equal 3dB couplers and varying L_2

It can be seen that with an increase in the difference between arm lengths L_1 and L_2 that the input power required to generate the π phase shift reduces. This characteristic is dependent on the percentage difference between L_1 and L_2 and not the length of the fibre, for example, the L_1 = 1km and L_2 = 0.9km or 1.1km switching function is the same as L_1 = 2km and L_2 = 1.8km or 2.2km. When both arms are of equal length, the light is output from the opposite port. Unfortunately the Mach Zehnder interferometer is sensitive to environmental fluctuations as any environmental effect that results in a change in phase along one of the arms disrupts the output.

5.3.2 • Fibre Loop Mirrors

The fibre loop mirror, also known as the Sagnac interferometer, works on a similar principal to the Mach Zehnder interferometer and comprises of a fibre coupler with a

long length of fibre connecting two output ports to form a loop. This time the coupler at the base of the loop acts as both the input and output coupler in the Mach Zehnder, therefore $\alpha_1 = \alpha_2$. Light enters from the input port and is split along both arms of the loop and (assuming uniform fibre) pass each other at the mid-point of the loop. As the fractured signals propagate along the same path, not only is SPM involved, but also XPM will occur.

With only light induced into the input, the forwards and backwards propagating light can be described using the coupler equations 5.3 and 5.4 giving;

$$A_f = \sqrt{\alpha} A_{in}, \tag{5.15}$$

$$A_b = i\sqrt{1-\alpha} A_{in}, \tag{5.16}$$

with the backward field attaining a $\pi/2$ phase shift compared to the forwards field. After propagating around the loop, with both fields crossing and the mid-point, and attain a linear and a nonlinear phase shift, resulting in the fields at the coupler;

$$A'_f = A_f \exp\left[i\beta L + i\gamma\left(\left|A_f\right|^2 + 2\left|A_b\right|^2\right)L\right], \tag{5.17}$$

$$A'_b = A_b \exp\left[i\beta L + i\gamma\left(\left|A_b\right|^2 + 2\left|A_f\right|^2\right)L\right]. \tag{5.18}$$

The transmitted output can be given by [150.151];

$$P_{out} = P_{in}\left(1 - 2\alpha(1-\alpha)\left[1 + \cos\left(\left[1-2\alpha\right]\gamma P_0 L\right)\right]\right). \tag{5.19}$$

There is no linear phase shift due to its exact cancellation; the only phase remaining is the intensity dependent nonlinear phase. Depending on the phase of the counter-propagating optical beams, the light will either be transmitted or reflected. If there is no loss or gain imbalance in between the arms and a 3dB coupler is used, the loop act like a mirror; with all of the light being reflected out of the input port. In order to use this as a switching device, the symmetry of the loop mirror must be broken.

Many methods exist for breaking the symmetry of the loop. Using a non-3dB coupler effects the power in the forwards and backwards direction, generating different nonlinearity and altering the nonlinear phase for each path, although this changes the contrast ratio at the outputs [152]. This can also be seen in Fig 5.6 where equation 5.19 has been solved for various coupling ratios. Here, L = 2.0km, γ= 1.6W^{-1}km^{-1}, and α= 0.1, 0.2, 0.3, 0.4 and 0.5.

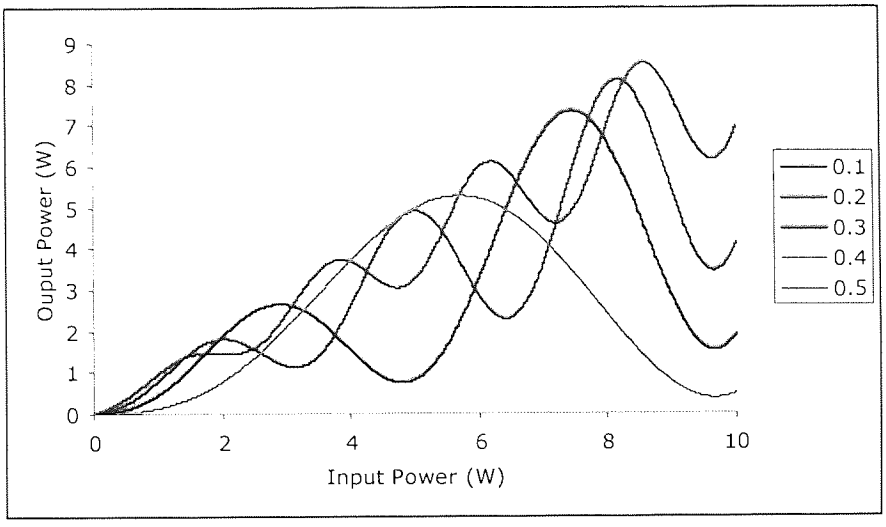

Figure 5.6: Output Power (W) against Input Power (W) for a Sagnac interferometer with a 2.0km loop and varying α

It can be clearly seen that the contrast ratio is improved as coupling ratio tends to 0.5, but as the power difference between the clockwise and counter clockwise signals is smaller, a greater input power is required to generate the π phase shift necessary for switching.

The result of changing the fibre length in equation 5.19 can be seen in Fig. 5.7 where the Output Power (W) is plotted as a function of Input Power (W) where $\alpha = 0.4$, $\gamma = 1.6\text{W}^{-1}\text{km}^{-1}$, and $L = 0.1\text{km}$, 0.5km, 1.0km, 2.0km and 4.0km.

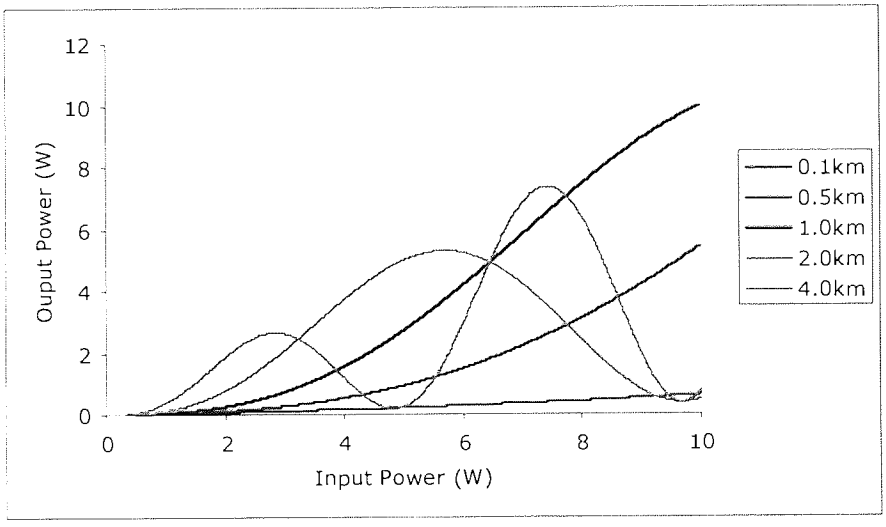

Figure 5.7: Output Power (W) against Input Power (W) for a Sagnac interferometer with a 3dB coupler and varying loop length L

The power required to induce the π phase shift necessary for switching is dependent on the fibre length. For the 4.0km loop, an input power of 2.85W is required and for the 2.0km loop the required power has doubled to 5.70W, as the increase in power is required to compensate for the loss in length. For a fibre of length 500m, a power of 22.8W is required, clearly this is becoming impractical for a system and a longer length of fibre (or a fibre with smaller effective are) would be more practical. Like the Mach Zehnder, any temporary environmental effects such as vibrations, that adjusts the phase of one side of the loop a not the other, results in noise at the output or a reduction in the contrast ratio.

Introducing an amplifier into one arm of the loop generates asymmetry even in the presence of a 50:50 coupler at the input that maintains the contrast ratio [153]. Introducing a pump probe that propagates with a signal in one direction can be used to induce switching within a Sagnac loop. The pump signal interacts with one of the counter-propagating pulse and generates a XPM-induced phase shift, whilst the other signal component experiences no phase shift [154].

Another introduction can be that of a nonlinear element, offset from the centre, in order to disrupt the nonlinearity of one signal with respect to the other in time. With such a device embedded within the loop, the length of fibre necessary for nonlinearity can be reduced. A semiconductor optical amplifier (SOA) is used passively for this purpose in a semiconductor amplifier in a loop mirrors (SLALOMs) [155], and actively in terahertz optical asymmetric demultiplexers (TOADs) [138, 139]. In the TOAD a pump signal is coupled into the loop in order to saturate the amplifier, changing the refractive index, resulting in any signal pulses entering the SOA before it recovers seeing a different phase shift to the other signal pulses. This can be used OTDD if the pump pulse is at a clock bit rate. Another method is by changing the dispersion in one arm with respect to the other in order to unbalance the loop [156]. Such devices are known as dispersion imbalance loop mirrors (DILMs).

5.4 • Dispersion Imbalanced Loop Mirrors

Dispersion imbalanced loop mirrors work on the same principles as the conventional 3dB coupled fibre loop mirror, with the exception that unbalanced dispersion fibre is used within the loop to break the symmetry of the device. By creating a loop consisting

of two fibre sections, one with a low amount of dispersion and the other with a much greater amount of dispersion an asymmetric map is obtained. This setup can be seen in Fig. 5.8 where the longer length of low dispersion fibre is on the clockwise arm and the shorter high dispersion fibre is on the counter-clockwise arm.

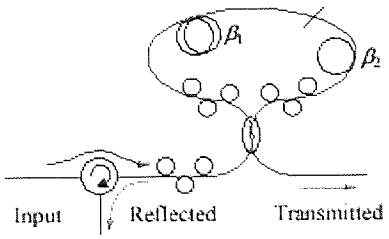

Figure 5.8: Illustration of the experimental setup used for characterisation of the DILM transmission and reflection against input power.

The signal propagating in the counter-clockwise direction disperses quickly and then remains broad in the second segment, inducing little nonlinear phase shift. The pulse in propagating clockwise suffers little dispersion and maintains it's shape, and as such it acquires a large amount of nonlinear phase shift that is both intensity dependent and proportional to the fibre length. On return back to the coupler ports, both pulses have experienced the same dispersion effects but have generated different nonlinear phase shifts. CW signals are not affected by dispersion, so the CW components propagating in the clockwise and counter-clockwise direction see the same phase shift and, like a conventional $\alpha = 0.5$ Sagnac interferometer, are reflected. This can be used to reject unwanted CW signals in communication systems, such as ASE, whilst allowing the pulse to propagate.

Fig. 5.8 also includes the additional components necessary for the experimental characterisation and operation of a DILM. The input to the DILM consisted of a circulator, to monitor the reflected signal and a polarisation controller to set the input polarisation. The DILM consisted of 2020m of dispersion-shifted fibre (DSF), 372m of dispersion-compensating fibre (DCF), a balanced 50:50 coupler and two polarisation controllers within each arm of the interferometer. The DSF provided a zero-dispersion wavelength at 1556.7nm and the DCF possessed a dispersion of –92.4ps/nm/km at 1550nm. For characterisation, an input signal at the desired bit rate is launched through the circulator and through a polarisation controller into the DILM. Initially a signal of low optical power is launched into the DILM to maintain linearity (reflection) and

prevent the phase shift necessary for transmission. The polarisation controllers within the DILM are set to balance the fibre loop and minimise the transmission power (or maximise the reflected power), ensuring correct linear operation. Once the loop is balanced, the power is increased in order to generate the nonlinear phase shift and switch the input signal out of the transmission path, at this point the input polarisation controller is aligned so that signal entering the loop is in the optimum polarisation state for transmission. The switching characteristic of the DILM, presented in Fig. 5.9 was generated using this method.

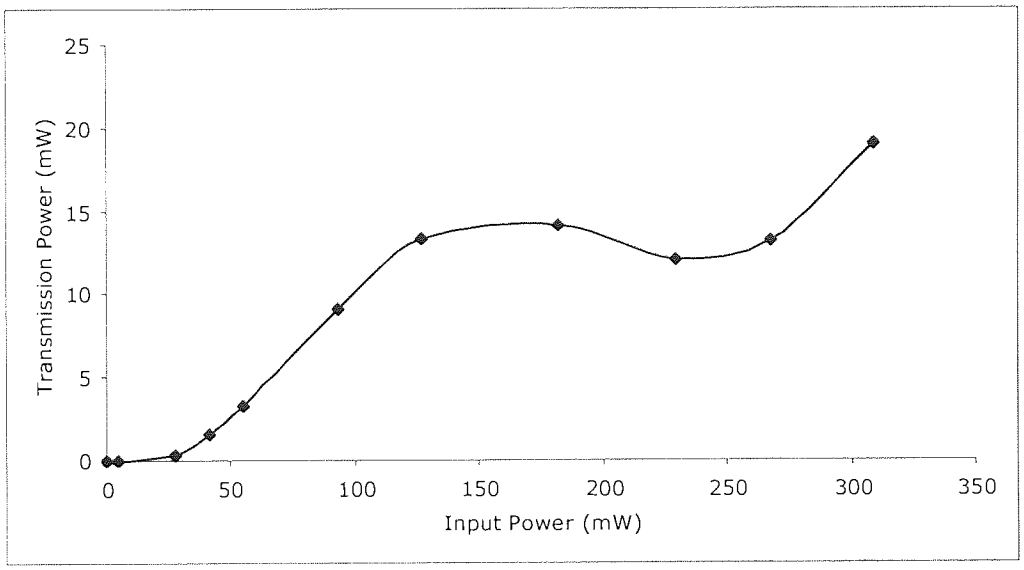

Figure 5.9: The switching characteristic, input power (mW) against transmission power (mW), of the DILM used as a nonlinear filter within the 40Gbit/s to 10Gbit/s demultiplexer

Clearly the resultant switching profile is nonlinear, any input less than 17dBm is attenuated to 3dBm, whereas larger signals of 21dBm are attenuated to 11dBm. The DILM acts similarly to a Saturable absorber (SA). SAs are semiconductor-based devices that have a high loss for a signal below its saturation threshold and a low loss for signals greater that its saturation threshold. These are often multi-quantum-well (MQW) devices that work in reflection and would require a circulator, similar to the DILM reflection monitor. When a SA is subjected to a high input signal and is in its transparent state, the loss is the consistent for all powers beyond this level. Therefore a SA would increase the contrast ratio between a '0' and a '1', but it would not reduce any intensity noise on the '1's. The DILM similarly increase the contrast ratio by

reflecting the CW and lower power components and transmitting than the higher power ones, but also the DILM would provide reduce some intensity noise. For the DILM described in Fig 5.6 an input signal was noise on the '1's between 120mW and 220mW (3dB of amplitude jitter) would be transmitted with only 1dB of jitter.

5.5 • DILM Enhanced Demultiplexing

Due to the damage sustained by the EAM, another method of OTDD was required to demultiplexer down from 40Gbit/s to 10Gbit/s. $LinNbO_3$-based Mach-Zehnder electro-optic modulators (EOM) are used to encode the data on the source before OTDM occurs, although their switching window (around 45ps depending on bias conditions and drive voltages) is much greater than the 40Gbit/s bit window. EAMs are now more easily available but are sensitive and require additional thermal stabilisation circuitry. Also EAMs suffer catastrophic optical damage when even signals at moderate input powers, (10mW peak power, 1dBm average) are input. Conversely, the EOM can sustain greater input powers (10dBm) and impart little chirp on the data. Directly replacing the EAM with an EOM would result in impartial demultiplexing. As the switching window of the EOM is greater than the bit window one channel will propagate with minimal attenuation whilst one or more of the others will suffer greater attenuation but would still be detectable at the receiver, resulting in noise. Using a DILM as a nonlinear filter and exploiting its SA like properties could satisfy the demultiplexing demands of a 40Gbit/s OTDD employing a $LiNbO_3$ EOM. The fast response of a DILM can be used to offset the slower operation of the modulator to provide successful demultiplexing of optical time division multiplexed data. This section examines the use of a nonlinear filter to enhance the OTDD performance of a $LiNbO_3$ EOM.

The experimental configuration depicting the use of a DILM with a $LiNbO_3$ amplitude modulator to demultiplex to 10Gbit/s from a 40Gbit/s OTDM source is shown in Fig. 5.10. The experimental layout is very similar to the EAM based demultiplexer show in Fig. 5.2, with the EAM being replaced by a $LiNbO_3$ EOM (AM) and the DILM. The PriTel UOC-3 wavelength tuneable mode-locked fibre laser source provided pulses with a FWHM of 2.7ps at the operating wavelength of 1550nm and a 10Gbit/s 2^{31}-1

PRBS data pattern was imposed on the pulse stream by a Lithium Niobate amplitude modulator.

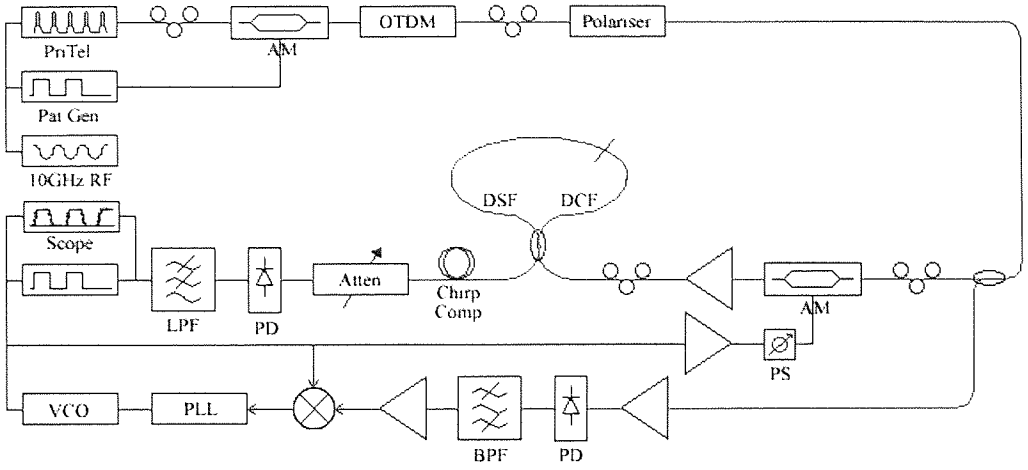

Figure 5.10: Schematic diagram of the experimental configuration showing the 40Gbit/s data source and the 40Gbit/s to 10Gbit/s demultiplexer

The resultant bit stream was optically time division multiplexed up to a bit rate of 40Gbit/s using the fibre delay line multiplexer described in section 4.4. In the multiplexer, the relative delay and amplitude of the four 10Gbit/s bit streams was equalised, the latter with the aid of the output polariser, which also bestowed a single polarisation state on the 40Gbit/s signal. At this point, a fraction of the optical output was split from the data stream and converted into an electrical signal for the clock recovery unit. The 10Gbit/s clock recovery unit operated on the electrical phase-locked loop feedback principle disclosed in section 5.2. The recovered 10GHz clock signal was then used to drive the demultiplexing modulator, via a phase shifter, and also to trigger the bit-error rate (BER) measurement equipment. The other branch of the 40Gbit/s data propagated through a polarisation controller, to reduce the PDL of the modulator, and was then demultiplexed to 10Gbit/s by a $LiNbO_3$ modulator. The modulator was driven by a sinusoidal signal with a frequency of 10GHz and each 10Gbit/s channel was selected by varying the phase of that signal. The resultant signal was subsequently transmitted through a narrowband filter and amplified by an EDFA, broadening the pulse FWHM to 6ps before being inputting into the DILM based nonlinear filter.

The nonlinear filter was based around the DILM described in section 5.4, and comprised of 2020m of dispersion-shifted fibre (DSF), 372m of dispersion-

compensating fibre (DCF). The characteristic of the DILM can be seen in Fig. 5.9. 2km of conventional single-mode fibre (SMF) was used after the DILM, to compensate for the pulse chirp imposed by the DILM. A circulator was used on the input for the initial characterisation, but in this experiment it was removed as the Isolators within the EDFA attenuated signals rejected by the DILM and prevented the light re-entering the EOM.

After amplification, the signal power for the channel designated for demultiplexing will have the power necessary to be transmitted by the DILM and the attenuated channels will be rejected. Initially the 40Gbit/s OTDM signal was demultiplexed without the aid of the nonlinear filter. Even at the optimal driving conditions for the $LiNbO_3$ modulator, error free demultiplexing was not achievable, and for this case the best BER was at a level of $4.3x10^{-8}$. The high error rate is a result of the wide switching window of the highly linear $LiNbO_3$ modulator, which does not fully suppress the adjacent OTDM channels. However, error-free performance was easily achieved by including the nonlinear filter.

By examining the eye diagrams taken without (upper) and with the filter (lower) in Fig. 5.11, the improvement in signal quality can be readily seen. Both screen shots show the received optical eye on a 32GHz photodiode above and the electrical eye, broadened by the 5GHz low pass filter, below. Contrasting the optical eyes for the selected OTDM channel on the fast diode, they are both clear and open, although they have different dimensions due to the chirp induced and compensated by the filter. A comparison of the two optical eyes shows that without the filter adjacent TDM channels have not been fully suppressed by the modulator whereas when the filter is used, the adjacent TDM channels are fully suppressed. The resulting electrical eye viewed by the BER tester without the filter is more closed than the nonlinear filtered electrical eye.

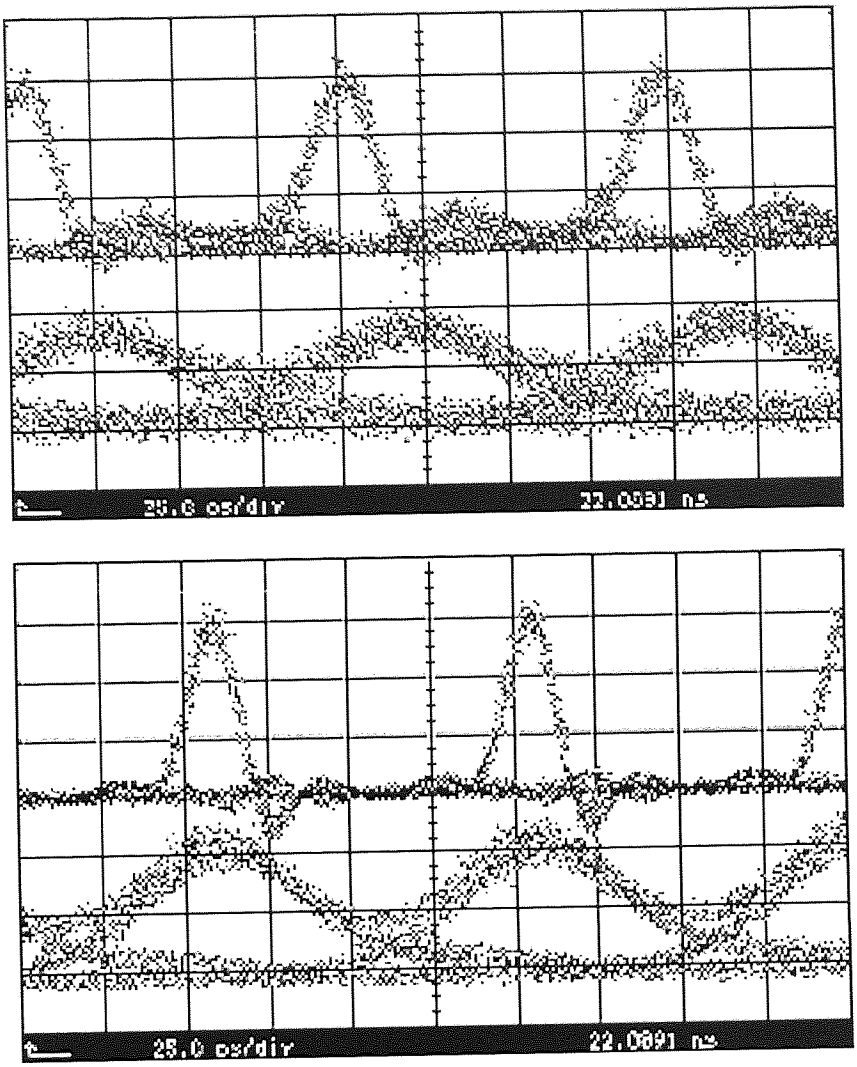

Figure 5.11: Recovered eye diagrams for the transmission with solely a LiNbO3 (above) and with the aid of the nonlinear filter (below). Scale 25ps/div. The received power for the unfiltered eye was –7.6dBm and –0.6dBm for the filtered case.

The BER measurements, presented in Fig. 5.12, show that the BER is dramatically reduced when the nonlinear filter is introduced, particularly for the 'worst-case' channel (the upper line in each group of lines). In addition to that, there is substantial difference in the unfiltered BERs for each OTDM channel, whereas the filtered results follow the same slope and are tightly grouped together. Utilising the filter attenuates the signal due to the intrinsic loss of the DILM (measured at 7dBm). This is easily outweighed by the gained suppression of parasitic signal components as the eye diagrams show filter superiority even when incorporating the DILM loss. For example, the worst case unfiltered channel has a BER of $1x10^{-7}$ at a power of 2dBm the equivalent BER is

obtained at a power of −10dBm for the worst case filtered channel, a difference of 12dB. As a result, successful demultiplexing of 4 x 10Gbit/s signals is achieved when using the filter.

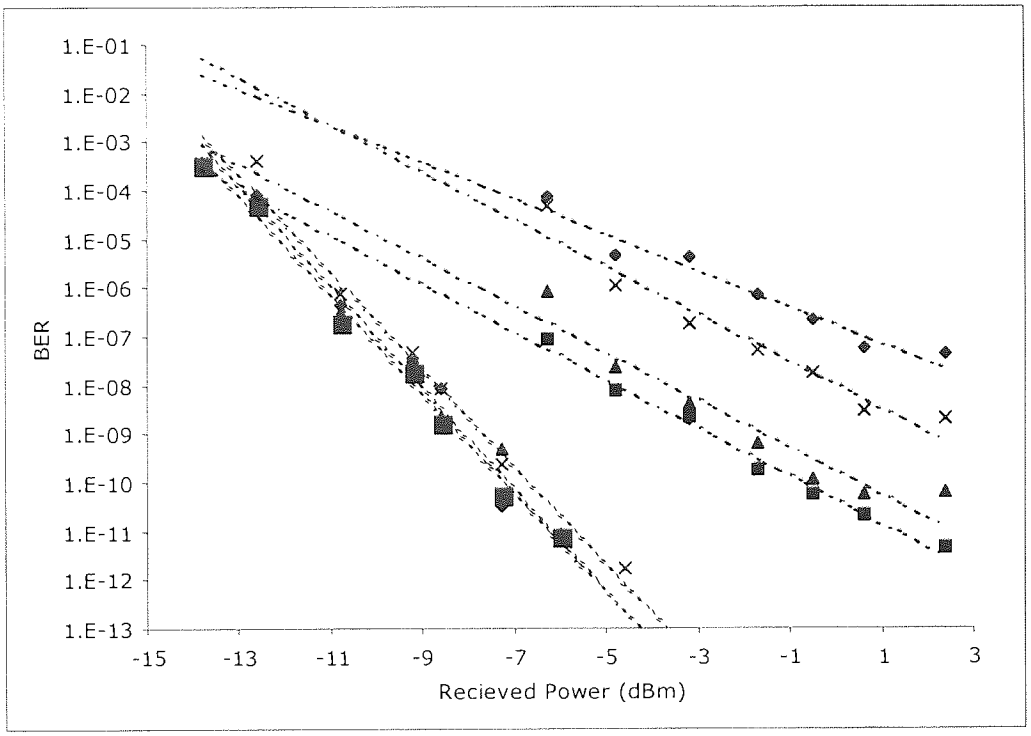

Figure 5.12: BER as a function of received power with and without the nonlinear filter. The upper lines in each group show the 'worst-case' channels without (red) and with (green) the DILM

Transmission over span of 104 km of SMF and DCF, setup similar to that shown in Fig. 5.2, and comprising of 17km SMF, 8km DCF, 44km SMF, 8km DCF and 27km SMF. Transmission without the nonlinear filter produced no recoverable data, whereas using the filter provided BERs of $1x10^{-10}$ for all four DILM channels. Unfortunately due to a problem with one of the AOMs and a lack of time before the research changed direction, the recirculating loop was not available when working with the DILM and no long distance transmission results were taken.

Clearly using the DILM with the EOM is superior than using the EOM alone, although no direct comparison of the EOM and DILM based demultiplexer was compared with that of the EAM. When working with the DILM, stability issues were of a prime concern, large changes in noise could affect the resultant BER and it is not clear whether the device would be suitable for a system. To use a DILM in a commercial

system it would need to be maintained at a constant temperature in a vibration and soundproof chamber, even thought the EOM would not require this. Fluctuation in span loss would not adversely affect the required performance of an EAM, as when used for OTDD it has no intensity dependent profile, whereas the output DILM has a nonlinear response with respect to input power. One large benefit frequently offered by advocates of NOLMs is their low cost, as they require only a few kilometres of fibre. This is misleading, as to operate the DILM, large input powers are required, hence the need of an expensive high-powered optical amplifier. For the purpose proposed, the DILM was ideal as an EAM was not available whereas there was the fibre, amplifier and EOM, resulting in an EOM based demultiplexer that was able to successfully demultiplex from 40Gbit/s to 10Gbit/s. The filtering provided by the DILM could also be used with an EAM in a similar method described here, but to demultiplex at higher data rates

5.6 • Summary

In summary, methods for OTDD of a 40Gbit/s data signal down to a single 10Gbit/s channel were explored. All the OTDD methods explored required the use of a 10GHz phase locked loop which operated in feedback by mixing the recovered clock with the filtered 10GHz harmonic of the 40Gbit/s data. The PLL recovered clock was used to trigger devices such as BER equipment and sampling scopes. The EAM based 40Gbit/s OTDD also used this recovered clock. By adjusting the phase of the incoming clock with respect to the incoming data, isolation of a single channel was achieved. The EAM was a power sensitive device that eventually suffered catastrophic damage when it was exposed to the ASE of and amplifier of a moderately large input power. Due to the demise of the EAM, only the demultiplexed eye diagrams from the EAM OTDD were shown.

Both the Mach-Zehnder and the Sagnac nonlinear interferometeric devices were investigated. The equations of operation for both devices were found to be similar, although the nonlinear phase shift in the Sagnac NOLM is also dependent on XPM. To generate switching in the Mach-Zehnder the symmetry can be broken by varying the length of one arm with respect to the other arm. The greater this difference the less power is required to obtain the first π phase shift. For the Sagnac interferometer, the

symmetry can be broken by varying the loss or gain on one side with respect to the other or by using a non-3dB coupler. It was found that the closer the coupling coefficient progressed to 0.5, the greater the contrast ratio between the transmitted and reflected ports became. This was at the expense of the power required to obtain the π phase shift, as the closer the coupling coefficient came to 0.5, the greater was the power required for switching. These devices are not bit rate dependent and are only limited by the speed of the nonlinear interaction.

The DILM works on the same principles as the Sagnac interferometer but the loop is comprised from two fibres, one of low dispersion and the other of high dispersion. In the DILM one pulse first experiences little broadening and a large nonlinear interaction then intense broadening and little nonlinear interaction, conversely the opposite pulse experiences intense broadening and small nonlinear interaction followed by little broadening and little nonlinear interaction. It is the phase difference between these two pulses that breaks the symmetry of the device. CW components are not subject to dispersion, and so the symmetry of the loop mirror remains unbroken for them. The experimental characteristic of the DILM used for nonlinear filtering was obtained and method of operation was described.

As no EAM was available for OTDD, an OTDD comprising of a $LiNbO_3$ modulator and DILM was constructed and successfully used to demultiplex 40Gbit/s to 10Gbit/s. The OTDD used the same PLL based clock recovery but the EAM was replaced by a EOM and a DILM. The DILM was used as a nonlinear filter to suppress the adjacent channels that were not fully attenuated by the EOM. Transmission over 100km was permitted with the aid of the filter, although when the DILM was removed even transmission back-to-back was not possible.

Chapter 6

WDM System Simulation

6.1 • Introduction

In this section transmission at 40Gb/s with return-to-zero (RZ), chirped-return-to-zero (CRZ) and non-return-to-zero (NRZ) data modulation formats over 600km of SMF with an amplifier separation of 100-km will be investigated by the use of computer simulation. The first section of this chapter examines the principles behind computer-based simulation and the major features of the simulation tool used. Initially the propagation effects of a single 40Gbit/s channel are studied and it is found that the dispersion managed soliton approach is not suitable for terrestrial systems that comprise of long amplifier spans with fibres of high local dispersions. The model is then expanded to incorporate 16 x 40Gb/s channel for WDM transmission with a channel separation of 100GHz. This introduces additional problems such as need for residual dispersion compensation and the addition of more nonlinear interactions. Due to the bandwidths constraints imposed by the ITU grid, the optima found for the single channel case are no longer sustainable and the system is forced to adopt pulses with a greater width. Finally, to overcome the limitation of the ITU grid, the channel spacing is varied between 50GHz and 200GHz. This increases the effect of residual dispersion whilst decreasing the interchannel interaction.

6.2 • Simulation Design

Laboratory prototypes of potential systems are an obvious pre-requisite before installing or upgrading any communication link as it provides the opportunity to test all the components under a variety of different environments locally. Unfortunately by their very nature, laboratory experiments are constrained by the availability of physical components and the time that is required to construct the experiment and vary elements. In the modern world, where increasing emphasis is placed on productivity

and turnover, the ability to quickly generate accurate mathematical models of systems in order to reduce the time to market is of increasing importance. Mathematical simulations are now commonplace in the industry and are used in parallel with laboratory and field experiments. Simulating experiments first provides an opportunity to reduce the seemingly endless permutations of fibre and components, guiding the experimentalist and eliminating the need for extraneous work. Not only this, but simulations also offer the ability to highlight the effects of selective system attributes without having to worry about physical implication. By removing or adding the relevant components from equations, simulations can examine the contribution that any element has on a system.

The aim of the communication simulation is to simulate the propagation of modulated signal along a span of fibre and through a variety of electrical and optical components. The simulation aims to model the properties of hardware in the system, without the requirements of the use of hardware. As a signal propagates it encounters effects that are both deterministic and stochastic, the simulation must be able handle both. Deterministic signals can be described by a function in time as an independent variable, conversely stochastic signals have uncertainty about their current value in time. A filter is one example of a deterministic component, in that it attenuates the incoming signal by a given mathematical function, whereas the amplified spontaneous emission noise of an amplifier would be random in time. Random numbers are generated using recursive formulas that require a seed number to start the random generation process. Each seed will generate a set of pseudo-random numbers, and by altering the seed a new set of pseudo-random numbers will be generated.

The random processes in systems leads to randomness at the output that can in turn lead to errors. Experimentally the bit-error-rate (BER) is measured by setting a threshold level to determine if the input signal is a one or a zero, this is compared with the known input sequence and the fractional number of errors transmitted in the sequence is given. This is the most straightforward way of analysing the data and will give a good indication about the performance of a system, but it will provide little information with regards to where the errors are originating. The Monte Carlo estimation procedure takes the output of the decision decoder at the end of the system and compares it with a delayed version of the original data. By measuring the value of the waveform on the decision detector at sampling instants, probability density functions (pdf) can be generated. For Monte Carlo estimations of error in an error

detector, a pdf can be generated for the voltage of the ones and a pdf can be generated for the voltage. These pdfs provide the foundation for various error estimation processes. In these simulations, these mean and standard deviation of the pdfs were used to generate the Q values as described section 4. Other simulation techniques for estimating BER exist, such as importance sampling where a known increase in artificial increase is introduced, or tail extrapolation where assumptions are made regarding the tail region of a pdf [157], but are not described here.

Even when errors have been calculated from the pdfs of the ones and zero voltage levels, questions can still be raised about the reliability of those pdfs. The stochastic elements within the simulation tool are dependent on the seed used for the generation of the random variables, which in turn affect the distribution of the pdfs. Even though these sequences are generated randomly, there is the possibility that these may contort the outcome of the simulation. For example, the pattern generated for the PRBS data may lead to a pattern that has less ISI or it may lead to the generation of more ISI, it may also lead to favourable or unfavourable noise characteristics. It may be true that in a real system, there is the possibility that the data transmitted may lead to the reduction in ISI, although there is no knowledge (unless some coding or scrambling scheme is involved) about what interaction the random pattern to be transmitted will generate. Therefore it is necessary to adopt a simulation strategy that accounts for the psuedo-random generation. Parsing multiple simulations each with a different seed, will provide a variation in the pdfs used for generating Q predictions and in turn lead to a variation in that Q (although Q is not the only feature that can be used to quantify a system). This will provide a maximum and a minimum Q value for each simulation configuration. In the case of Q values, the worst-case scenario adopts the minimum Q and the best-case scenario would adopt the maximum Q values, also the average or mean of the Q variations can be taken.

In the simulations performed, a fixed seed was used for the generation of random numbers necessary for noise generation to reduce the time taken for simulation. Using a fixed seed, results in the same pseudo-random sequence and noise effects being generated for each simulation. Running multiple simulations with varying seeds increases the accuracy of the simulation by further randomising the stochastic processes although this is at the expense of greater simulation time.

When examining simulations with multiple wavelengths, a comparison is made of the results obtained for each channel for a given pulse duration and launch power, and the

minimum value is recorded. This is not an analysis of the worst case due to variations in the seed. This is used to provide a summary for all of the channels and an overview of a system as a whole. Due to the used of a fixed seed, minimum and maximums are taken from variations in the results for each channel.

6.3 • The Treatment of Simulation Output

In Monte Carlo simulations results are based on the pdfs that are generated for the 1's and 0's. Pdfs can also be generated for the min-max approach to simulation. The worst-case value may seem like the obvious choice to take, as it shows how well the system copes with the worst variations in the stochastic effects, although this may not be suitable for all simulations. Simulations that adopted the worst-case method whilst attempting to examine a detrimental effect such as PMD would result in an overly critical analysis. Even though there is the probability that the total PMD would align in such a way as to result in no recoverable data, the probability of this lies within the tails of a Gaussian distribution, and would only happen for a short period of time. The worst-case approach would lead to a conclusion that the system could not tolerate PMD. Mean and the standard deviation of these pdfs can be generated, and are used in Q estimation, yet it is not know how accurate these values are. A point estimate of a parameter is a number, which is calculated from a given sample and serves as an approximation of the unknown exact value of the parameter. Mean and standard deviations are such parameters of a normal distribution and also the maximum likelihood method is another such estimation. Whenever a mathematical approximation formula is used, we should try to find out how much this approximate value can deviate from the unknown true value. For a sample we cannot draw conclusions about the population that are 100% certain, therefore it is necessary to determine two numerical quantities that confer a probability that the exact unknown value is contained between them. This is known as an interval estimate or a confidence interval. The magnitude of this confidence interval depends on the confidence level (95%, 99%) and the sample size. For a greater confidence level, the larger the confidence interval, conversely the larger the sample size the smaller the confidence interval. In the case of the Monte Carlo method, this is the number of samples used to

determine the pdfs for the one and zero levels, and for the min-max method this is the number of simulations with varying seeds.

For the analysis of errors Monte Carlo methods are adopted in the receiver in order to deduce a Q value. The number of samples for the pdfs was set at 50; this value was not tested nor optimised. Confidence intervals for the pdfs for the ones and zeros were not performed, as the simulation tool does not provide an output of the pdf data. As a fixed seed was used, confidence intervals for the min-max method were also not generated.

6.4 • Simulation Tool

A proprietary simulation tool known as preSTAR was used for simulation. This software is owned by BTexact, was developed in house and was based around an their earlier Monty simulation tool [158, 159]. PreSTAR deals with both electrical and optical signals that are represented by a finite number of sampling points. The higher the number of samples used the longer the time interval that can be represented (and the wider simulation bandwidth), however as there are more points to process the time taken to complete the simulation will rise. Power outside of this Fourier window is stored separately as simple power spectrum and contains no phase information. Both the "in-band" and "out-band" spectrums are passed from one block to the next, with the phase sensitive information such as signals transmitted "in-band", and the phase insensitive information such as spontaneous emission noise being carried "out-band". The split-step Fourier method is used to solve the NLSE for pulse propagation within the in-band [160]. The split-step Fourier method will not be described in this thesis although a brief description will be given. The split-step Fourier method assumes that when a signal is propagating over a short distance, dispersion and nonlinear effects act independently whereas, in general, they act together. This distance is split into two independent stages, one where nonlinearity is accounted for and the dispersion and absorption components are assumed to be zero, and the other stage accounts for dispersion and the nonlinear components are assumed to be zero. A further method involves including nonlinearity in the middle of the segment as opposed to at the end and is referred to as the symmetriesed split-step Fourier method. If the step size is incorrectly specified then inaccuracies in the results can occur so it is necessary to perform additional simulations to ensure the accuracy of the model. In preSTAR,

these steps are spread evenly throughout the whole transmission path and in order to improve the accuracy the total number of steps must be increased. In addition, if this bandwidth were too narrow, signal energy would be carried out-band and would only contain simple power information. Therefore both the split step length and the number of sample points must be optimised in order to minimise the simulation time whilst maintaining simulation accuracy. For the single channel experiments, an initial sweep over a single 100km fibre span was conducted with 16384 sample points and was reduced. It was found that 4096 sample points showed a marginal difference to 16384 sample points. Running a simulation with a small step size of 25m and increasing it to 1000m found that and step size of 250m was similar to that of the shorter step lengths. When the single channel experiments were changed to incorporate 16 wavelengths, the number of sample points was not increased and errors were noticed. This was due to the external channels falling out-band. The process of optimising the sample points began again and it was found the 16384 sample points was similar to 65536 sample points. The optimum split step length was found to be the same as for the single channel experiment. The total out-band bandwidth used for the simulation was from 1500nm to 1600nm, with a central frequency of 1550nm used for the in-band.

The tool has a pseudo-graphical user interface (GUI) that allows the user to string together multiple blocks in order to create a complete system. The block sequences are arranged hierarchically with preSTAR processing all of the blocks within the first block sequence before passing the information to the next. Each block is individually configurable and is used to describe a system element or component. The block parameters can remain fixed throughout the simulation process or can be changed per block sequence (for loops within a set of blocks) or per simulation (for multiple loops of a simulation) by inserting an array of numbers. Three main block sequences were created, one for the transmitter, one for the fibre span, and one for the receiver.

The transmitter comprised of block that generated a pseudo-random stream of electrical ones and zeros at a given frequency and pulse shape, this information was then passed to electrical-to-optical-converter block. The converter then produced and ideal monochromatic source of a given wavelength and pulse shape that was modulated by the electrical wave of the previous block. In order to evaluate the amount of power carried in the wide band spectrum, this block also estimated the mean power density in the tails of the modulated spectrum. The final block in the transmitter block-sequence was the phase modulator that was set at the clock frequency. The signals

from each transmitter were added to the mux block, which combined all the channels. The block sequence was looped for the required number of data channels.

The fibre span consisted of six blocks, a fibre block, a limiting-amplifier block and optical-filter block. The fibre block contains the main fibre parameters such as length, attenuation, dispersion and so forth. There are two models available for the fibre, linear and nonlinear. The linear model assumes that the Kerr coefficient is zero whereas the nonlinear model takes into account the non-linear nature of the refractive index of silica. The limiting-amplifier block contains user definable noise figure, gain, central frequency and bandwidth. The block takes the gain set for the amplifier in dB and applies it to the input signal to generate a new output signal then the mean-noise-power-density is calculated from the noise figure. The optical-filter block module provides a number of filter shapes; Gaussian, raised cosine, rectangular and a 2^{nd} order Butterworth and the filter profile applied to the signals around a given centre wavelength for a given filter bandwidth. Each one of these modules was use twice to generate the 100km span with amplification and dispersion compensation. The entire fibre block-sequence could be repeated as many times as was required before the information was handed to the next block-sequence.

The receiver consisted of the optical-filter block described above, an optical-to-electrical-converter block, a low-pass-electrical-filter block and a Q-estimator block. The optical to electrical converter acts as an ideal optical receiver, whereby the incoming optical power is converted into a photo current without receiver noise generation. The incident optical fields from both polarisations are squared up and added together to give a power array, which is scaled by the quantum efficiency parameter. The low pass electrical filter can apply three types of filter profiles scaled to a user configurable 3dB bandwidth. The filter profiles available were a first and third order Butterworth, a fifth order Bessel-Thompson and a raised-cosine. The Q estimator sampled the incoming signal by a number of sample points and generated the Q value from both the Bergano technique [128] and another technique developed by Anderson and Lyle [161]. The Anderson technique was created to avoid the spurious patterning effects, which limit the accuracy of Q. A low pass filter would affect a one embedded within a string of ones differently than an isolated one in the receiver. The patterning on each bit is dependent on the bit preceding it and the one following it. Using this fact it is possible to relate each bit to one of eight unique patterns. If the bits in the sequence are sorted by pattern the mean and standard deviation of each pattern can be

calculated. Each of these distributions gives the probability of error from that particular pattern, p, and as such the assumption that the noise is Gaussian is still maintained. This can be calculated by;

$$p = erfc\left(\frac{|D - \mu_p|}{\sigma_p}\right) \tag{6.1}$$

where D is the decision level, μ_p the mean of pattern p and σ_p the standard deviation of pattern p. Both of these Q values were monitored during simulation and compared to each other as an aid to identify when a simulation was running incorrectly.

Test runs of the simulations were performed in order to minimise the number of sampling points and maximise the split-step length. Test runs were also made filter bandwidth of the electrical filter in the receiver and an optimum was found at 30GHz.

6.5 • Simulation of Terrestrial Optical Transmission Systems

40Gbit/s wavelength-division multiplexed (WDM) transmission has been studied [162, 163] with transmission distances beyond 1500km at 1Tbit/s being achieved. The current trend in these high bit rate systems is to employ new fibre types such as reverse dispersion fibre (RDF) and non-zero dispersion shifted fibre (NZ-DSF) in order to keep low average dispersion and a high local dispersion. Techniques such as dense dispersion managed soliton (DDMS) transmission [164] and operating with shorter amplifier separation [165] are also utilised to circumvent the transmission limitation imposed by the dispersion length [166]. Currently much of the terrestrial infrastructure has a data rate no higher than 10Gbit/s and an upgrade to 40Gbit/s transmission is attractive possibility. For these network operators, exploiting newer transmission methods can render their prevailing network ineffectual and upgrading to the entire network becomes expensive. The obvious, but not necessarily simple, solution is to modify the system to increase the bandwidth for a relatively low expenditure. Some work has been performed on modifying terrestrial systems, such as transmitting over conventional single mode fibre (SMF) with long amplifier spans and analysing the differences between modulation formats [167-171], although the majority of this work has been performed at 10Gbit/s per channel. Increasing the data rate beyond 10Gbit/s and operating at terrestrial amplifier separations requires an increase in the optical

power; this makes it increasingly difficult to control the detrimental nonlinear interactions.

Historically, NRZ was regarded as the modulation format for transmission as both optical spectrum and peak power are minimised, reducing the detrimental effects of group-velocity dispersion (GVD) and fibre nonlinearity [172]. Presently NRZ is generally deemed inferior to RZ transmission as results have demonstrated [173], and NRZ has also been shown to give a 2dB receiver power penalty compared to RZ modulation [174]. One of the advantages of RZ is the ability to utilise the balance between GVD and self-phase modulation (SPM) for soliton and soliton-like transmission [175], although the low local dispersion in soliton based transmission results in large timing jitter (see 2.7.1). Achieving the linear and non-linear equilibrium required for soliton-like transmission indicates that there is sufficient power to induce other unwanted non-linear effects such as cross-phase modulation (XPM) and four-wave mixing (FWM). Any mismatch between the linear and nonlinear effects results in the soliton adapting by shedding energy in the form of dispersive waves, although launching at a special point [176] or equivalently pre-chirping the soliton-like pulse can reduce the amount of dispersive wave created [177].

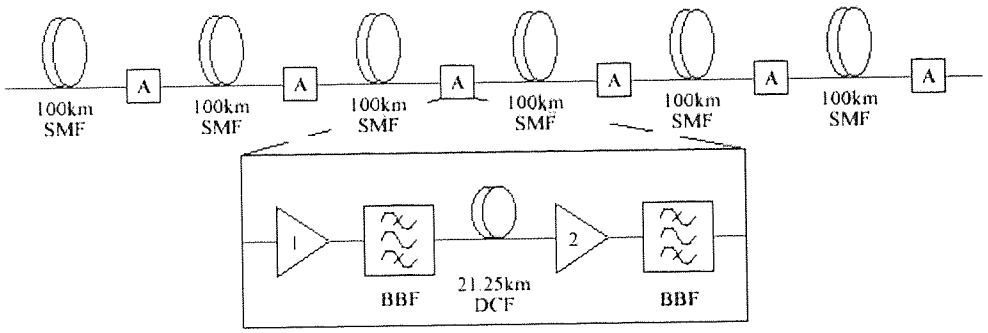

Figure 6.1: Schematic diagram describing the configuration of the 600Km single-mode transmission fibre, including the amplifier positions and dispersion map

The BT fibre network comprises of nodes, which are used to add and drop channels and these are situated, on average, every 100km [178] and are connected by single mode G652 fibre with a longest span length around 600km. It was from these premises that the design of an SMF based 600km fibre span originate. This is not the same as the installed fibre, as the installed fibre is not exactly periodic, as some spans stretch over 200km [178]. The transmission span used for simulation can be seen in Fig. 6.1

Component	Parameter	Value
SMF at 1550nm	Length	100 km
	Split Step Length	0.25 km
	Attenuation	0.2 dB/km
	Effective Area	80.0 μm^2
	Dispersion	17.0 ps/(nm.km)
	Dispersion Slope	0.06 ps/(nm^2.km)
DCF at 1550nm	Length	21.25 km
	Split Step Length	0.25 km
	Attenuation	0.35 dB/km
	Effective Area	25.0μm^2
	Dispersion	-80.0 ps/(nm.km)
	Dispersion Slope	0.06ps/(nm^2.km)
Black Box Amplifier	Noise Figure	5dB
	Amplifier Width	30nm
Broad Band Filter	3dB Bandwidth	10nm Single Channel
		30nm WDM
	Filter Profile	Rectangular
Receiver Filter	3dB Bandwidth	Channel Spacing
	Filter Profile	Rectangular
Electrical Filter	3dB Point	30GHz
	Filter Profile	5^{th} Order Bessel-Thompson

Table 6.1: Summary of the parameters used for the components in the simulation

The transmission path incorporates six 100km lengths of SMF each with an attenuation of 0.2dB/km and an effective area of 80μm^2. The SMF dispersion was 17.0ps/(nm.km) at the operating wavelength with a dispersion slope of 0.06ps/(nm^2.km). As shown in Fig. 6.1, after each 100km length of SMF, an amplifier and a dispersion compensation module are utilised to compensate for the span loss and dispersion. For compensation, 21.25km of dispersion compensating fibre (DCF) was used to reduce the accumulated dispersion to zero. Prior to each length of DCF, an amplifier was used to compensate for the loss imposed on the signal by the DCF. As the strength of the nonlinearity coefficient, γ, is dependent on the effective area, we can expect greater nonlinear interactions within the DCF than those experience in SMF due to it smaller effective area. Consequently to avoid increasing any nonlinear effects, a low input power into

the DCF was consistently maintained throughout the simulations. After the DCF, a second amplifier is used to control the launch power in the following section. Both amplifiers had a noise figure of 5dB and after each amplifier broad band-pass filters, with a 3dB bandwidth of 6.0nm, were utilised to reduce any build up of ASE. Owing to the limitations of commercially available components, the maximum average transmission power was limited to 24dBm throughout all the simulations. Table 6.1 provides a summary of the parameters of the components in the span. The parameters of the SMF used were based on parameters supplied to BTexact by Corning and represented the more recent SMF-28 and the DCF parameters were taken from the Sumitomo's dispersion compensating module range. These are similar to, but do not exactly match the fibre installed in the BT network, and the author does not know the exact values of the fibre in the network. One limiting factor of the older fibres used in the BT network is PMD. This is not accounted for in this simulation and is a major limiting factor for transmission at higher data rates.

The dispersion of each span of DCF at 1550nm was -80.0ps/(nm.km) and the dispersion slope was -0.23ps/(nm^2.km), this provides approximately 80% slope compensation for the fibre map. The accumulated dispersion is shown below in Fig. 6.2. It is worth noting the differences between transmission length and span length. As these simulations are designed to simulate older installed terrestrial systems, where operation was at 1300nmm there was no DCF was needed, the span length only incorporates the SMF. Physically, the DCF would be inserted at the amplifier positions along the span and would not contribute to the span length, although the signal does propagate through the DCF resulting in a total transmission distance of 727.5km, greater than the span length.

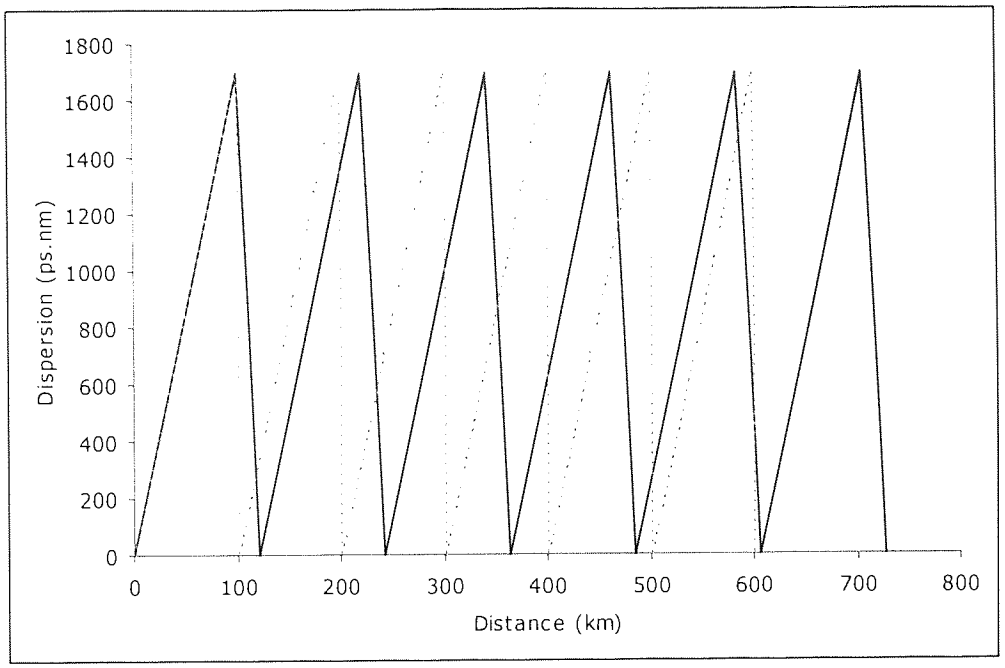

Figure 6.2: Accumulated dispersion for transmission at 1550nm. The dark line is the transmission length (SMF) whereas the light dashed line is the distance along the span (including DCF)

Fig. 6.3 shows the results obtained from equation 3.1 for map strength against the FWHM pulse width (ps) and wavelength (nm) for the fibres used in the simulation. The top graph shows the results for the pulse widths used in the simulations and clearly shows the square dependence that map strength has for pulse width, with pulses of 2.0ps generating map strengths over 800. At 14ps, the broadest pulses used in the WDM simulation, the map strength is just below 6 and still does not reach the map strength of 1 for soliton like propagation. The lower graph focuses on the pulse durations that approach the map strength required for DMS transmission. At 40ps the map strength is just over 2 and would allow propagation that is more soliton like, yet this pulse duration is a lot greater than the bit slot, and would lead to pulses that are totally overlapped by the pulses on both sides. The map strength is marginally affected by the wavelength, and there is a variation of ±1.9% for the minimum and maximum wavelengths from 1550nm. Clearly the dispersion-managed soliton is not a viable solution for this fibre map at 40Gbit/s. In order for dispersion-managed solitons to be feasible in this system, the fibre lengths would have to be reduced by more than one third.

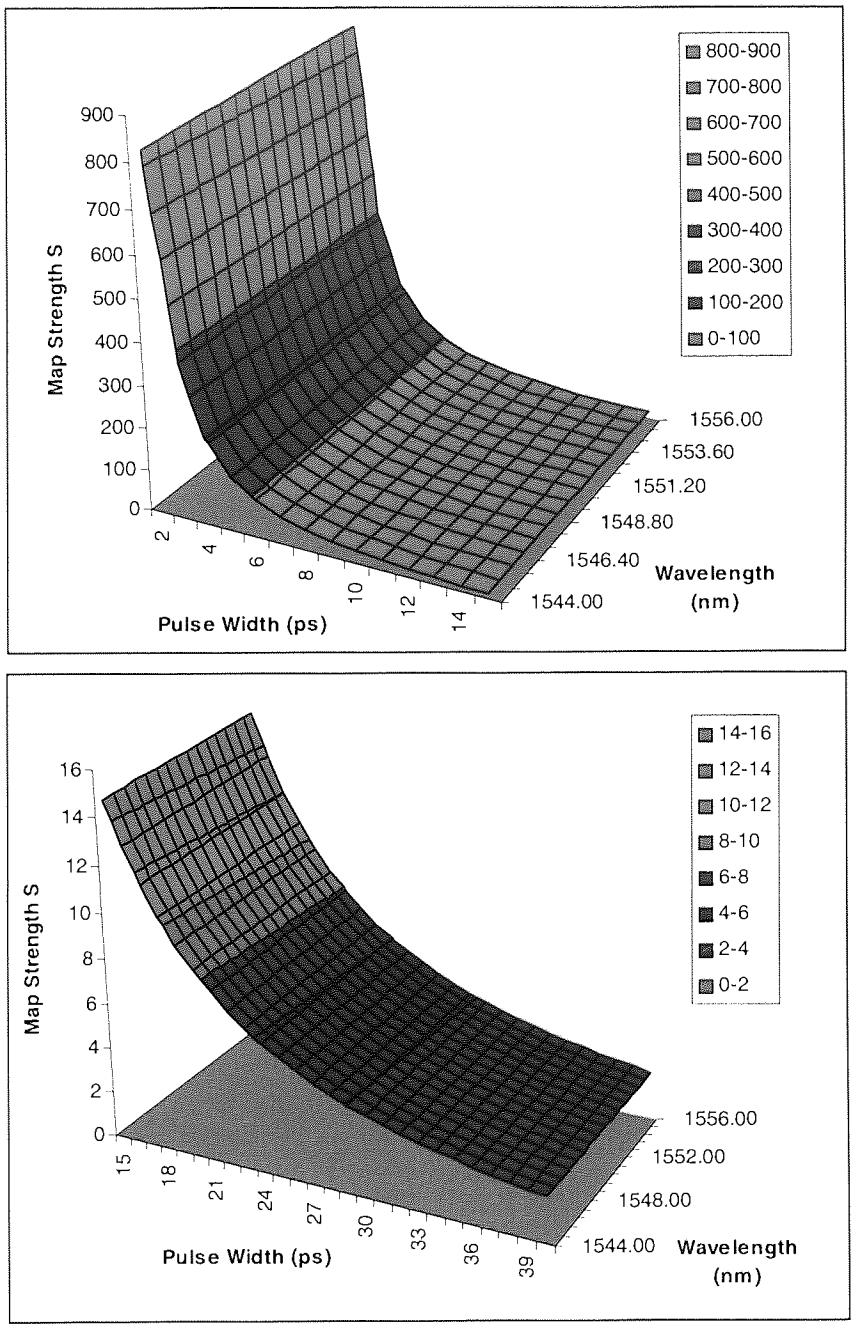

Figure 6.3: Map Strength, S, against Pulse Width (ps) and Wavelength (nm) for the fibres used in the simulation. The top graph show the result for the pulse duration used in the simulation whereas below they show the pulse durations for map strengths required for dispersion managed solitons

Optimisation of bandwidth requirements reduces costs for a network operator as reducing the number of components on a span saves installation and maintenance costs. Increasing the number of WDM channels increases the required optical bandwidth and it also requires more expensive and complex gain flattened amplifiers, WDM routers, and optical switches. By using TDM to increase the system bandwidth, by transmitting at a higher base data rate, the need for these WDM components is removed. Therefore for some parts of a network, single channel transmission can be preferred over WDM. Another advantage is as only one wavelength is in operation, there are no inter-channel effects being created, also there is little limitations on the optical bandwidth available per channel, so narrower pulse widths are sustainable. Increasing the base data rate increases introduces its own problems. To sustain the same power per pulse, the average launch power needs to be increased and current system amplifiers may not be able to generate the additional energy required. Also new electronics are required at the transmitter and receiver to cope with the change in base frequency.

The system configuration for the single channel transmission simulation is shown in Fig. 6.4 and the arrangement of the transmission span was shown earlier in Fig. 6.1.

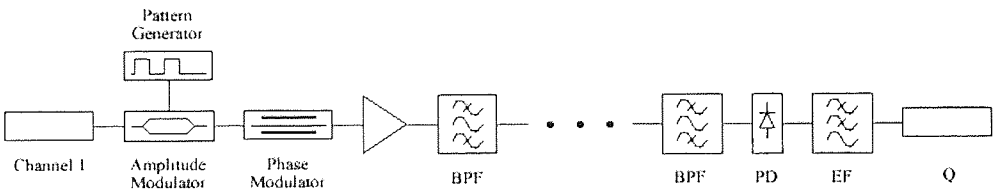

Figure 6.4: Configuration of the 40Gbit/s single channel transmitter and receiver depicting both amplitude modulation and phase modulation components

A single channel at a wavelength of 1550nm and with a bit-rate of 40Gb/s was simulated without using time division multiplexing or polarisation multiplexing. Three different data modulation formats were used for transmission: NRZ, RZ, and CRZ. When either of the RZ transmission formats was used, the source was a pulse laser producing pulses with a Gaussian profile as opposed to a CW laser source used for NRZ transmission. Previous results have shown that by optimisation of the path-

averaged dispersion, single channel propagation can be improved [173]. However, as the aim of the simulations was to expand the single channel system to a WDM system centred at 1550nm, the span used for all the simulations was configured such that the average dispersion at the central WDM frequency was zero.

Initially we consider the dependence of single channel transmission on launch pulse width for both the RZ and CRZ formats. To optimise the chirp for CRZ transmission, the phase modulation index for the phase modulator was varied between -2π and 2π. As the average fibre dispersion was zero large chirps were not required to compensate for GVD, therefore the optimum phase modulation index was found to be close to zero at $\pi/18$.

Fig. 6.5 shows the results as a contour plot of the system Q as a function of the input pulse width and the launch power. These were obtained by parsing a single simulation, retrieving the Q value and then incrementing the pulse width and/or power. Matrices of the results were generated and the graphs acquired. From these results it is apparent that both modulation formats have a similar dependence on pulse width and transmission power with both formats achieving similar Q areas. The chirp applied to RZ data is normally used to counteract the effects of residual dispersion on external channels. As this is a single channel system operating at the dispersion zero, the application of chirp on the signal has made little difference. CRZ has a marginally better performance than RZ with a peak around a pulse width of 3ps and a transmission power of 12dBm although RZ is marginally more tolerant to the variations of power and pulse width. The optimum parameters tend to be in the region of 3ps to 7ps and powers of 11dBm to 13dBm. For a Gaussian pulse, this would result in a bandwidth between 1.64nm and 0.71nm. As the pulse width broadens, the spectrum decrease and for a 10ps Gaussian this reduces the bandwidth to 0.5nm. In a real system, SBS would become an issue at the power levels described for bandwidths narrower than this, although in this simulation SBS is not considered. As this is a single channel system, there is little penalty for using large bandwidth, and a large gain by the enhancement obtained in SNR.

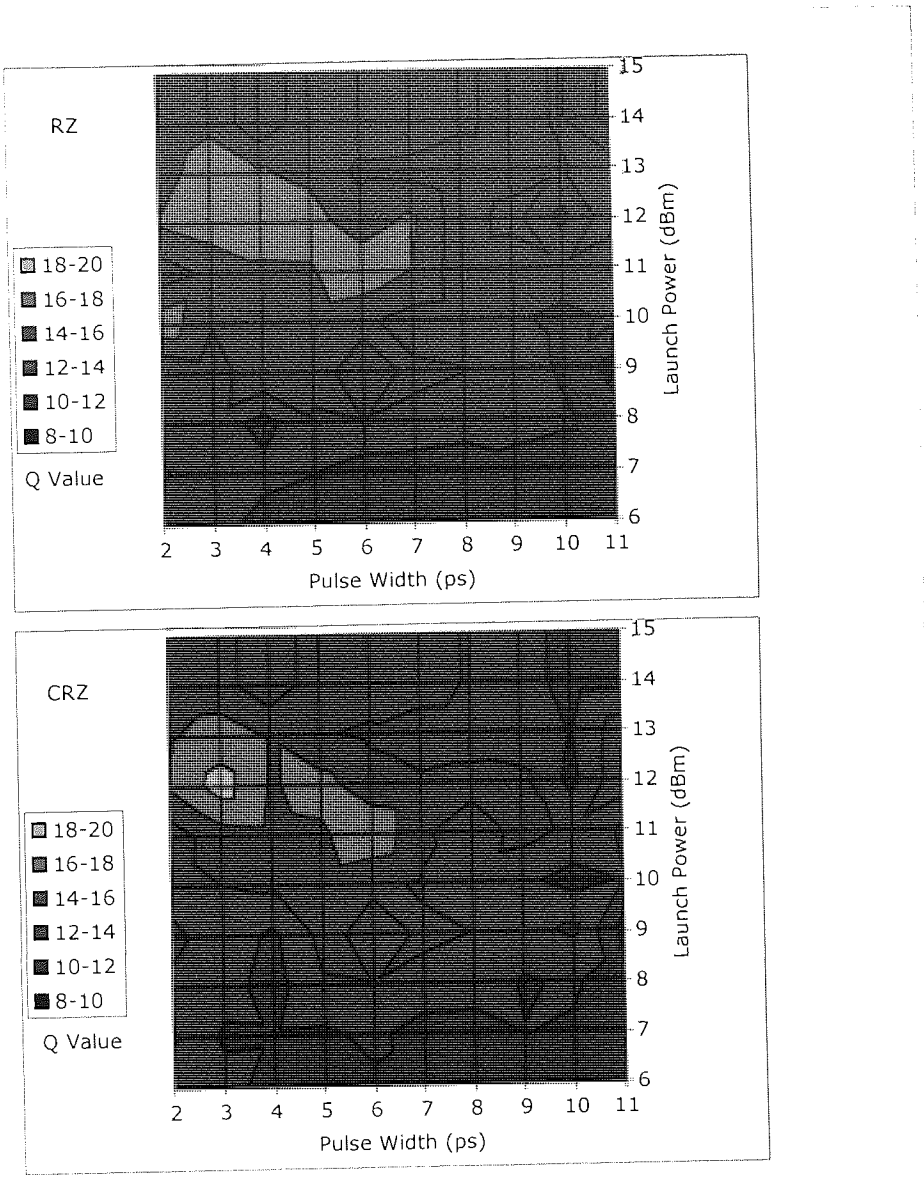

Figure 6.5: Q maps illustrating the dependence of pulse width and launch power for RZ and CRZ transmission over 600-km of SMF

As mentioned in the introduction, one of the strengths of simulations is to examine selected elements in order to gain an understanding of system operation. By removing the nonlinear components from the simulation we can identify in which regimes these nonlinear components are limiting the system. In Fig. 6.6, RZ and CRZ single-channel transmission simulations were repeated with the nonlinear components removed.

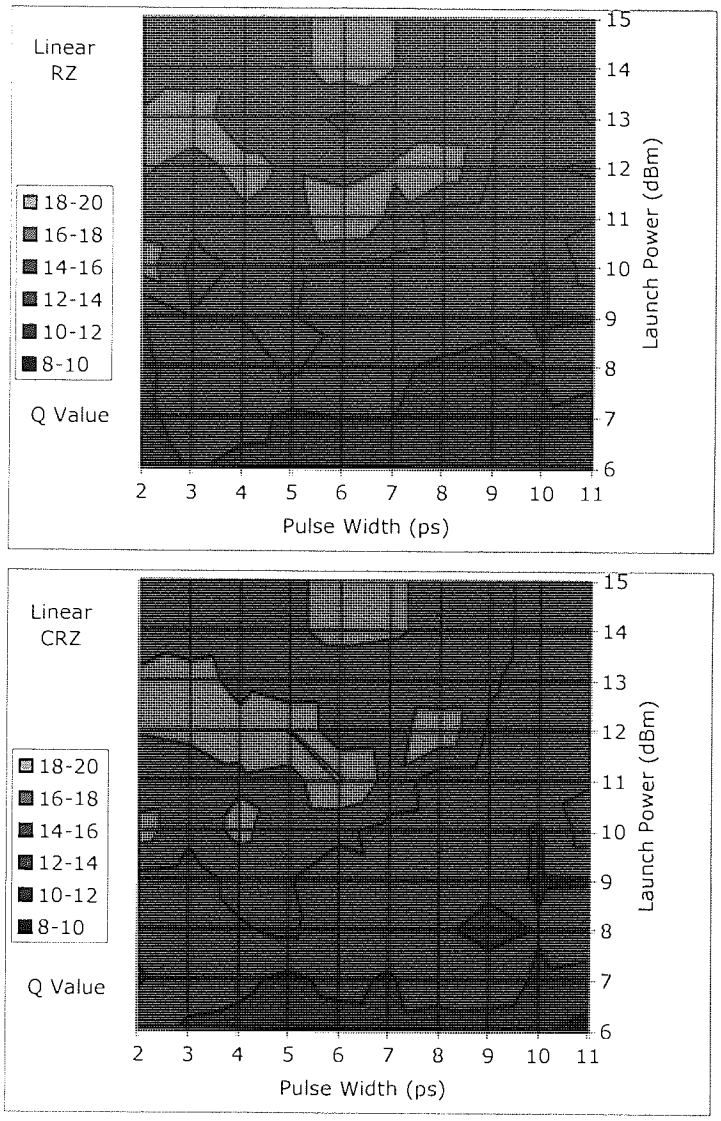

Figure 6.6: Received Q mapped against pulse width and launch power for RZ and CRZ transmission when nonlinear components are removed from the simulation

For a nonlinear system an increase in power increases the signal to noise ratio (SNR) which in turn increases the perceived Q value although, as the power increases, unwanted nonlinear interactions start to negate the gains made by increasing the SNR. On the other hand, for a linear system there are none of the nonlinear interactions that are detrimental to the SNR, so increasing the power increases the Q value. As the improvement figures portray, there is a general trend, for both modulation formats, showing the Q increasing as the launch powers. The optimum region now extends down to 2ps and up to 8ps, although this time there seems to be little penalty for

increasing the launch power beyond 13dBm. This has been highlighted in Fig. 6.7, which depicts the improvement in Q gained by the removal of the nonlinear components.

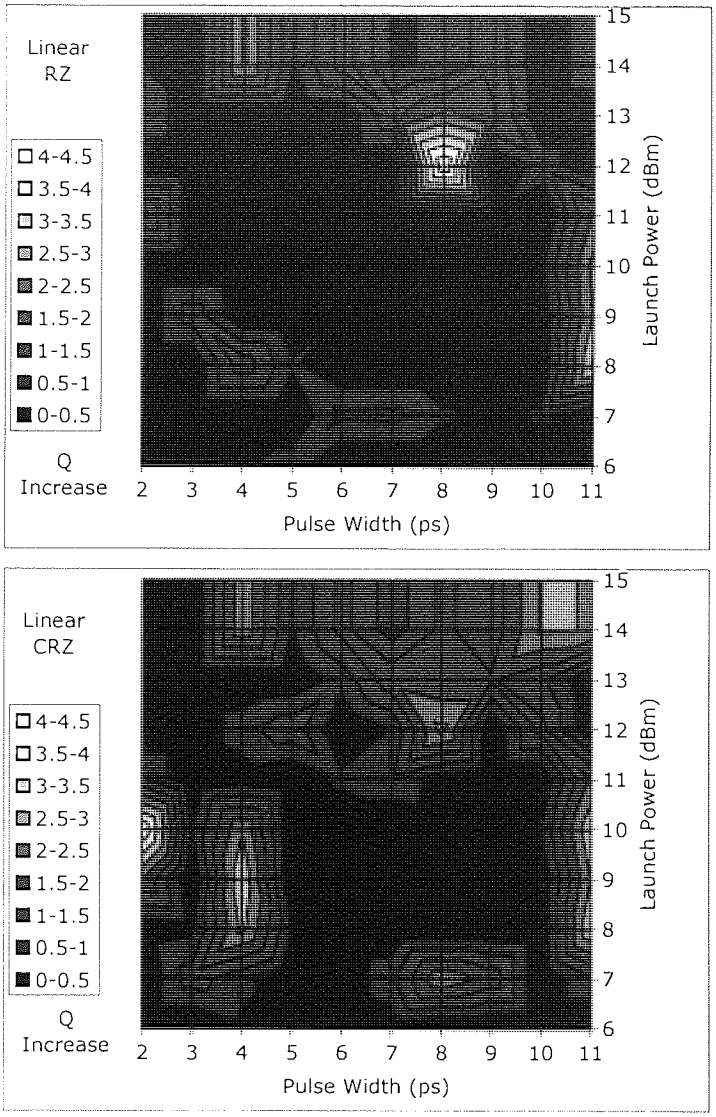

Figure 6.7: Improvement in received Q mapped against pulse width and launch power for RZ and CRZ transmission when nonlinear components are removed from the simulation

Again, due to the full dispersion compensation, there is very little difference between the chirped and unchirped cases in a single channel system. Both formats suffer from increasing nonlinear interaction around similar power levels and exhibit similar trends for broader pulse widths. Also both linear Q boundaries for both formats are a lot more

defined and exhibit fewer fluctuations within Q regions than their nonlinear counterparts.

Fig. 6.8 displays the performance of the NRZ modulation format against both RZ formats over the 600km of SMF.

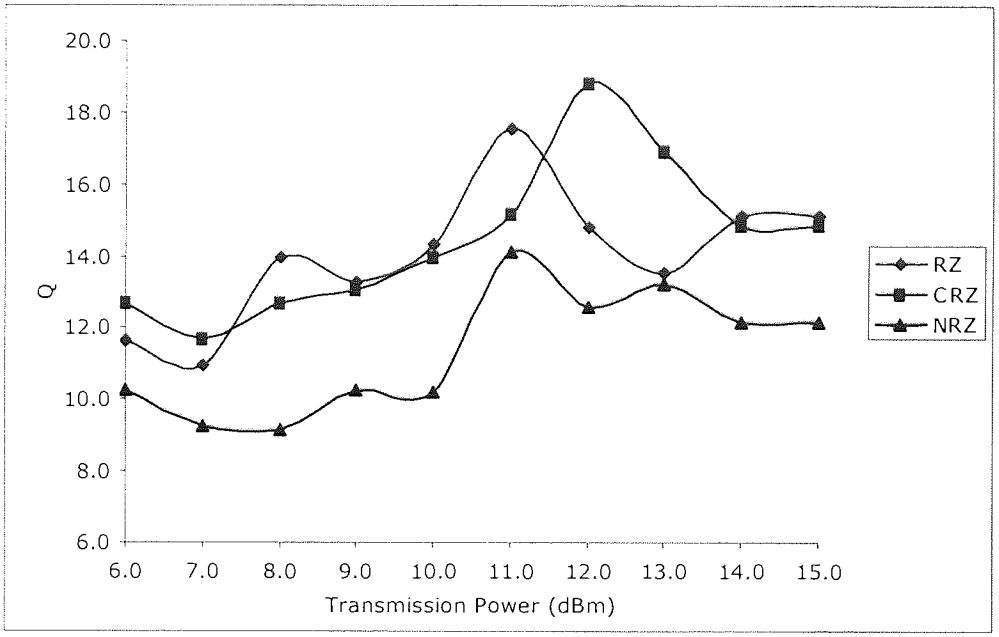

Figure 6.8: Q value as a function of transmission power for single channel transmission of NRZ, RZ and CRZ modulation formats at 40-Gb/s over 600-km SMF. The pulse widths of the RZ and CRZ data are 6-ps and 3-ps respectively

The pulse widths for RZ and CRZ were chosen from the optimum Q values from the nonlinear transmission simulations. All three formats exhibit a similar trend with the Q increasing linearly towards a maximum and then a reduction in Q occurs. At the lower power levels, the improvement in SNR gained by increasing the transmission power results in an increase in the estimated Q. This continues until the nonlinear interactions are sufficiently negative to reduce the Q value. The performance of NRZ surpasses that of the target bit error rate for commercial systems of $1x10^{-15}$ (when a Gaussian noise distribution is assumed, this equates to a Q of 8), although it does not achieve as high a level of performance as the RZ formats. All three modulation formats provide their maximum Q values at similar launch powers, 11dBm for NRZ and RZ, and 12dBm for CRZ. Overall CRZ provides the highest Q value although the CRZ performance is very similar to that of standard RZ and both RZ formats are superior to NRZ.

Fig. 6.9 shows (from top to bottom) the input spectrum, the received spectrum, the received eye and the received bit stream for the RZ modulation format for four pulse widths.

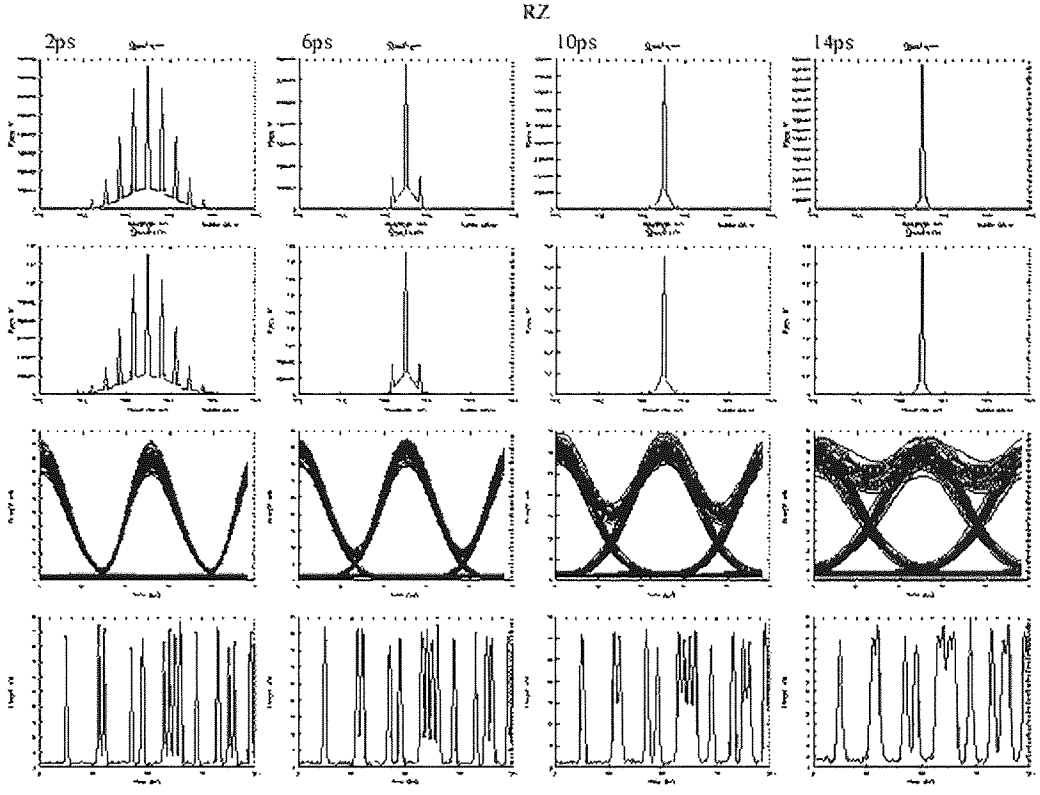

Figure 6.9: Examples of simulation output files for single channel RZ transmission at 40Gbit/s over 600km. The results are for varied launched pulse widths from 2ps to 14ps.

Due to the matched dispersion compensation the output optical spectrum is almost identical to that of the input spectrum for all cases. The relationship between spectral bandwidth and pulse width is also clearly visible with the narrower pulses exhibiting a much broader spectrum than narrower pulses (2.5nm for a 2ps pulse and 0.4nm for a 14ps pulse). The bottom set of graphs show the received eye and the amplitude received bit stream in time. The narrow pulse widths provide a clear eye diagram with a well-resolved data stream and an enhanced OSNR. Whereas the larger pulse widths tend to overlap when there are longer streams of ones resulting in greater noise on the one level of the eye diagram. Out of the four simulations, the 6ps pulse width provided highest Q value due to its maximised eye width and height, although all received Q values are well above a Q of 8.

Similarly to Fig 6.9, Fig. 6.10 shows (from top to bottom) the input spectrum, the received spectrum, the received eye and the received bit stream for a 6ps CSZ data with an applied phase modulation of $-\pi$ to π in $\pi/2$ steps.

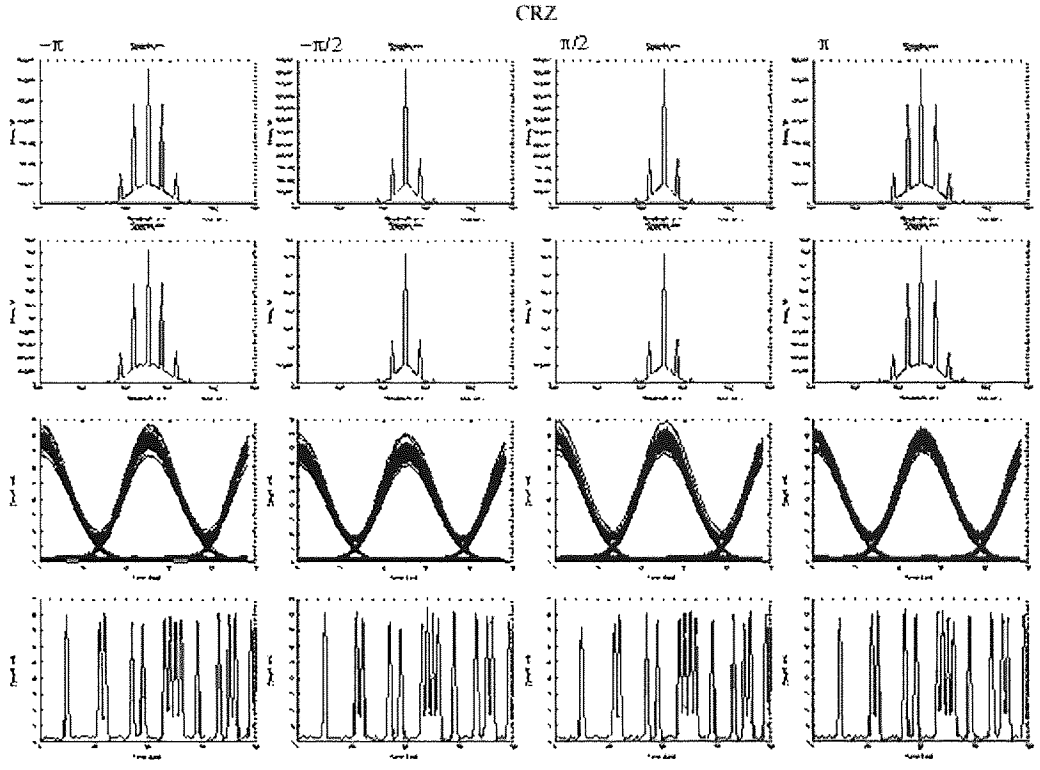

Figure 6.10: Examples of simulation output files for single channel CRZ transmission at 40Gbit/s over 600km with a launched pulse width of 6ps. The phase modulation index was varied between π and $-\pi$.

Due to the complete dispersion compensation at 1550nm, the input spectrum matches the output spectrum. When phase modulation is applied, the greater the magnitude of the phase modulation, the greater the spectral broadening and the more sidebands are introduced. This is not dependent on the sign of the phase. There is very little discernable difference between the various received eye diagrams. The positive phase modulation of π provided eye with the and highest Q value and also exceeds the 6ps RZ case by a small margin, but again all Q values were well over 10. This is due to the sign of the chirp applied to the data marginally counteracting the broadening of the pulse as it is launched into the anomalous fibre, whereas the opposing sign adds to the broadening of the anomalous dispersion. Due to the complete dispersion compensation, this effect is minimal. With the addition of phase modulation, the

spectral bandwidth increased for all four values when compared to the RZ case, this would suggest that the benefits gained by CRZ would be outweighed by interchannel interference for WDM transmission when the dispersion map is equally matched.

Fig. 6.11 shows (from top to bottom) the input spectrum, the received spectrum, the received eye and the received bit stream for NRZ data with various rise and fall times.

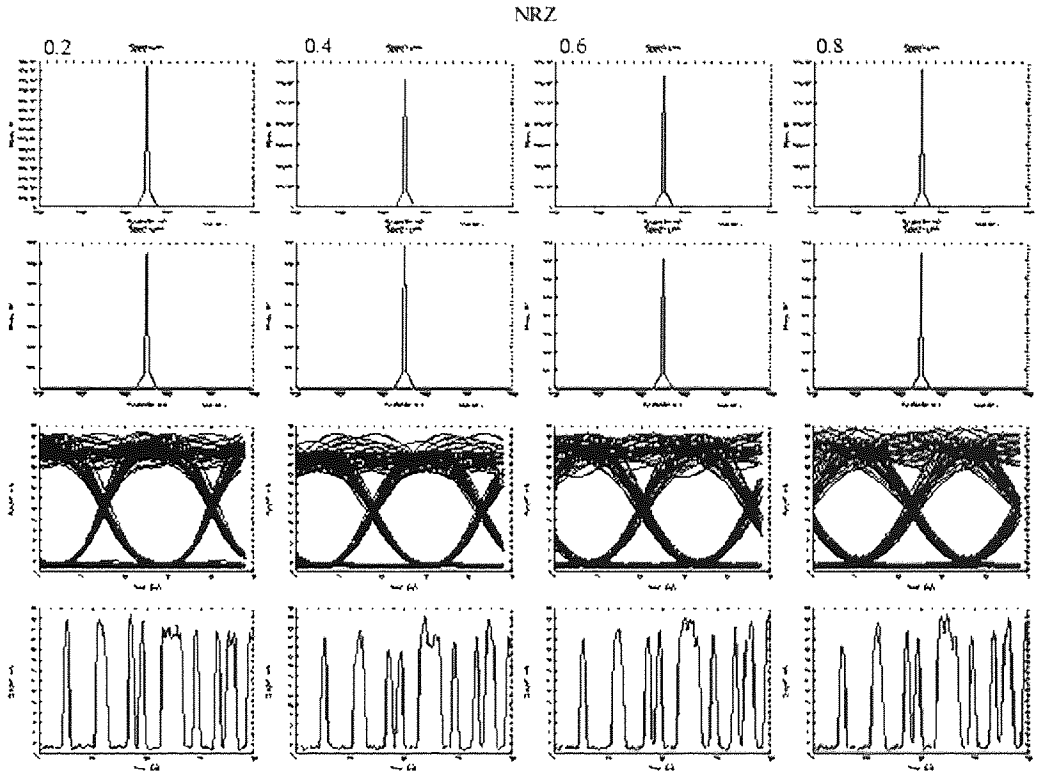

Figure 6.11: Graphical output from single channel NRZ transmission at 40Gbit/s over 600km. The modulator rise and fall time was varied such that $T_r = T_f$ between 0.2 and 0.8

For Fig 6.11, the modulator rise time, T_r, and fall time, T_f, both described as a fraction of half the bit slot, T_b, was varied between 0.2 and 0.8. At 40Gbit/s, this results in a rise and fall time of 2.5ps for $T_r = T_f = 0.2$ and a rise and fall time of 10ps for $T_r = T_f = 0.8$. This can be seen on the received eye diagrams, as they clearly show that the rising and falling eye edges are at a steeper angle for $T_r = T_f = 0.2$ than they are for $T_r = T_f = 0.8$. The faster the rise time, the more open the eye is in the time domain. Although the more pulse like the data becomes, the greater enhancement in SNR due to the higher peak power. The balance between the two effects was found at $T_r = T_f = 0.4$, although this was a marginal increase over the 0.2 case. For the greater values, the slower rise

time closes the eye diagram in the time domain resulting in lower Q values, all of which are still beyond a Q of 8. This variation of rise and fall time should not significantly affect WDM transmission as the spectrums for the NRZ are all very narrow due to its more CW like nature, particularly over long strings of ones.

6.7 • WDM Transmission with 100GHz Channel Spacing

Due to the effects of Kerr nonlinearity, multiplexing multiple wavelengths introduces additional nonlinear effects in the form of the inter-channel interactions. Phase shifts caused by XPM, are converted into amplitude fluctuations due to the GVD of optical fibre and FWM induces new frequencies that can collide with the frequencies of signal channels. Optimisation of the channel spacing and dispersion map can help to suppress these interactions. Here however, the dispersion map and channel spacing are fixed for SMF dispersion, a terrestrial 100km amplifier separation and the ITU standard of 100GHz channel spacing. WDM also imposes restrictions on the maximum amount of optical bandwidth available per channel, as any sidebands that extend into neighbouring channels will create inter-channel interference, decreasing the optical SNR. Consequently the single channel optima may no longer be sustainable in a WDM environment.

The modifications made to the transmitter (top) and the receiver (bottom) in order to incorporate WDM transmission is shown in Fig.6.12. The wavelengths of the 16 optical channels are separated by 100GHz and are spaced evenly around the spans zero average-dispersion wavelength of 1550nm. The transmission fibre for the 16x40Gb/s WDM transmission was unchanged from that of the single channel 40Gb/s transmission displayed in Fig. 6.1 although, to accommodate the additional channels, the 3dB bandwidth of the broad band-pass filters within the span was extended to 30nm to cover the spectrum of all 16 channels. As indicated in the fibre parameters listed in Table 6.1, the DCF provides 80% dispersion slope compensation, resulting in residual dispersion that builds up after each span of SMF and DCF. Residual dispersion is a large problem for WDM systems and if left uncorrected generate large intersymbol interference at the receiver. Fig. 6.13 shows the residual dispersion for the 600km SMF, DCF fibre map for various DCF slope compensations for the wavelengths range of 1544nm to 1556nm.

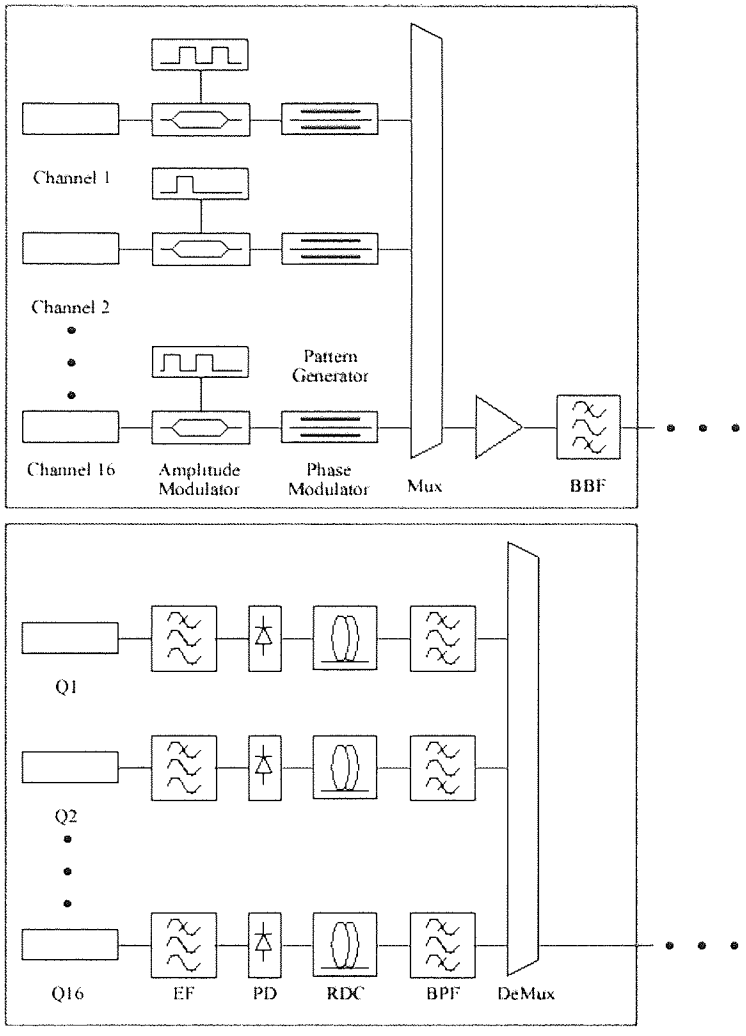

Figure 6.12: Schematic diagram of the configuration of the 16-channel WDM transmitter and receiver. The transmitter is depicted on the top and the receiver is shown on the bottom

It is clear to see that the effect of residual dispersion is not equal for all the channels, as the dispersion slope of the DCF does not compensate for the dispersion slope of the SMF. The result is that the further away a channel is from the zero-dispersion wavelength of 1550nm, the larger the accumulated residual dispersion. The DCF dispersion slope is greater than that of the SMF, although there is much less DCF in the system so it does not fully compensate the SMF slope, resulting in more than 50ps.nm of dispersion for the wavelengths furthest from the zero-dispersion wavelength. To compensate for the undesired pulse distortions caused by the residual dispersion, short lengths of positive and negative dispersion fibre are used at the

receiver to achieve post-system compensation. In order to optimise the residual dispersion compensation in the receiver of each channel, the dispersion of the RDC modules was varied and the corresponding improvement or degradation of the received Q value was monitored.

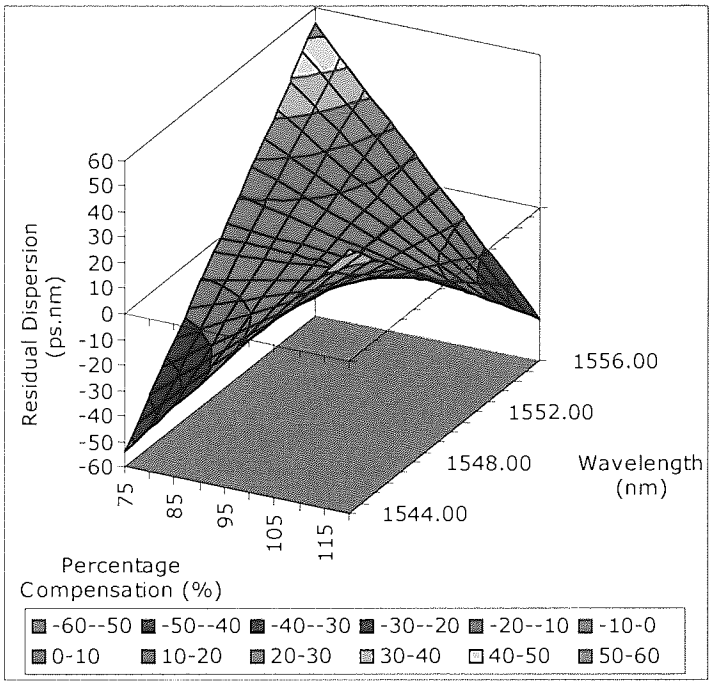

Figure 6.13: Mathematical profile of the residual dispersion versus DCF slope compensation and wavelength for the 600km simulation dispersion map.

Fig. 6.14 through to 6.16 display the results from the RDC optimisation process. The lower channel numbers require a positive amount dispersion to offset the accumulated dispersion and the higher channels require the opposite. Fig. 6.14 shows the estimated Q value against RDC for the RZ modulation format. The central channels require very little RDC as they are close to zero-dispersion wavelength, when too much RDC is introduced the data is broadened resulting in a reduced Q value. Due to the lack of 100% slope compensation, the channels at the wavelength extremities require greater RDC and the estimated Q shows an improvement of more than 2 for channels requiring both positive and negative RDC

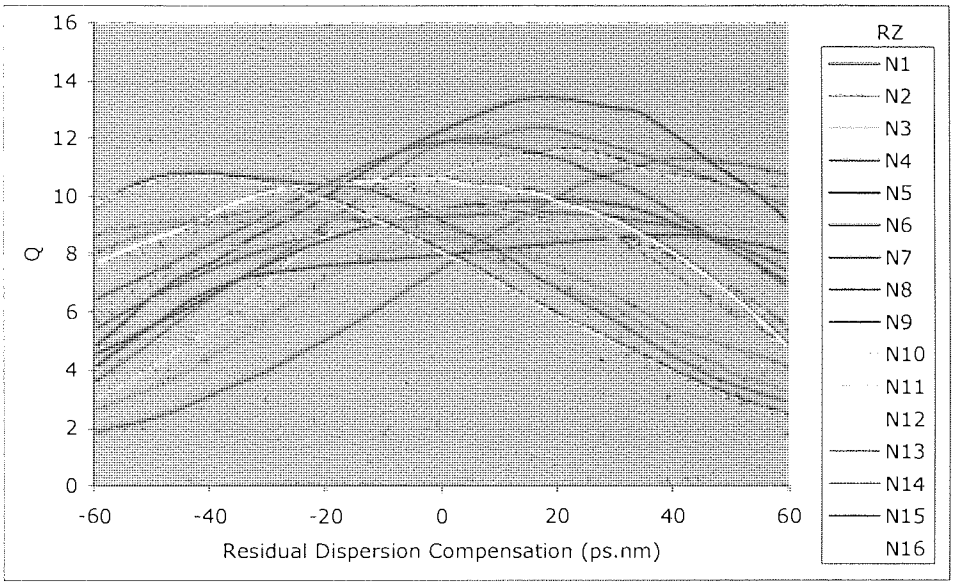

Figure 6.14: Residual dispersion versus received Q value for RDC module optimisation for RZ channel numbers 1 through 16

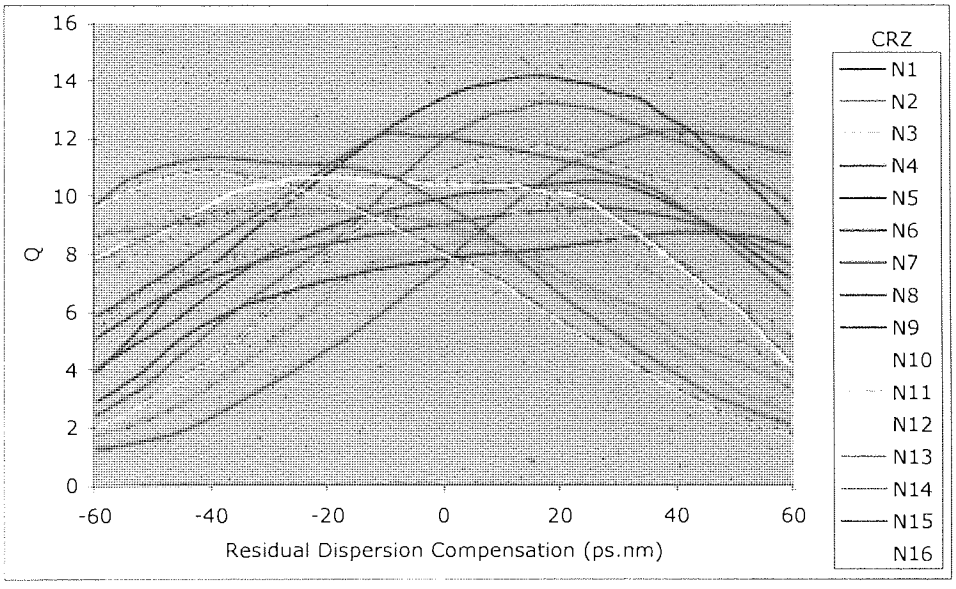

Figure 6.15: Residual dispersion versus received Q value for RDC module optimisation for CRZ channel numbers 1 through 16

Fig. 6.15 shows the estimated Q value against RDC for the CRZ modulation format. The results mirror the improvement for the RZ case, with the central channels

requiring little RDC and the outermost channels requiring the largest RDC of around ±50ps.nm.

Fig. 6.16 shows the estimated Q value against RDC for the NRZ modulation format. Due to the narrower bandwidth of NRZ it is more tolerant to residual dispersion accumulation, with an improvement in Q of 1 for optimisation of the external channels. Also the optimum RDC value for the external channels is not the theoretical ±50ps.nm, but is reduced to nearer ±40ps.nm.

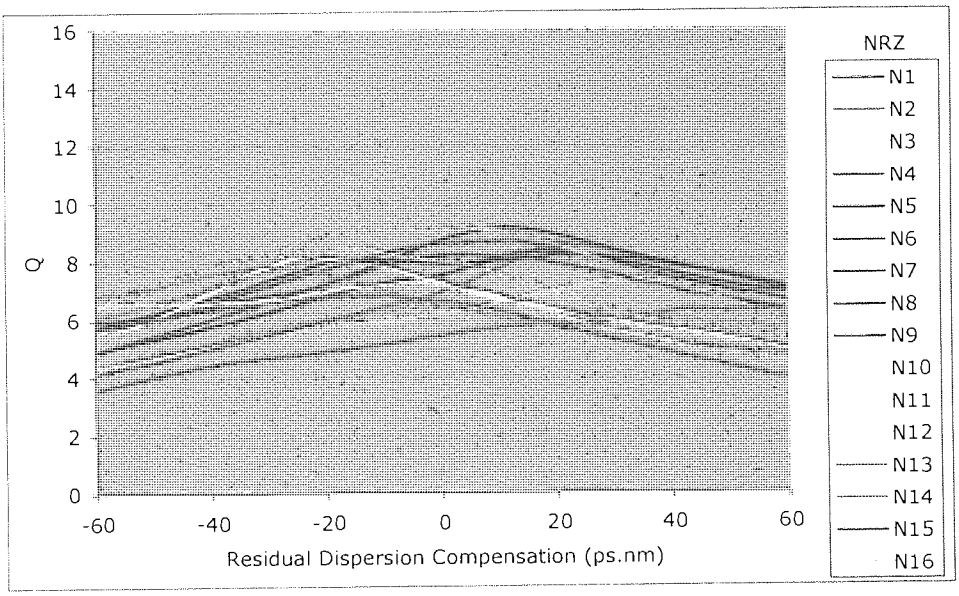

Figure 6.16: Residual dispersion versus received Q value for RDC module optimisation for NRZ channel numbers 1 through 16

Fig. 6.17 shows the improvement in Q value (bottom) for each channel by utilising the residual dispersion compensation for NRZ, RZ and CRZ data and the dispersion value attained from RDC optimisation (top).

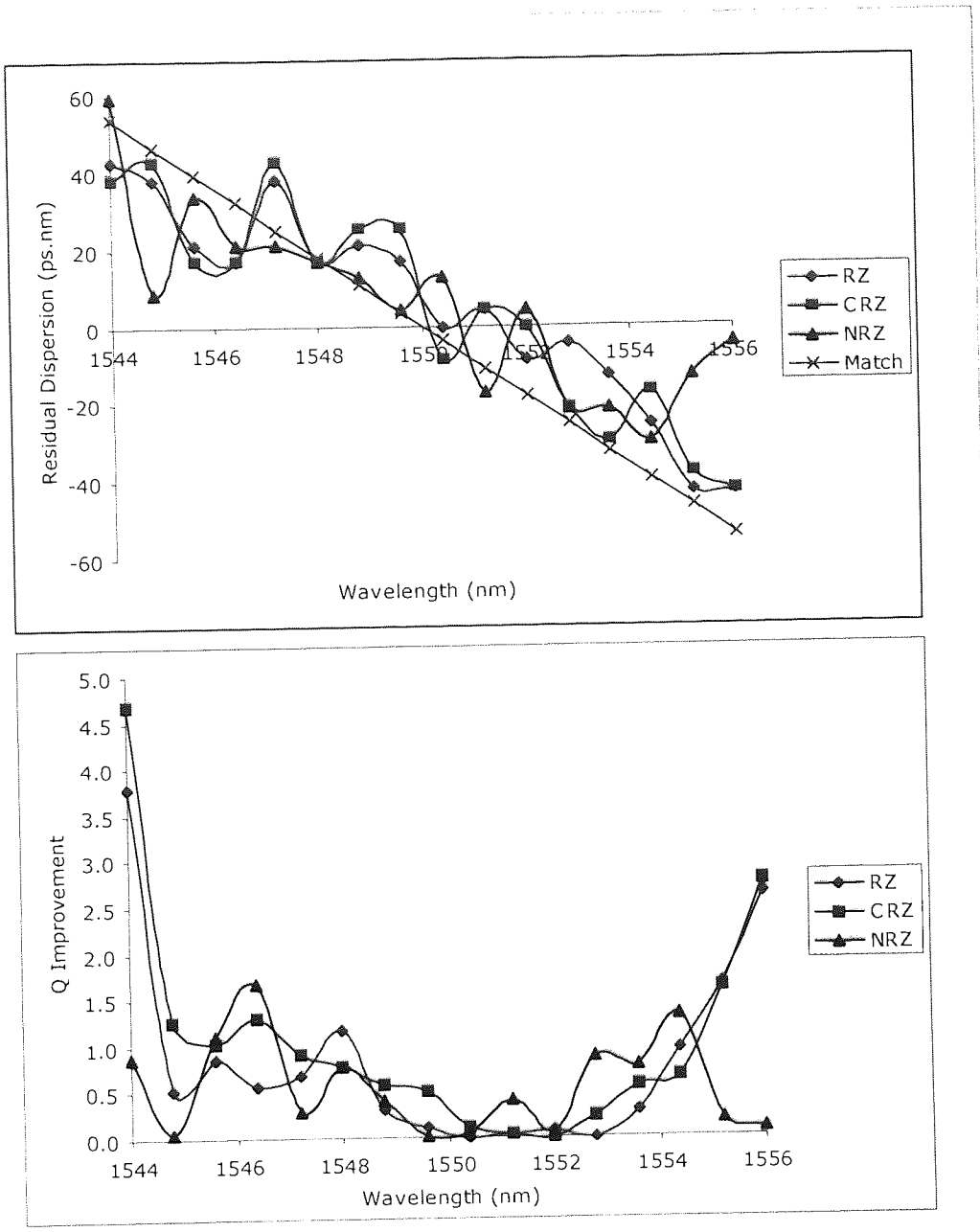

Figure 6.17: Optimised residual dispersion against wavelength (top) and the improvement in received Q value by the use of residual dispersion compensation at the receiver (bottom) for 16 x 40Gbit/s 100GHz WDM transmission

Plotted alongside the optimised RDC are the theoretical RDC values necessary to reduce the overall system dispersion back to zero. All three modulation formats tend to follow the trend set by the theory, although in general the RDC is optimal when it does not fully compensate the accumulated dispersion and leaves a small amount of positive dispersion. With the DCF providing 80% slope compensation, the residual dispersion is almost optimised for WDM NRZ as the received Q is only slightly improved by

employing additional compensation. RZ and CRZ on the other hand are more dependent on full dispersion compensation with the channels on the outermost wavelengths, which suffer from larger local dispersion, improving significantly with the use of compensation, unlike NRZ, which shows no significant Q improvement between wavelengths. This is due to the greater optical bandwidths of the RZ and CRZ modulation formats result in a greater sensitivity to dispersion, whereas the NRZ format is broader and more CW like so is less sensitive. Notice also the asymmetry with channels at longer wavelengths performing slightly better for the RZ formats. This is an indication of the partial compensation of nonlinearity as a result of the net system anomalous dispersion.

With the residual dispersion compensation optimised, the investigation into the effect transmission power plays on the system was conducted. The dependence of the WDM transmission performance for each channel on the launch pulse width and transmission power for both the RZ and CRZ formats is analysed in Fig. 6.18 and Fig. 6.19 respectively. Both figures show the estimated Q mapped against pulse width and transmission power. The result of both the minimum and the average Q over all the wavelengths for a given transmission power and pulse width are also given. These provide a trend to how the overall system is behaving.

Unfortunately, to exploit bulk purchasing discounts, commercial systems are generally constructed from banks of transponders operating with similar parameters and it may not be possible to tune individual launch pulse widths. It becomes necessary to look at the system from a worst-case perspective so that a set of operating parameters, that are proficient for all channels, can be identified in order to create a benchmark for the system components. Fig. 6.20 highlights the minimum Q value for all channels for both RZ and CRZ transmission.

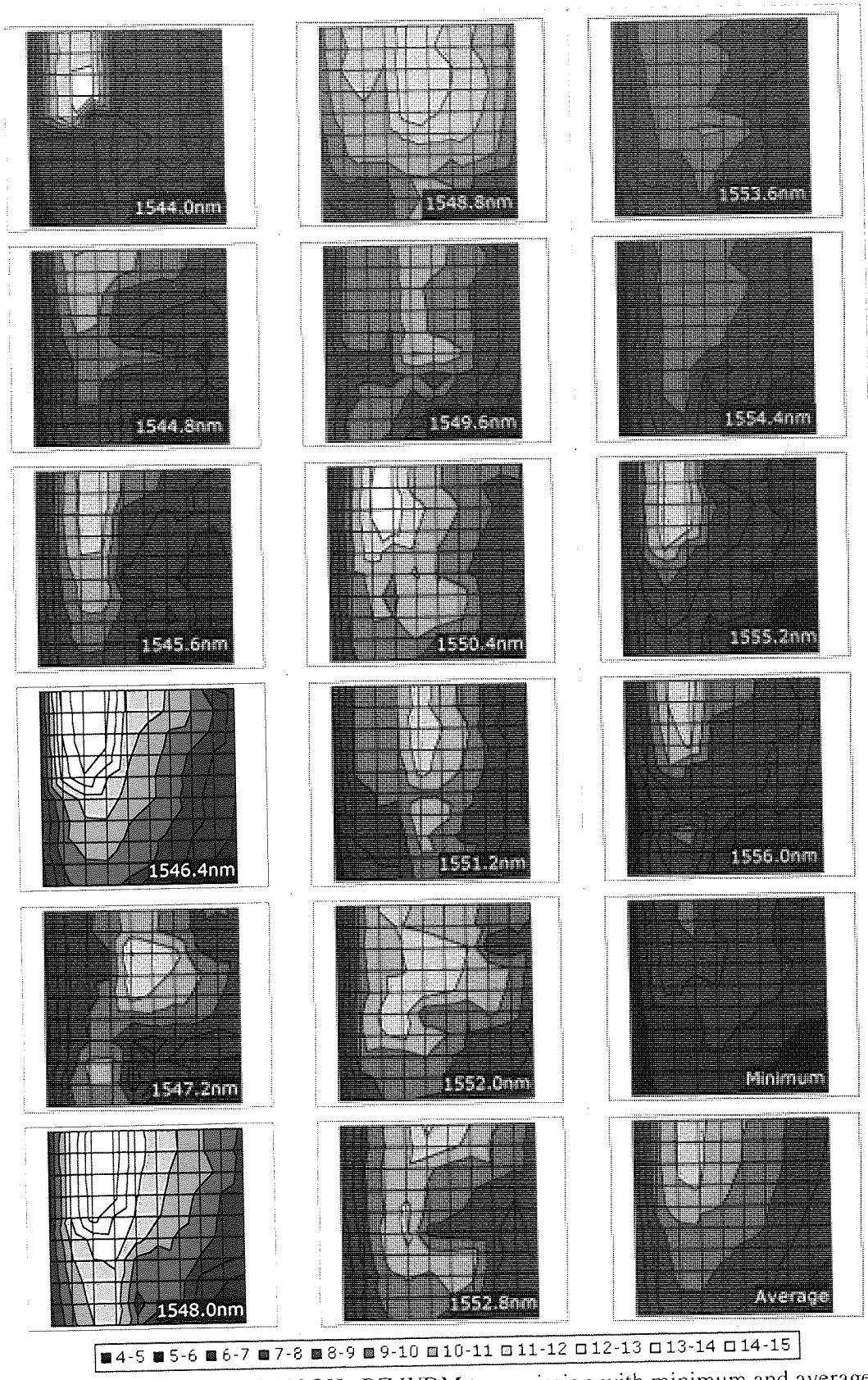

Figure 6.18: 16 Channel 100GHz RZ WDM transmission with minimum and average results. (X = Pulse Width: 5-14ps, Y = Launch Power: 15-24dBm, Z = Q)

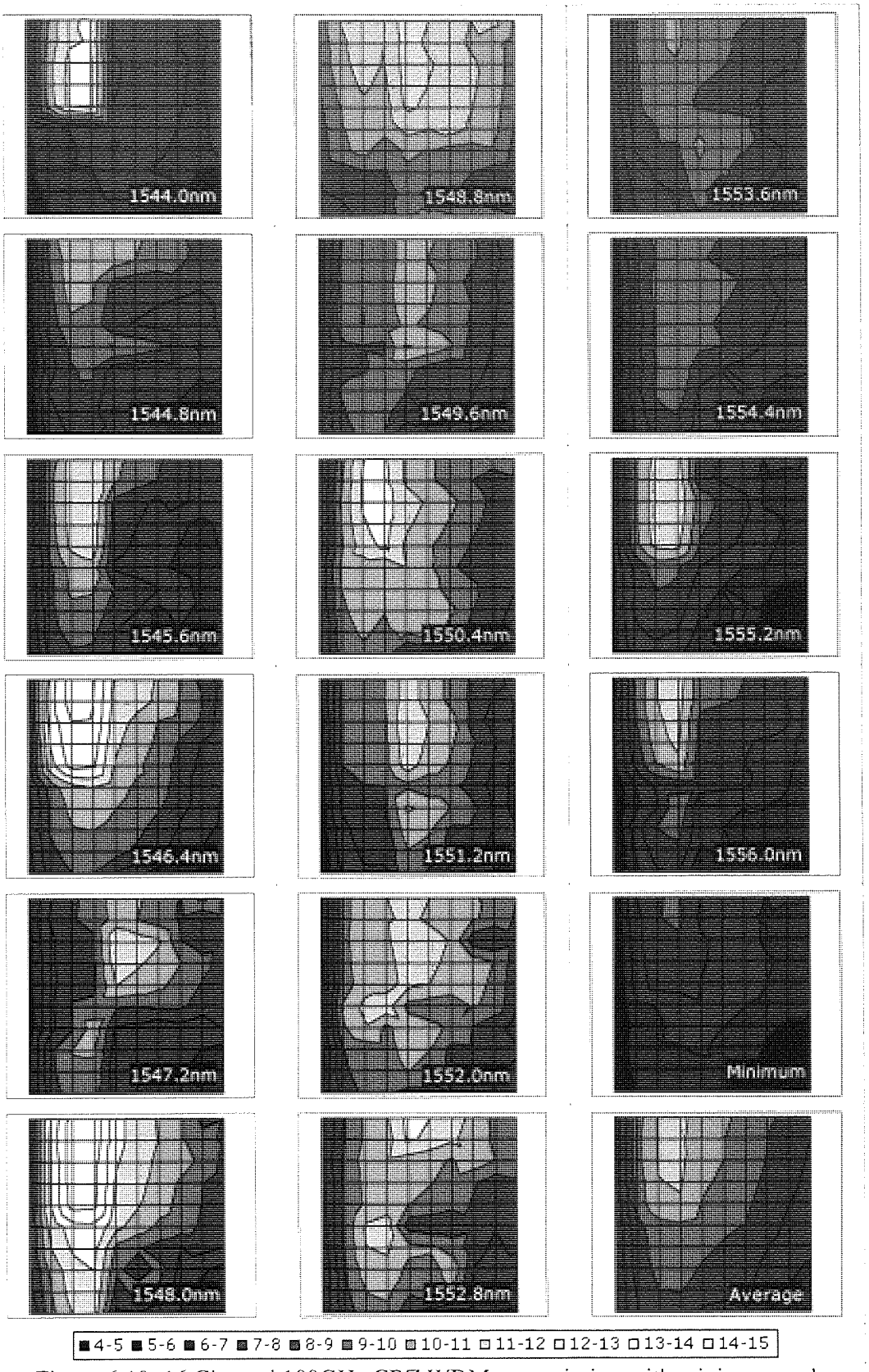

Figure 6.19: 16 Channel 100GHz CRZ WDM transmission with minimum and average results. (X = Pulse Width: 5-14ps, Y = Launch Power: 15-24dBm, Z = Q)

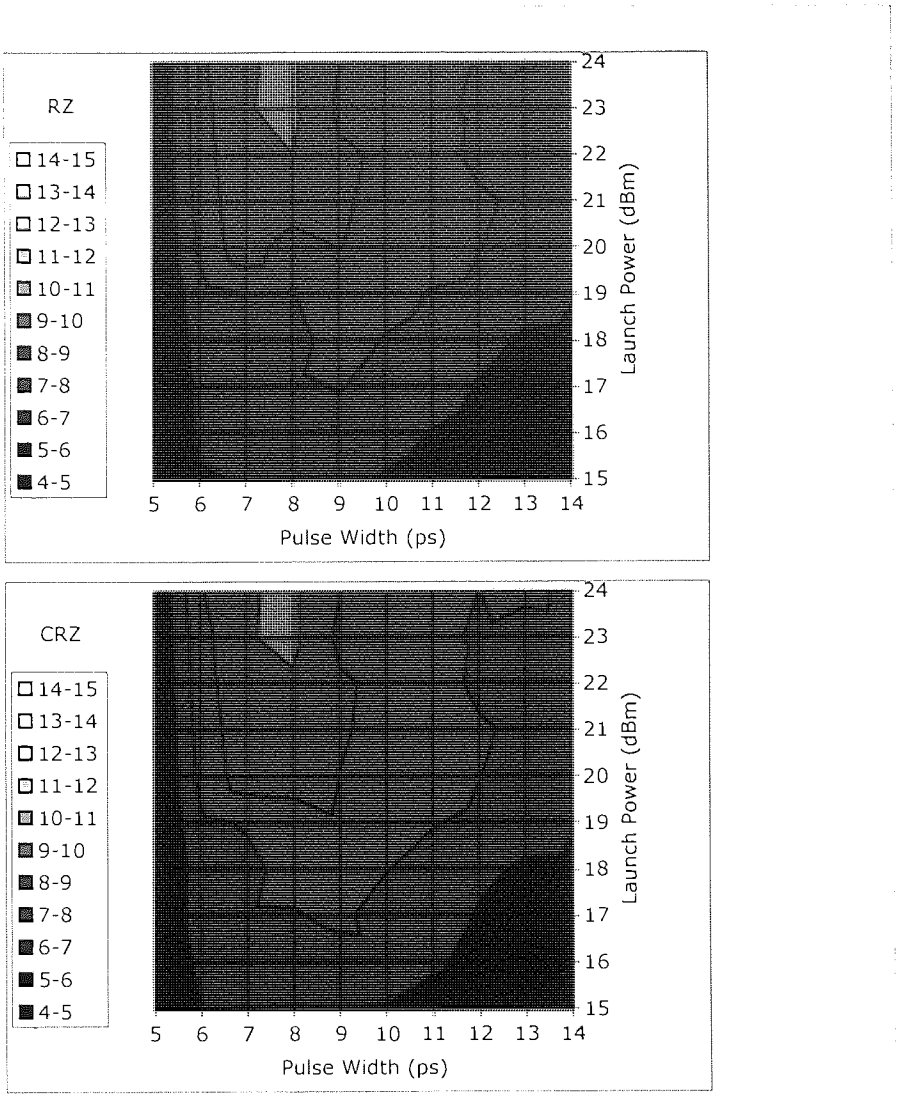

Figure 6.20: Minimum received Q value for all 16 channels against pulse width and launch power for 100Ghz WDM for RZ and CRZ data formats

Again, RZ and CRZ produce similar performances over the 600km with the worst channel performance peaking at a transmission power of 23dBm and a pulse width of 8ps. Although the maps are similar, the map provided by the CRZ format does provide a marginally greater area than RZ for equal Q values. Comparing these results with those for single channel transmission yields a notable increase for the optimum launched Gaussian pulse width; whereas the optimum transmission power has remained the same for RZ at 11dBm per channel (23dBm average power) and has reduced by 1dBm per channel for CRZ. This increase in optimum pulse width is due to the inverse relationship between time and optical frequency. The optimum is found at

8ps, resulting in a bandwidth of 0.62nm for a Gaussian pulse. For pulse widths below this, the spectral side bands interact with those in the neighbouring channels, and this interaction causes the transmission performance to degrade quickly for narrower pulse widths. Also, the filter at the receiver is mapped to the ITU grid, and has a 3dB bandwidth of 0.8nm. Consequently any pulses narrower than 6.2ps would exhibit a greater loss in power due to the attenuation suffered by optical filter in the receiver. Another consequence of increasing the pulse width is that the peak power is reduced, lowering the strength of interchannel interaction. Due to the high local dispersion of the fibres used, the pulses would broaden quickly and the peak powers would diminish rapidly, reducing nonlinear interactions. Therefore, the main reason for WDM optima requiring a greater pulse width is due to the interaction sustained due to power overlapping in the spectral domain.

Fig. 6.21 shows the Q value of each channel for NRZ, RZ and CRZ modulation formats for simulation results optimised for maximum worst channel performance.

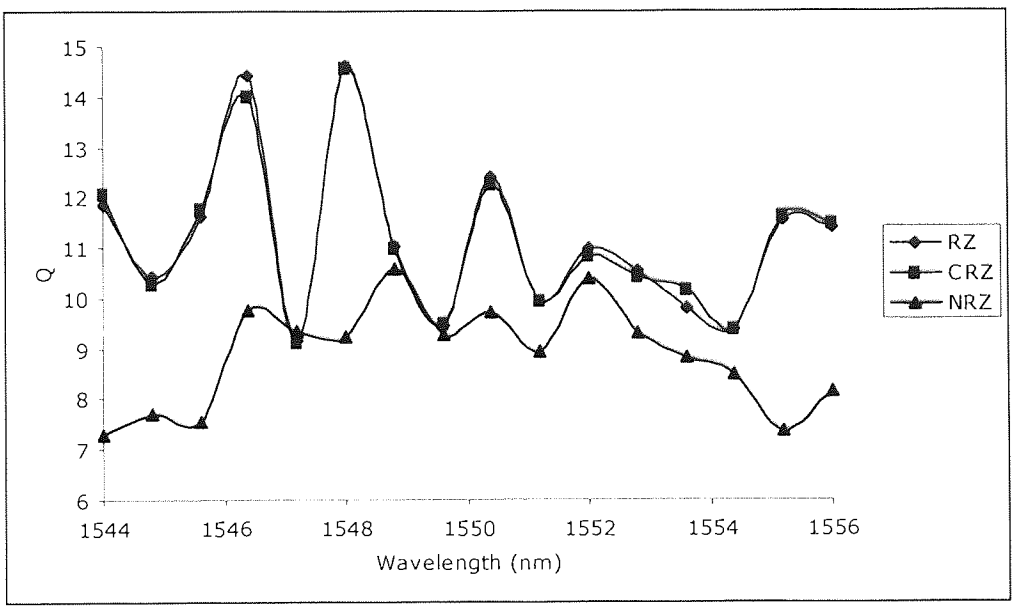

Figure 6.21: Q value for 16 WDM channels transmitted over 600km for NRZ, RZ and CRZ modulation formats.

NRZ performance is moderately consistent with the central channels outperforming the outermost channels, indicating that even with optimised residual dispersion compensation the outer channels still suffer from greater dispersive effects than the central channels. RZ and CRZ accomplish superior transmission performance to that of

NRZ, which achieved worst-case channel Q values greater than 9. With the RDC introduced, estimated Q's tend to be around 11 although the transmission performance between adjacent channels fluctuates quite severely. This fluctuation in Q is due to the fixed launch pulse width, as the pulse width chosen is less than ideal for a number of the channels, and is situated on the rapidly declining slopes of their Q maps (Figs. 6.11 and 6.12).

6.8 • WDM Transmission with Varying Channel Spacing

For the single channel case, the estimated optimal conditions were found for small pulse widths of around 4ps, yet this requires an optical bandwidth of 110GHz per channel. Clearly the ITU grid imposes a limitation on the system designer. By increasing the channel spacing, we hope to be able to increase the transmission performance and reduce or even negate inter-channel effects such as four-wave mixing at the expense of residual dispersion, which can be compensated for at the receiver. For these simulations, the configuration of the system components was the same as that of the 100GHz WDM simulation shown in Fig. 6.12 with the exceptions of the residual dispersion compensation and amplifier bandwidths, which were optimised for the increased channel bandwidths. To test this, the channel spacing was varied from half the ITU 100GHZ spacing (50GHz) to twice the ITU spacing (200GHz) in 25GHz increments in order to evaluate the change in transmission performance. In order to keep the result consistent with the previous work, the wavelength span of the channels was centred at 1550nm and the span and components are outlined in Table 6.1.

The three graphs in Fig. 6.22 show the effect channel spacing has on the received Q value for transmission over 600km for all the considered modulation formats for the RZ (top) CSRZ (middle) and NRZ (bottom) modulation formats. The graphs plot the average estimated Q value for the WDM channels at a given channels spacing. The upper and lower bars around each average show the maximum and minimum estimated Q respectively.

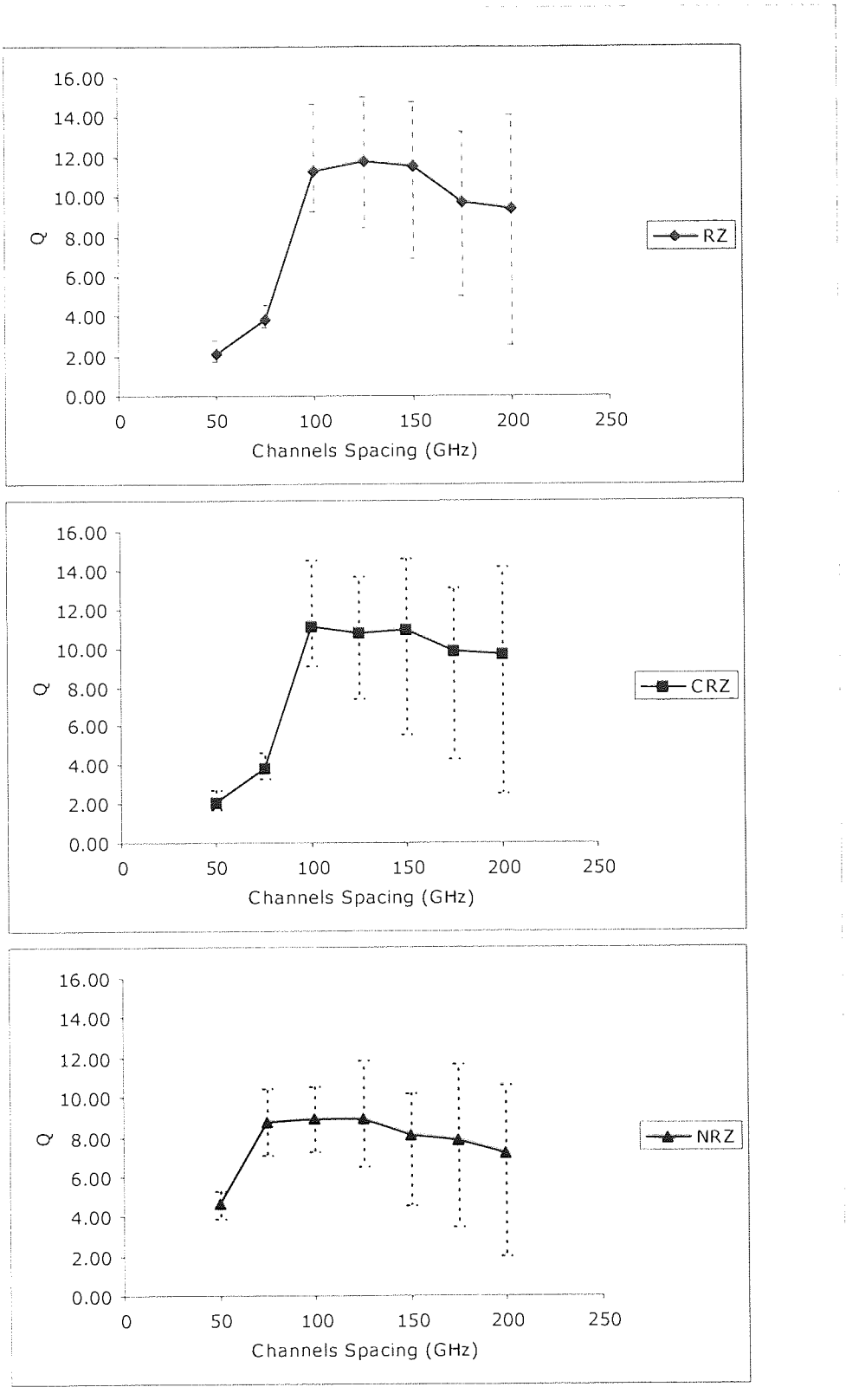

Figure 6.22: Q value against channel spacing for RZ, CRZ and NRZ 16 channel WDM transmission over 600km SMF

NRZ, as with all the three formats, has its low received Q values at the narrowest channel spacing of 50GHz although when the spacing is increased to 75GHz there is a dramatic increase with the average Q almost doubling in value and even the worst channel provides a Q greater than 7. Between 50 and 75GHz, the performance of NRZ exceeds the values for RZ and CRZ transmission although, as the spacing increases the performance of RZ and CRZ supersedes that of NRZ. This is due to NRZs narrower bandwidth, and the sidebands of the modulation format do not extend into the adjacent channels to as much as the sidebands of the RZ and CRZ format.

Beyond 100GHz all formats exhibit the same tendencies. There is a disparity in the trend of the minimum Q compared with the trends for the average and maximum Q values. Whilst the average and maximum Q values tend to remain moderately consistent there is a gradual deterioration in the minimum Q values, these tended to arise from the outer wavelengths whereas the average and maximum results come from the more centrally orientated channels. This drop in performance by the outer channels reduces the minimum system Q resulting in an optimum channel spacing being found at 100GHz even though, for some formats, maximum Q values were attained at broader channel spacing.

On analysing the behaviour of the maximums and minimums we find that below 100GHz the Q values are all closely spaced together indicating that negative inter-channel interactions affect all channel similarly. Increasing the channel spacing exaggerates the effects of dispersion and tends not to significantly reduce any of the nonlinear effects that hamper the transmission performance of all channels. Any reduction of inter-channel effects gained by increasing the channel spacing is negated by the increased dispersion for each channel, even though the residual dispersion was compensated.

6.9 • Conclusions

The performance for 640Gbit/s WDM transmission over 600km with various channel separations has been presented. Throughout the simulations there has been little difference between both RZ modulation formats with the CRZ format providing no significant advantage over conventional RZ for the considered system. Previous work has also shown close results between RZ and CRZ over this distance [171] and it is

expected that CRZ will outperform RZ over longer distances. Performance for both RZ modulation formats is strongly dependent on the transmission pulse width. Optimisation of this parameter is necessary to maximise performance for both single channel and WDM transmission particularly with the narrow bit slot at 40Gbit/s. Both modulation formats provided a marked improvement over the NRZ format, although they are less tolerant to dispersion. Throughout the simulations there has been little difference between both RZ modulation formats with the CRZ format providing no significant advantage over conventional RZ for the considered system. Previous work has also shown close results between RZ and CRZ over this distance [171] and it is expected that CRZ will outperform RZ over longer distances.

Out of all the possibilities presented, the most suitable in terms of a network upgrade would be a 16 x WDM RZ 40Gbit/s with 100GHz channel separation. Deviating from the grid results in greater errors from inter channel interaction when the spacing is reduced and errors for dispersive effects when the channel spacing is increased. Additionally, by operating at frequencies specified by the ITU grid, it may be possible to salvage some of the passive optical components, such as band pass filters, in the receiver and reduce the cost of upgrading. The marginal performance gained by utilising CRZ does not compensate for the cost (both financial and in regards to reliability) incurred in the introduction of additional component. For future upgrades, NRZ may become a viable option. As the available bandwidth for new frequencies is reduced, the narrow spectrum of NRZ allows more channels to be closely packed together with less of an impact on system performance. Based on a 100GHz channel separation, RZ clearly surpasses the performance of the NRZ format. Residual dispersion must be carefully optimised to compensate for the non-complete slope compensation of the DCF.

The system would not be suitable for dispersion managed soliton transmission due to the long amplifier separation and the high local dispersion. Dispersion managed solitons are more suited to systems with lower local dispersion or shorter amplification spans, such as newly installed oceanic systems. It is also worthwhile noting that with these long amplifier spans Raman amplification would be beneficial as by utilising backwards pumping, lower launch powers could be used, although this was not accounted for in the simulations.

6.10 • Summary

In summary, the performance for 640Gbit/s WDM transmission over 600km with various channel separations has been presented. The simulations were performed with BTexact's preSTAR simulation tool that utilised the split step Fourier transform method to solve the nonlinear Schrödinger wave equation. The simulation tool incorporated the nonlinear effect of SPM, XPM and FWM. The simulated span comprised of SMF and 80% slope compensating DCF, with and 100km amplifier separation resulting in a total system length of 600km.

For the single channel 40Gbit/s system, RZ and CRZ performed similarly and both provided larger estimate Q values than that of the NRZ format. Narrow pulses in the region of 4ps tended to perform best as their higher peak power provided a greater contrast ratio. Normally one would expect negative nonlinear interaction to occur for these narrow pulse widths, although due to the long fibre lengths and the high local dispersion, this was not evident.

The system was then expanded to incorporate 16 x 40Gbit/s channels with a 100GHz separation. Due to the non-complete slope compensation of the DCF, residual dispersion was evident on all channels, although it had a greatest effect on those furthest away from the dispersion zero wavelength of 1550nm. When RDC was introduced, the large improvements were made in the Q for the channels at the extremities for the RZ and CRZ formats. Due to its narrower optical spectrum, NRZ showed a greater tolerance to the residual dispersion and smaller improvement in Q were found for this format. Even though NRZ was more dispersion tolerant, RZ and CRZ still outperformed NRZ with and without RDC. The best performance was found to be RZ with an estimated Q of 9.3, whereas NRZ never provided a Q greater than 8. Due to the bandwidth restrictions, the narrow pulse widths used for single channel operation were no longer sustainable for WDM, and optimal performance was found at 8ps, twice the pulse width of the single channel case.

The channel separation was decreased to 50GHz and then increased through to 200GHz in 25GHz steps. Due to their larger bandwidth requirements, the RZ and CRZ formats were outperformed by the NRZ format for the narrower channel separations of 50GHz and 75Ghz. Again, the performance of the RZ and CRZ formats were very similar, with CRZ providing marginally better performance than RZ. At the larger

channel separations, the RZ and CSRZ formats outperformed the NRZ format. When the channels were close together, the system was limited by the inter channel interaction, whereas when the system.

The most suitable format out of the three analysed with respects to upgrading a system for 16 x 40Gbit/s WDM, was found to be the RZ format with a 100GHz channel separation. This was due to its superior performance over the NRZ format and that it has a lower component count than the CRZ format.

Chapter 7

Thesis Conclusions

7.1 • Introduction

This aim of this thesis was to investigate the suitability of dispersion managed solitons transmission for systems operating at 40Gbit/s. This chapter provides a summary of the investigation in this thesis and provides conclusions regarding the main bodies of research.

After the introduction to fibres and systems, the theory behind dispersion, SPM and solitons was explained in order to provide an introduction for the investigation into dispersion managed soliton and the other nonlinear effects that can occur in high-speed TDM and WDM systems. With the aims of eventually experimentally transmitting DMS at 40Gbit/s over a fibre test bed the suitable OTDM sources available were characterised and analysed, along with the modulator necessary for the application of data. The operation of the recirculating loop, crucial for transmission over long distance with limited amplifiers and fibre, was shown. Due to damage that rendered the sole EAM inoperable, the EAM based OTDD designed for the demultiplexing of 40Gbit/s down to 10Gbit/s could no longer function and the available EOMs were inadequate for this task, therefore a new method for OTDD was required. In order to allow demultiplexing with the EOM, the operating principles of fibre based loop mirrors were introduced and a DILM was constructed to aid the EOM with demultiplexing. This research was interrupted by the move to BTexact, where the research shifted away from the experimental and in the direction of terrestrial simulation. A simulation of a terrestrial style system based on SMF was undertaken with the aim of 40Gbit/s WDM transmission around 1550nm.

The ability of the soliton to counteracting the chirp of dispersion by utilising SPM theoretically is ideal, although the solitons susceptibility to timing jitter results in a format that is unsuitable for communications systems. The low path averaged dispersion of a dispersion map allows the DMS to propagate in a similar way to the conventional soliton, but timing jitter is reduced. Like the soliton, the dispersion managed soliton was found to require a balance of fibre dispersion, length and pulse width in order for it to propagate. They also require a symmetric dispersion map with an initial half step of anomalous dispersive fibre. The map strength is a useful equation that balances these parameters and results in a parameter that can be used to define the type of transmission, with values close to 1 generating the most soliton like conditions. It is unlikely that any currently installed systems would be able to sustain DMS due to their operating restrictions. DSF systems have no need to adopt the DMS as they operate around the dispersion zero and have little need for dispersion mapping. SMF based systems have high local dispersion in both the transmission and compensating fibre, so to reduce the map strength, wider pulses are required, increasing the required bit slot. Where the DMS is practical is in new high speed TDM systems with short amplifier separations as they would be able to utilise newer NZDSF which maintains the lower dispersion and allows narrower pulse durations. The high speed TDM DDMS is an impractical solution due to the short periodic nature of the fibre maps and the small bit windows leave a system susceptible to PMD.

The dispersion managed soliton does not coexist well with WDM systems due to the additional nonlinear effects that are introduced when multiple frequencies copropagate. The energy enhancement of DMS exists because of the periodic return to the chirp free point where the peak power is at a maximum. As the efficiency of XPM and FWM is at a maximum when the signals are in phase, this would lead to the generation of large nonlinear interactions at the chirp free points. The narrow pulse widths required to generate the high powers for DMS transmission result in a broader spectrum per channel that will again lead to greater inter-channel interactions. This can be reduced by increasing the separation of the channels, although this reduces the spectral efficiency and reduces the available amplifier bandwidth for future upgrades.

For the upgrading of systems, quasi-linear WDM transmission would allow the introduction of pulse widths that can be optimised to reduce their spectral bandwidth and inter-channel nonlinearities. It places no specific requirements on the fibre span and allows for future upgrades.

In conclusion the dispersion managed soliton is not a suitable solution for the majority of systems and wavelength division multiplexing is a lot more flexible solution.

7.3 • Devices For High Speed Transmission

Like the soliton, loop mirrors utilise nonlinearity in a positive manor. The nonlinear phase shift generated by SPM and XPM allows optical switching when the symmetry of interferometers has been broken. Due to the almost instantaneous response of these nonlinear interactions, these devices can be utilised at extremely high data rates. Yet at bit rates that are currently obtainable, solutions based around concatenating multiple EAM for demultiplexing operate well.

The device examined was the dispersion imbalanced loop mirror. This works on the operating principles of the Sagnac interferometer although the symmetry of the DILM is not broken by loss/gain, but by the dispersion. The pulse propagating along the high dispersion arm initially experiences intense broadening followed by little nonlinearity and the pulse propagating along the low dispersion arm experiences high nonlinearity followed by intense broadening. This results in a phase difference between the two pulses when they overlap and allows switching. One advantage to the DILM is that it rejects CW components such as ASE. As the CW components are not affected by dispersion, when they cross at the mid point, both waves have the same intensity and no phase shift is generated resulting in the light being reflected.

In practice, these devices are susceptible to anything that can instigate changes in phase or polarisation, such as temperature fluctuations and vibrations that disturb the fibre. As such, they are not highly practical and a temperature and vibration safe housing would be required before they could be used in a system. EAM based devices are stable over long periods of time and, due to theirs small housing are easy to integrate into a system. As seen in this thesis, interferometers are useful when conventional demultiplexing devices have reached their maximum performance level. In this case presented here, this was for an EOM and the DILM allowed successful

demultiplexing where previously none had been attainable. In conclusion, traditional EAM based demultiplexers are preferable although when the bandwidth of these demultiplexers has been exhausted, interferometers would provide an extension to this bandwidth.

7.4 • Simulation of Terrestrial 40Gbit/s systems

Simulations over a six 100km amplifier spans was conducted for the RZ, CRZ and NRZ modulation formats at a bit rate of 40Gbit/s, both for a single channel and for 16 channels WDM. While not a direct map of the installed fibre in the UK this was an approximation of the terrestrial system found in UK with their long amplification spans and high local dispersions. Due to the limitations of time, a fixed seed was used for the simulations and only one pass of each simulation was a parsed, leading to a lack of confidence values being used in the results. While this does not mean that the simulation results are wrong, it does lead to possible inaccuracies and greater understanding of the results can be gained by utilising these simulation methodologies. The simulation also did not take into account PMD. In older SMF fibres that were used for slower bit rate systems, minimising PMD was not considered a priority resulting in fibres that have large PMD. This dispersive effect would severely limit transmission as the bit period is reduced.

The high local dispersion of the SMF and DCF coupled together with the large amplifier spans used in terrestrial systems, results in a system that does not lend itself well to the DMS approach. Even providing the pulses FWHM is equivalent to the 25ps bit window for 40Gbit/s this results in map strengths around 4.5 which starting to approaching the more soliton style behaviour. This leads to large overlapping in the time domain at the chirp free point, increasing intra-channel interaction and closes the received eye. Therefore a more linear approach should be taken when examining these systems.

As for the result based on the differing modulation formats, over the relatively short distance of 600km, CSZ provided little difference when compared to the RZ case for both the single channel and the WDM cases and is not worth considering over RZ for this distance. The reduced component count of RZ increases the cost of a real system and improves reliability by reducing the number of components from which something

could go wrong. These RZ formats outperformed the NRZ format in all aspects bar optical bandwidth. Even though NRZ is viewed by many as an old transmission, it narrow bandwidth lends itself to DWDM and reduces its susceptibility to dispersive effects and as such it should not be discounted. In fact the simulations led to the conclusion that for 75GHz spaced WDM, NRZ would out performed the RZ formats, highlighting the spectral efficiency of this format.

The lack of complete dispersion slope cancellation by the DCF also requires RDC at the receiver, although if DMS were sustainable, this would be required at each amplifier. The higher susceptibility of the RZ formats to dispersion leads to this being of greater importance to the RZ and CRZ cases than for the NRZ format. Practically, RDC is quite easy to compensate for by introducing fixed lengths of fibre before each receiver or by incorporating tuneable dispersion devices such as fibre Bragg gratings. As the gains provided by RDC are substantial and the application of a solution is straightforward, this should be employed in all systems that suffer from residual dispersion.

Increasing the channel separation reduces the spectral efficiency but also reduces the WDM based nonlinear interactions. For terrestrial systems, these nonlinear interactions did not dominate the errors due to the reduction in phase matching provided by the high local dispersion. As the channel spacing increased, the errors appeared on the external channels indicating the dispersion compensation was of greater importance, and the optimum was found to be a separation of 100GHz.

In conclusion, the DMS approach is not suitable for 40Gbit/s WDM transmission over 40Gbit/s and a quasi-linear approach is more appropriate for systems with high local dispersion and long amplifier separations.

7.4 • Suggestions for Future Work

The DILM was used for demultiplexing with an EOM, yet it would be interesting to obtain a direct comparison between the EOM-DILM demultiplexer and EAM based demultiplexers. The ability of the DILM to filter CW components could be further investigated by examining the effect of the dispersion map within the loop has on this. The ability to reduce the transmission of CW components would be ideal after an

amplifier mid span, although the suitability of this device in this position would need to be examined.

There are many aspects of terrestrial systems that need to be investigated before commencing an upgrade to the UK terrestrial network. As mentioned above PMD has been largely ignored throughout this thesis, yet this will have a large impact on 40Gbit/s systems, regardless of WDM. The values of the actual PMD of the fibre in the network must be obtained and PMD needs to be introduced.

The model of the EDFAs used in the span can be improved particularly with regards to WDM systems and effects such as gain tilt and polarisation hole burning could be introduced. It is unlikely that these would have a dramatic effect over short transmission distances and methods such as channel pre-emphasis could be employed to counteract gain ripples, although these should be performed to gain a more complete understanding of the systems expected performance.

Only the modulation formats of RZ, CSRZ and NRZ were considered and future work could investigate the suitability of others. The suppression of the sidebands of RZ formats would reduce the spectral overlap of channels and may allow a reduction in channel spacing improving the spectral efficiency. Employing multi-level modulation formats allows the transmission of 40Gbit/s over at 10Gbit/s window, improving spectral efficiency due to the broader pulses and reducing inter-channel nonlinear interaction. This would also reduce the effect of PMD, although this would place restrictions on SNR. The effect of coding schemes such as forward error correction could be introduced and the effect that various correction codes have on transmission could be examined.

Laboratory based experiments could be performed, and due to the short system length and with the provision of enough components, could even operate without the aid of the recirculating loop. This could then be used to perform a direct comparison between the model and the experiment, and highlight the limitations or suitability of the model. Once the experiment and the simulations have been optimised, system trials could be performed over the network.

List of Publication

R.A. Ibbotson, Y.W.A. Lee, S.A. Feiven, I.Y. Khrushchev and K.J. Blow, "Robust 40 to 10 Gbit/s Demultiplexer Comprising a Lithium Niobate Modulator and a Passive Non-linear Fibre Switch", Non-Linear Guided Waves (NLGW2001), Clearwater, Florida, U.S.A. , pp. TuA5 Mar 2001

R. A. Ibbotson, I.Y. Khrushchev and K.J. Blow "40Gbit/s and Beyond" Rank Prize Fund syposium on Terabit Optical Networks (RANK2001), Grassmere, UK. Mar 2001

R. A. Ibbotson, Y-R. Zhou, K. J. Blow, R. P. Davey and A. Lord "40Gb/s RZ- Versus NRZ- Versus CRZ Terrestrial Transmission over Standard Single Mode Fiber with Varying Channel Spacing" accepted Journal of Lightwave Technology subject to revisions, October 2002

References

[1] F. P. Kapron, D. B. Keck, and R. D. Maurer, "Radiation losses in glass optical waveguides" Appl. Phys. Lett., Vol. 17, No. 10, pp. 423-425, Nov 1970

[2] K. C. Kao, and G. A. Hockham, "Dielectric-fibre surface waveguides for optical frequencies" Proc. IEE, 133, pp. 1151-1158, 1966

[3] T. Miya, Y. Terunama, T. Hosaka and T. Miyashita, "An Ultimate Low Loss Single Mode Fiber at 1.55μm" Elec. Lett., No. 15, pp. 106, 1979

[4] A. Ghatak and K. Thyagrajan, "3.6 Loss Mechanisms" in Introduction to Fiber Optics, pp. 34, Cambridge University Press, Cambridge, 1998

[5] A. Ghatak and K. Thyagrajan, "10 Waveguide Dispersion and Design Considerations" in Introduction to Fiber Optics, pp. 191, Cambridge University Press, Cambridge, 1998

[6] Govind P. Agrawal, "2.3.1 Nonlinear Pulse Propagation" in Nonlinear Fiber Optics 2nd Edition, pp. 36, Academic Press, London, 1995

[7] Govind P. Agrawal, "2.3.1 Nonlinear Pulse Propagation" in Nonlinear Fiber Optics 2nd Edition, pp. 38, Academic Press, London, 1995

[8] Govind P. Agrawal, "2.3.1 Nonlinear Pulse Propagation" in Nonlinear Fiber Optics 2nd Edition, pp. 41, Academic Press, London, 1995

[9] C. R. Menyuk. "Application of Multiple-length-scale Methods to the study of Optical Fiber Transmission", Journ. Eng. Math., Vol 36 pp. 113-136, 1999

[10] Govind P. Agrawal, "3.2 Dispersion Induced Pulse Broadening" in Nonlinear Fiber Optics 2nd Edition, pp. 65, Academic Press, London, 1995

[11] Govind P. Agrawal, "3.2 Dispersion Induced Pulse Broadening" in Nonlinear Fiber Optics 2nd Edition, pp. 76, Academic Press, London, 1995

[12] Govind P. Agrawal, "3.2 Dispersion Induced Pulse Broadening" in Nonlinear Fiber Optics 2nd Edition, pp. 92, Academic Press, London, 1995

[13] A. Hasegawa and F. Tappert, "Transmission of Stationary Nonlinear Optical Pulses in Dispersive Dielectric Fibres 1. Anomalous Dispersion", Appl. Phys. Lett., Vol. 2, No.3, pp. 142-144, 1973.

[14] M. Nakazawa, Eyamada, H. Kubota, and K. Suzuki, "10Gb/s Soliton Data Transmission over One Million Kilometres", Electron. Lett., Vol. 27, pp. 1270-1272, 1991.

[15] L. F. Mollenauer, M.J. Neubelt, M. Honer, E. Lichtman, S. G. Evangelides, and B. M. Nyman, "Demonstration of Error-free Soliton Transmission at 2.5 Gbit/s over more than 14,000km," Electron. Lett., Vol. 27, pp. 2055-2056 1991.

[16] Govind P. Agrawal, "5.1 Modulation Instability" in Nonlinear Fiber Optics 2nd Edition, pp.134, Academic Press, London, 1995

[17] C. S. Gardener, J. M. Green, M. D. Kruskal, and R. M. Miura. "Method for Solving the Korteweg-de Vries Equation." Phys. Rev. Lett., Vol.19, pp. 1095, 1967

[18] V. E. Zakharov and A.B.Shabat. "Exact Theory of Two Dimentional Self Focusing and One-dimentional Self Modulation of Waves in Nonlinear Fibres", Soviet Phys. JETP, Vol. 34, pp. 62-69 1972.

[19] Govind P. Agrawal, "5.2 Fiber Solitons" in Nonlinear Fiber Optics 2nd Edition, pp.142, Academic Press, London, 1995

[20] T. Georges and B. Charbonnier, "Reduction of the Dispersive Wave in Periodically Amplified Links with Initially Chirped Solitons", IEEE Photonics Tech. Lett., Vol. 9, No. 1, pp. 127-129, Jan 1997

[21] T. Georges and B. Charbonnier, "Continuum generated by chromatic dispersion and power variations in periodically amplified soliton links", Opt. Lett., Vol. 21, No. 16, pp. 127-129, Aug 1996

[22] K. J. Blow and N. J. Doran, "Average Soliton Dynamics and the Operation of Soliton Systems with Lumped Amplifiers", Phot. Tech. Lett., Vol. 3, No. 4, Apr 1991

[23] S. Kumar, A. Hasegawa and Y. Kodama, "Adiabatic soliton transmission in fibers with lumped amplifiers: Analysis" Journ. Opt. Soc. Amer. B, Vol. 14, No., 4 pp. 888-894, Apr 1997

[24] L. F. Mollenaur, S. G. Evangelides, Jr. and H. A. Haus, "Long-distance Soliton Propagation using Lumped Amplifiers and Dispersion Shifted Fiber", Journ. Light. Tech. Vol. 14, pp. 194-197, 1991

[25] D. J. Richardson, R. P. Chamberlin, L. Dong and D. N. Payne, "High-Qualtiy Soliton Loss-Compensation in 38km Dispersion-Decreasing Fiber", Electon. Lett., Vol. 31, No. 19, pp. 1681-1682, Sep 1995

[26] C. Pare, "Higher-order Quasi-solitons along a Dispersion-profiled Fiber", Optics Comms., Vol. 154, No.1-3, pp. 9-13, Aug 1998

[27] D. J. Richardson, L. Dong, R. P. Chamberlin, A. D. Ellis, T Widdowson and W. A. Pender, "Periodically Amplified System based on Loss Compensating Dispersion Decreasing Fibre" Electon. Lett., Vol. 32, No. 4, pp. 373-374, Sep 1996

[28] H. Kawakami, T. Kataoka, Y. Miyamoto, K. Hagimoto and H. Toba, "Transmission Line with Distributed Erbium-doped Fiber Amplifier", Journ. Light. Tech. Vol.19 No.12, pp. 1887-1891, Dec 2001

[29] H. Li and X. L. Yang, "Study of Distributed Erbium Doped Fiber Amplifier", Int. Journ. Infrared and Millimeter Waves., Vol. 17, No. 11, pp. 1977-1986, Nov 1996

[30] A. Altuncu, A. S. Siddiqui and A. D. Ellis, "Spectral Characteristics of Long Span Distributed Erbium Doped Fibre Amplifiers (DEDFAs) for Soliton Transmission", Electron. Lett., Vol. 33, No.18, pp. 1558-1559, Aug 1997

[31] Govind P. Agrawal, "8.2 Loss-Managed Solitons", in Applications of Nonlinear Fiber Optics 1st Edition, pp. 377, Academic Press, London, 2001

[32] L. F. Mollenauer, J. P. Gordon and M. N. Islam, "Soliton Propagation in Long fibers with Periodically Compensated Loss", IEEE Journ. Quant. Electron. Vol. QE-22, No. 1, pp.157-173, Jan 1986

[33] K. J. Blow and N. J. Doran, "Bandwidth Limits of Nonlinear (Soliton) Optical Communication-systems" Electron. Lett., Vol. 19, No.11, pp 429-430, 1983

[34] J.P. Gordon, "Interaction Forces Among Solitons in Optical Fibers", Opt. Lett., Vol. 8, No., 11, pp 596-598, 1983

[35] Govind P. Agrawal, "5.4.4 Soliton Interaction", in Nonlinear Fiber Optics 3rd Edition, pp176-178, Academic Press, London, 2001

[36] S. Chi, J. C. Dung and S. F. Wen, "Improving the Undoing of Soliton Interaction with Optical-Phase Conjugation by Phase Alteration between Neighbouring Solitons" Opt. Comms., Vol. 117, No. 1-2, pp. 61-64, May 1995

[37] A Mostofiand and P. L. Chu "Reversal of Soliton Interactions in Optically Phase-conjugated Systems with Unequal-amplitude and Alternating-phase Solitons" Opt. Comms., Vol. 141, No.5-6 pp. 259-264 Sep 1997

[38] Govind P. Agrawal, "5.4.3 Soliton Interaction", in Nonlinear Fiber Optics 2nd Edition, pp172, Academic Press, London, 1995

[39] K. Bertilsson and P. A. Andrekson, "Numerical Study of Moderate Distance High Bit-rate Alternating-amplitude Soliton Systems", Journ. Light. Tech., Vol 14, No. 3, pp. 237-242, Mar 1996

[40] M. Suzuki, N. Edagawa, H. Taga, H. Tanaka, S. Yamamoto and S. Akiba, "Feasibility Demonstration of 20 GBit/s Signle-Channel Soliton Transmission over 11500km using Alternating-Ampitude Solitons", Elec. Lett., Vol. 30, No. 13, pp. 1083-1084, Jun 1994

[41] Govind P. Agrawal, "8.5 WDM Soliton Systems", in Applications of Nonlinear Fiber Optics 1st Edition, pp. 417-420, Academic Press, London, 2001

[42] A. Yariv, "Signal-to-noise Considerations in Fiber Links with Periodic or Distributed Optical Amplification" Opt. Lett., Vol. 15, No. 19, pp. 1064-1066, 1990

[43] J. P. Gordon and H. A. Haus, "Random Walk of Coherently Amplified Solitons in Optical Fiber Transmission" Opt. Lett. Vol. 11, No. 10, pp. 665-667, Oct 1986

[44] T. Georges and F. Favre, "Modulation, Filtering, and Initial Phase-control of Interacting Solitons" Journ. Opt. Soc. Am. B, Vol. 10, No. 10, 1880-1889, Oct 1993

[45] D. Marcuse, "An Alternative Derivation of the Gordon-Haus Effect" Vol. 10, No. 2, pp. 273-278, Feb 1992

[46] L. F. Mollenauer, "Method for Nulling Nonrandom Timing Jitter in Soliton Transmission" Opt. Lett., Vol. 21, No. 6, pp. 384-386, Mar 1996

[47] E. M. Dianov, A. V. Luchnikov, A. N. Pilipetskii and A. N. Starodumov. "Electrostriction Mechanism of Soliton Interaction in Optical Fibres" Opt. Lett., Vol. 15, No. 6, pp. 314-316, Mar 1990

[48] K. Smith and L. F. Mollenauer "Experimental Observation of Soliton Interaction over Long Fibre Paths: Discovery of a Long-range Interaction" Opt. Lett., Vol. 14, No. 22, pp. 1284-1286, 1989.

[49] Y. Kodama and A. Hasegawa. "Generation of Asymptotically Stable Optical Solitons and Suppression of the Gordon-Haus Effect" Opt. Lett., Vol. 11, No. 10, pp. 662-664, 1986

[50] V. V. Afanasjev, "Interpretation of the Effect of Reduction of Soliton Interaction by Bandwidth-limited Amplification" Opt. Lett., Vol. 18, No. 10, pp. 790-792, May 1993

[51] Y. Kodama and S. Wabnitz. "Analysis of Soliton Stability and Interactions with Sliding Filters", Opt. Lett. Vol 19, No. 3, pp 162-164, 1994

[52] J. C. Dung, S. Chi and S. Wen, "Reduction of Soliton Interactions by ZigZag-sliding-frequency Guiding Filters" Opt. Lett., Vol. 20, No.18, pp. 1862-1864, Sep 1995

[53] S. Wabnitz and E. Westin, "Optical Fibre Soliton Bound States and Interaction Suppression with High-order Filtering", Opt. Lett. Vol. 21 pp. 1235-1237, 1996

[54] A. Mecozzi, "Soltion Transmission Control by Butterworth Filters" Opt. Lett., Vol. 20, No. 18, pp.1859-1861, Sep 1995.

[55] J. C. Dung, S. Chi and S. Wen, "Reduction of Soliton Interaction by Sliding-frequency Second-order Butterworth Filters", Opt. Lett., Vol. 21, pp 339-341, 1996

[56] O. Leclerc, P. Brindel, S. Bigo, E. Brun-Maunand and E. Desurvire "2 x 20Gbit/s, 3500km Regenerated WDM Soliton Transmission with All-optical Kerr Fibre Modulation" Elec. Lett., Vol. 34. No. 2, pp. 199-201, Jan 1998

[57] N. J. Smith, K.J. Blow, W. J. Firth and K. Smith. "Soltion Dynamics in the Presence of Phase Modulators", Opt. Commun., Vol. 102, No. 3-4, pp. 324-328, Oct 1993

[58] T. Widdowson, D. J. Malyon, A. D. Ellis, K. Smith and K. J. Blow "Soliton Shepherding: All-optical Active Soliton Control over Global Distances" Elec. Lett., Vol. 30, No. 12, pp 990-991, Jun 1994

[59] V. S. Grigoryan and A. Richter "Efficient approach for modeling collision-induced timing jitter in DM return-to-zero dispersion-managed systems" Journ. Light. Tech., Vol. 18, No. 8, pp. 1148-1154, Aug 2000

[60] A. Naka, T. Matsuda and S. Saito, "Optical RZ signal straight-line transmission experiments with dispersion compensation over 5520 Km at 20Gbit/s and 2160 Km at 2 x 20 Gbit/s," Electron. Lett., Vol. 32, No. 18, pp. 1694-1696, 1996

[61] N. Edagawa, I. Morita, M. Suzuki, S. Yamamoto, H. Taga and S. Akiba, "20 Gbit/s, 8100km Straight Line Single Channel Soliton based RZ Transmission Experiment using Periodic Dispersion Compensation" in Proc. 21st European Conf. Optic. Comms. (ECOC'95), Brussels, Belgium, pp. 983-986 1995

[62] F. M. Knox, W. Forysiak, and N. J. Doran, "10-Gbit/s soliton communication over standard fiber at 1.55 μm and the use of dispersion compensation," J. Lightwave Tech., Vol. 12, No. 10, pp. 1955-1962, Oct. 1995

[63] C. Kurtzke "Suppression of fiber nonlinearities by appropriate dispersion management" Photon. Tech. Lett., Vol. 5, pp. 1250-1253, Oct 1993

[64] M. Suzuki, I. Moriata, S. Yamamoto, N. Edagawa, H. Taga, and S. Akiba, "Timing jitter reduction by periodic dispersion compensation in Soliton transmission," in Proc. Optic. Fiber. Comms., Washington DC, Optic. Soc. Amer. Postdeadline paper PD20, 1995

[65] N. J. Smith, W. Forysiak, and N. J. Doran, "Reduced Gordon-Haus Jitter due to Enhanced Power Solitons in Strongly Dispersion Managed Systems" Electron. Lett., Vol. 32, No. 22, pp. 2085-2086, 1996

[66] N. J. Smith, N. J. Doran, W. Forysiak, and F. M. Knox, "Soliton Transmission Using Periodic Dispersion Compensation," J. Lightwave Tech., Vol. 15, No. 10, pp. 1808-1822, Oct 1997

[67] A. R. Chraplyvy, A. H. Gnauck, R. W. Tkach, and R. M. Derosier, "8 x 10 Gb/s Transmission Through 280 km of Dispersion-Managed Fiber", IEEE Photon. Tech. Lett., Vol. 5, No. 10, pp. 1233-1235, Oct. 1993

[68] S.-M. Hwang and A. E. Willner, "Guidelines for Optimizing System Performance for 20 WDM Channels Propagating Through a Cascade of EDFA's", IEEE Photon. Tech. Lett., Vol. 5, No. 10, pp. 1190-1193, Oct. 1993

[69] C. Lin, H. Kogelnik, and L. G. Cohen, "Optical-pulse Equalization of Low-Dispersion Transmission in Single-mode Fibers in the 1.3-1.7 μm Spectral Region" Opt. Lett., Vol. 5, pp. 476, 1980

[70] S. K. Turitsyn, I. Gabitov, E. W. Laedke, V. K. Mezentsev, S. L. Musher, E. G. Shapiro, T. Schäfer, and K. H. Spatchek, "Variation Approach to Optical Pulse Propagation in Dispersion Compensated Transmission Systems" Opt. Comms., Vol. 151, No.1, pp. 117-135, May 1998

[72] J. P. Gordon and L. F. Mollenauer. "Scheme for Characterising Dispersion Managed Solitons", Opt. Lett., Vol. 24, No. 4, pp. 223-225, 1999

[71] A. R. Pratt , H. Murai and Y. Ozeki, "40Gbit/s Multiple Dispersion Managed Soliton Transmission over 2700km", in A. Hasegawa, "Massive WDM and TDM Soliton Transmission Systems, A ROSC Symposium", pp. 309-326. Kluwer Academic Publishers, Dordrecht, 2000

[73] J. H. B. Nijhof, W. Forysiak, and N. J. Doran. "Dispersion-Managed Solitons in the Normal Dispersion Regime: a Physical Interpretation", Opt. Lett., Vol. 23, No. 21, pp. 1674-1676, Nov 1998

[74] A. Berntson, N. J. Doran, W. Forysiak, and J. H. B. Nijhof "Power Dependence of Dispersion-managed Solitons for Anomalous, Zero, and Normal Path-averaged Dispersion" Opt. Lett., Vol. 23., pp. 900-902, June 1998

[75] S. K. Turitsyn, J. H. B. Nijhof, W. K. Mezentsev, and N. J. Doran, "Symmetries, Chirp-Free Points, and Bistability in Dispersion-Managed Fiber Lines", Opt. Lett., Vol. 24, No. 24, pp. 1871-1873, Dec 1999

[76] N. J. Smith, W. Forysiak, and N. J. Doran, "Enhanced Power Solitons in Optical Fibres with Periodic Dispersion Management", Electron. Lett., Vol. 32, No. 1, pp. 54-55, Jan 1996

[77] J. H. B. Nijhof, N. J. Doran, W. Forysiak and A. Berntson, "Energy Enhancement of Dispersion-managed Solitons and WDM" Electron. Lett., Vol. 34, No. 5, pp. 481-482, Mar 1998

[78] J. H. B. Nijhof, N. J. Doran and W. Forysiak, "Energy Enhancement of Dispersion managed Soltions for Strong Dispersion Maps" in Technical Digest of Opt. Fiber Comms. Conf., paper ThC4, 1998

[79] T. Yu, E. A. Golovchenko, A. N. Pilipetskii, and C. R. Menyuk,. "Dispersion-managed Soliton Interaction in Optical Fibers" Opt. Lett., Vol. 22, No. 11, pp. 793-795, Jun 1997

[80] L. J. Richardson, W. Forysiak and N. J. Doran, "Trans-Oceanic 160Gb/s Single-Channel Transmission using Short-period Dispersion Management" IEEE Photon. Tech. Lett., Vol. 13, No. 3, pp. 209-211, Mar 2001

[81] A. Maruta, Y. Yamamoto, S. Okamoto, A. Suzuki, T. Morita, A. Agata, and A. Hasegawa "Effectiveness of Densely Dispersion Managed Solitons in Ultra-high speed transmission" Electron. Lett., Vol. 36, No. 23, pp. 1947-149, Nov 2000

[82] J. Mårtensson and A. Berntson, "Dispersion-managed Solitons for 160-Gb/s Data Transmission" IEEE Photon. Tech. Lett., Vol. 13, No. 7, pp. 666-668, Jul 2001

[83] R.-J. Essiambre, G. Raybon and B.Mikkelsen, "Pseudo-Linear Transmission of High-Speed TDM Signals: 40 and 160Gbit/s" in I Kaminow and T Li, "Optical Fibre Telecommunications IVB Systems and Impairments", pp. 233, Academic Press, London, 2002

[84] P. V. Mamyshev and N. A. Mamysheva, "Pulse-overlapped dispersion-managed Data Transmission and Intrachannel four-wave mixing" Opt. Lett., Vol. 24, No. 21, pp. 1454-1456, Nov 1999

[85] R.-J. Essiambre, B. Mikkelsen and G. Raybon, "Intrachannel Cross-Phase Modulation and Four-Wave Mixing in High-Speed TDM Systems" Electron. Lett., Vol. 35, pp. 1576-1578, 1999

[86] S B Alleston and P Harper and I S Penketh and I Bennion and N J Doran, "1220km propagation of 40Gbit/s single channel RZ data over dispersion managed standard (non-dispersion shifted) fibre", in Tech. Digest Opt. Fiber Comms. Conf pp. PD3, San Diego, California, Feb 1999

[87] K. Fukuchi, T. Kasamatsu, M. Morie, R. Ohhira, T. Ito, K. Sekiya, D. Ogasahara, and T. Ono, "10.92Tbt/s (273 x 40Gbit/s) Triple-band/Ultra-dense WDM Optical Repeated Transmission Experiment" in Tech. Digest Opt. Fiber Comms. Conf., postdeadline paper PD24, Mar 2001

[88] L. J. Richardson, V. K. Mezentsev and S. K. Turitsyn, "Limitations of 40Gbit/s based dispersion managed WDM transmission: solitons versus quasi-linear propagation regime" in Tech. Digest Opt. Fiber Comms. Conf., paper MF5-1, 2000

[89] G. P. Agrawal, "Stimulated Raman Scattering" in Nonlinear Fibre Optics, Third Edition, Academic Press, London, pp. 298, 2001

[90] P. Bayvel and R. Killey, "Nonlinear Optical Effects in WDM Transmission" in Optical Fibre Telecommunications IVB, Systems and Impairments. Academic Press, London, pp. 619-633, 2002

[91] G. P. Agrawal, "Cross Phase Modulation" in Nonlinear Fibre Optics Third Edition, Academic Press, London, pp. 260-293, 2001

[92] S. V. Chernikov and J. R. Taylor, "Measurement of Normalization Factor for n_2 for Random Polarization in Optical Fibers," Optics Lett., Vol. 21, No. 19, pp. 1559, 1996

[93] T. K. Chiang, N. Kagi, T. K. Fong, M.E. Marhic and L.G. Kazovsky, "Cross-Phase Modulation in Fiber Links with Multiple Optical Amplifiers and Dispersion Compensators", IEEE Jour. Light. Tech., Vol. 14, No. 3, pp.249-259, 1996

[94] A. Mahapatra and E. J. Murphy, "Electooptic Modulators" in Optical Fibre Telecommunications IVA, Components, Academic Press, London, pp 282, 2002

[95] G. P. Agrawal "10.1: Origin of Four Wave Mixing" in "Nonlinear Fiber Optics" Third Edition, pp. 389-392, Academic Press, London, 2001

[96] G. P. Agrawal "10.3 Phase-Matching Techniques" in "Nonlinear Fiber Optics" Third Edition, pp. 405, Academic Press, London, 2001

[97] P. Bayvel and R. Killey "Nonlinear Optical Effects in WDM Transmission" pp. in I Kaminow and T Li, "Optical Fibre Telecommunications IVB Systems and Impairments" pp. 618-619, Academic Press, London, 2002

[98] G. P. Agrawal "7.6 Four-Wave Mixing" in "Applications of Nonlinear Fiber Optics" First Edition pp. 344-348, Academic Press, London, 2001

[99] E. Desurvire, D. Bayart, B. Desthieux and S. Bigo, "Nonlinear Effects in WDM Transmission" from "Erbium-Doped Fiber Amplifiers Devices and Systems" pp. 497-503, Wiley Interscience, London, 2002

[100] D. A. Ackerman, J. E. Johson, L. J. P. Ketelsen, L. E. Eng, P. A. Kiely and T. G. B Mason, "Telecommunication Lasers" pp 587 in I Kaminow and T Li, "Optical Fibre Telecommunications IVA Components", Academic Press, 2002

[101] O. Mizuhara, T. V. Nguyen, L. D. Tzeng, and P. D. Yeats, "10Gbit/s Transmission Experiment using Direct Modulation including an 8:1 Time-division-multiplex" Electron. Lett. Vol. 31, pp. 660-662, 1995

[102] D. Adams, C. Rolland, n. Puetz, R. Moore, F. Shepherd, H. Kim, and S. Bradshaw, "Mach-Zender Modulator Integrated with a Gain-coupled DFB Laser for 10Gbit/s, 100 km NDSF Transmission at 1.55μm" Electron. Lett., Vol. 32, pp. 485-486, 1996

[103] M. Aoki, T. Sudi, D. Tsuchiya, D. Takemoto, and S. Tsuji, "85-C-10 Gb/s Operation of 1.3μm InGaAlAs MQW-DFB Laser", in Proc. Eur. Conf. Opt. Commun. 2000, paper 3.3.1, 2000

[104] F. N. Timofeev, I. A. Kostko, P. Bayvel, O. Berger, R. Wyatt, R. Kashyap, I. F. Lealman and G. D. Maxwell, "10 Gbit/s Directly Modulated, High Temperature-stability External Fibre Grating Laser for Dense WDM Networks" Electron. Lett., Vol. 35, pp. 1737-1739, 1999

[105] A. Ebberg, F. Auracher, and B. Borchet, "10 Gbit/s Transmission using Directly Modulated Uncooled MQW Ridge Waveguide DFB lasers in TO package", Electron. Lett., Vol. 36, pp. 1476-1477, 2000

[106] A. B. Massara, K.A. Williams, I. H. Wjhite, R. V. Penty, A. Galbraith, P. Crump and P. Harper "Ridge Waveguide InGaAsP Lasers with Uncooled 10 Gbit/s Operation at 70C" Electron. Lett., Vol. 35, pp. 1646-1647, 1999

[107] P. A. Morton, G. E. Shtengel, L. D. Tzeng, R. D. Yadvish, T. Tanbun-Ek, and R. A. Logan "38.5km Error Free Transmission at 10 Gbit/s in Standard Fibre using a Low Chirp, Spectrally Filtered, Directly Modulated 1.55μm DFB Laser", Electron. Lett., Vol. 33, pp. 310-311, 1997

[108] A. J. Taylor, J. M. Wiesenfeld, G. Eisenstein, and R. S. Tucker, "Timing Jitter in Mode-locked and Gain-switched InGaAsP Injection Lasers," Applied Physics Lett., Vol. 47, pp. 448-450, Sept. 1985

[109] A. G. Weber, W. Ronghan, E. H. Böttcher, M. Schell, and Dieter Bimberg, "Measurement and Simulation of the Turn-on Delay Time Jitter in Gain-switched Semiconductor Lasers" IEEE J. Quantum Electron., Vol. 28, No. 2, pp. 441-445, Feb 1992

[110] D. Seo, D. Y. Kim, and H. Liu, "Timing Jitter Reduction of Gain-switched DFB Laser by External Injection-seeding" Electron. Lett., Vol. 32, No. 1, pp. 44-45, Jan 1996

[111] I. Y. Khrushchev, I. H. White, and R. V. Penty, "High-quality Laser Diode Pulse Dompression in Dispersion-imbalanced Loop Mirror" Electron. Lett., Vol. 34, No. 10, pp. 1009-1010, May 1998

[112] M. D. Pelusi, and H. Liu, "Higher Order Soliton Pulse Compression in Dispersion-decreasing Optical Fibres" IEEE J. Quantum Electron., Vol. 33, No. 8, pp. 1430-1439, Aug 1997

[113] A. D. Ellis, R. J. Manning, I. D. Phillips, and D. Nesset, "1.6ps Pulse Generation at 40GHz in Phaselocked Ring Laser Incorporating Highly Nonlinear Fibre for Application to 160Gbit/s OTDM Networks" Electron. Lett, Vol. 35, No. 8, pp. 645-646, Apr 1999

[114] A. Hirano, Y. Miyamoto, K. Yonenaga, A. Sano, and H. Toba, "40Gbit/s L-band Transmission Experiment using SPM-tolerant Carrier-suppressed RZ Format", Electron. Lett., Vol. 35, pp. 2213-2215. 1999.

[115] Y. Miyamoto, K. Yonenaga, S. Kuwahara, M. Tomizawa, A. Hirano, H. Toba, K. Murata, Y. Tada and Y. Umeda, "1.2-Tbit/s (30 x 42.7-Gbit/s ETDM optical channel) DM transmission over 376 km with 125 km Spacing using Forward Error Correction and Carrier-suppressed RZ Format", in Proc. Opt. Fiber Commun. Conf., postdeadline paper PD26, 2000.

[116] N. Bergano, C. Davidson, M. Mills, P. Corbett, B. Evangelides, B. Petersen, R. Menges, J. Zyskind, J. Sulhoff, A. Srivastava, C. Wolf and J. Judkins, "Long-haul WDM Transmission using Optimum Channel Modulation: A 160Gbit/s (32 x 5Gb/s) 9,300km Demonstration" in Proc. Opt. Fiber Commun. Conf., postdeadline paper PD16, 1997

[117] K. Yoneneaga and S. Kuwano, "Dispersion-tolerant Optical Transmission System using Duobinary Transmitter and Binary Receiver", IEEE J. Lightwave Technol. Vol. 15 pp. 1530-1537, 1997

[118] C. R. R. Pollack, "Fundamentals of Optoelectronics" pp. 200, McGraw-Hill, New York, 1995

[119] M. Suzuki, H. Tanaka, K. Utaka, N. Edagawa, and Y. Matusuchima, "Transform-limited 14 ps Optical Pulse Generation with 15 GHz Repetition Rate by InGaAsP Electroabsorption Modulator" Electron. Lett., Vol. 28, No. 11, pp. 1007-1008, May 1992

[120] D. A. B. Miller, D. S. Chemia, T. C. Damen, A. C. Gossard, W. Wiegmann, T. H. Wood, and C. A. Burrus, "Band-edge Electroabsorption in Quantum Well Structures: the Quantum-confined Stark Effect" Phys. Rev. Lett., Vol. 53, No. 22, pp. 2173-2176, Nov 1984

[121] P. Harper, S. B. Alleston, and N. J. Doran, "80Gbit/s RZ Transmission Over 523km Using Dispersion Compensated Standard Fibre" in Proc. 26th Europ. Conf. on Opt. Comm., Vol.2, paper pt. 2, pp. 143-145, Munich, 2000

[122] S. B. Alleston, P. Harper, I. S. Penketh, I. Bennion, N. J. Doran and A. D. Ellis, "1000km Transmission of 40Gbit/s Single Channel RZ Data over Dispersion Managed Standard (Non-dispersion Shifted) Fibre" Electron. Lett, Vol. 35, No. 10, pp. 823-824, May 1999

[123] T. Ito, K. Fukuchi, K. Sekiya, D. Ogashara, R. Ohhira, and T. Ono. "6.4Tb/s (160 x 40Gb/s) WDM Transmission Experiment with 0.8bit/s/Hz Spectral Efficiency" in Proc. Eur. Conf. Opt. Commun, postdeadline paper PD1.1, 2000

[124] N. S. Bergano, "Undersea Communication Systems" pp.188 in, I Kaminow and T Li, "Optical Fibre Telecommunications IVB Systems and Impairments", Academic Press, 2002

[125] E. Desurvire, D. Bayart, B. Desthieux and S. Bigo, "Erbium-Doped Fiber Amplifiers Device and System Developments", John Wiley and Sons, New York, pp. 466-467, 2002.

[126] N. S. Bergano, "Undersea Communication Systems", in I. Kaminow and T. Li "Optical Fiber Telecommunications IVB", chapter 4, pp. 180-183, Academic press, San Diego, 2002.

[127] M. G. Taylor, "Observation of New Polarisation Dependence Effect in Long Haul Optically Amplified System", IEEE Photon. Tech. Lett., Vol. 5, No. 10, pp. 1244, 1993.

[128] N. S. Bergano and C. R. Davidson, "Circulating Loop Transmission Experiments for the Study of Long-haul Transmission System using Erbium Doped Fibre Amplifiers." IEEE Journ. Light. Tech. Vol. 13 pp. 879-888, 1995

[129] N. S. Bergano, "Undersea communication systems" pp.173 in, I Kaminow and T Li, "Optical Fibre Telecommunications IVB Systems and Impairments", Academic Press, 2002

[130] D. Marcuse, "Derivation of Analytical Expressions for the Bit-Error Probablility in Lightwave Systems with Optical Amplifiers," Journ. Light. Tech. Vol. 8, pp. 1816-1823, 1990

[131] P.A Humblet and M. Azizoglu, "On the Bit Error Rate of Lightwave Systems with Optical Amplifiers", Journ. Light. Tech, Vol. 9, pp. 1576-1582, 1991.

[132] V. J. Mazurczyk and D. G. Duff, "Effect of Intersymbol Interference on Signal-to-Noise Measuremens," Conf, on Optical Fiber Communication, paper WQ1, 1995.

[133] N.s Bergano, F. W. Kerfoot and C. R Davidson, "Margin measurements in optical amplifier systems", IEEE Photon. Tech. Lett., Vol. 5, No. 4, 1997

[134] G. Raybon, B. Mikkelsen, R.-J. Essiambre, A.J. Stentz, T.N. Nielsen, K. Dreyer, J.E. Johnson, L. Hsu, D.W. Peckham and NJ, L. Gruner-Nielsen, "320 Gbit/s Single Channel Pseudo Linear Transmission over 200km of NZDSF", in Technical Digest, Conf. on Opt. Fiber Comms., Postdeadline paper PD29 2000

[135] P.Harper, S.B.Alleston and N.J.Doran, "Experimental Comparison of SF/DCF and Short Period NZDSF Maps for 40 Gbit/s RZ Data Transmission", Proceedings of the 26th European Conf. on Opt. Comm. (ECOC'00), 2000

[138] J.P. Sokoloff, P. R. Prucnal, I. Glesk, and M. Kane, "A Terahertz Optical Asymmetric Demultiplexer (TOAD)" IEEE Photon. Technol. Lett., Vol 5, No. 7, pp. 787-790, July 1993

[139] J.P. Sokoloff, P. R. Prucnal, I. Glesk, and M. Kane, "Performance of a 50 Gbit/s Optical Time Domain Multiplexed System using a Terahertz Optical Asymmetric Demultiplexer" IEEE Photon. Technol. Lett., Vol 6, No. 1, pp. 98-100, Jan 1994

[140] S. B. Alleston, I. S. Penketh, P. Harper, A. Niculae, I. Bennion, and N. J. Doran, "16,000km, 10Gbits-1 Soliton Transmission over Standard Fibre by Reduction of Interaction through Optimum Amplifier Positioning" in Conference on Optical Fiber Communications, OFC99, Technical Digest, WC4, Feb 1999

[141] E. Yamada, H. Kubota, T. Yamamoto, A. Sahara, and M. Nakazawa, "10Gbit/s 10,000km Dispersion-allocated Soliton Transmission using Conventional1.3μm Single Mode Fibers" Electron. Lett, Vol. 33, No. 7, pp. 602-603, Mar 1997

[142] A. R. Pratt, H. Murai, and Y. Ozeki, "40 Gbit/s Single Channel Transmission over 3120 km of Dispersion Managed Standard Fibre" in Proc. 26th Europ. Conf. on Opt. Comm., Vol 4. paper pt. 4, pp. 43-44, Munich, 2000

[143] S.B.Alleston, P.Harper, I.S.Penketh, I.Bennion, N.J.Doran, A.D.Ellis, "1000 Km Transmission of 40 Gbit/s Single Channel RZ Data over Dispersion Managed Standard (Non-dispersion shifted) Fibre", Elec. Let., Vol. 35, pp. 823-824, 1999

[144] I.Y.Khrushchev, I.D.Phillips, A.D.Ellis, R.J.Manning, D.Nesset, D.G.Moodie, R.V.Penty, I.H.White, "OTDM Applications of Dispersion-Imbalanced Fibre Loop Mirror", Elec. Let., Vol. 35, 1183-118, 1999

[145] D.D. Marcenac, A.D. Ellis, and D. G. Moodie, "80 Gbit/s OTDM using electroabsorption modulators", Elec.Lett., Vol. 34, No. 1, pp. 101-103, Jan 1994

[146] M. Cavallari, M. Jones, P. Kean, D. Watley, and A. Hadjifotiou, "Single channel 160 GB/s OTDM propagation over 480 km of standard fiber using a 40 GHz semiconductor mode-locked laser pulse source", at Opt. Commun. Conf, Postconference Technical Digest, Vol. 1, No. 1, pp. 4-5, Mar 2002

[147] J. E. Midwinter "Photonics in Switching" Academic press, San Diego, CA. 1993

[148] G. P. Agrawal "Coupler Characteristics" in "Applications of Nonlinear Fiber Optics" pp62, Academic Press, London, 2001

[149] B. K. Nayar, N. Finlayson, N. J. Doran, S. T. Davey, W. L. Williams, and J. W. Arkwright, "All-optical Switching in a 200-m Twin-core Fiber Nonlinear Mach-Zehnder Interferometer" Opt. Lett. Vol. 16, No. 6, pp. 408-410, Mar 1991

[150] N. J. Doran and D. Wood, "Nonlinear-optical Loop Mirror" Opt. Lett., Vol 13, No. 1, pp56-58, Jan 1988

[151] B. K. Nayar, N. Finlayson, and N. J. Doran, "Concatenated all-optical Loop Mirror Switches" Journ. Of Modern Opt., Vol. 40, No. 12, pp. 2327-2332, 1993

[152] K. J. Blow, N. J. Doran and B. P. Nelson, "Demonstration of the Nonlinear Fibre Loop Mirror as an Ultrafast All-optical Demultiplexer" Electron. Lett., Vol 26, pp. 2008, 1990

[153] M. E. Fermann, F. Haberl, M. Hofer, and H. Hochstrasser, "Nonlinear Amplifying Loop Mirror" Opt. Lett., Vol 15, No. 13, pp. 752-754, July 1990

[154] K. J. Blow, N. J. Doran, B. K. Nayar and B. P. Nelson, "Two-wavelength Operation of the Nonlinear Fiber Loop Mirror" Opt. Lett., Vol. 15, No. 14, pp. 248-250, July 1990

[155] M. Eiselt, "Optical Loop Mirror with Semiconductor Laser Amplifier", Electron. Lett., Vol. 28, No. 16, pp. 1505-1507, 1992

[156] A. L. Steele, "Pulse Compression by an Optical Fibre Loop Mirror Constructed from Two Different Fibres" Electron. Lett., Vol. 29, No. 22, pp. 1972-1974, Oct1993

[157] M. C. Jeruchin, P. Balaban, and K. S. Shanmugan, "Simulation of Communication Systems" pp 492-520, Plenum Press, New York, 1992

[158] J. Wright and A. Lord, "Modelling of Subsea Cable Networks", Suboptic'97 proceeding, San Francisco, USA, pp. 878 – 885, May 1997

[159]: J. Wright, "Numerical Modelling of Transoceanic Cable Systems", IEE Colloq. 67 'Transoceanic Cable Comm.- TAT 12 and 13 Herald a new era', Savoy Place, London, UK, 1996

[160] F. D. Tappert and R. H. Hardin, "Computer Simulation of Long-Range Ocean Acoustic Propagation using the Parabolic Equation Method", 8th Applied Optics, Int Congr on Acoust, Contributed Pap, pp. 452, 1974

[161] C. J. Anderson and J. a. Lyle, "Technique for Evaluating System Performance using Q in Numerical Simulations Exhibiting Intersymbol Interference", Elec. Lett, Vol. 30, No. 1, pp. 71-72, Jan 1994.

[162] K. Suzuki, H. Kubota and M. Nakazawa, "1 Tb/s (40 Gb/s x 25 channel) DWDM Quasi-DM Soliton Transmission Over 1,500 km Using Dispersion-Managed Single-Mode Fiber and Conventional C-band EDFAs" in Proc OFC2001, paper TuN7-1, 2001

[163] L. J. Richardson, V. K. Mezentsev and S. K. Turitsyn, "Limitations of 40 Gbit/s Based Dispersion Managed WDM Transmission: Solitons Versus Quasi-linear Propagation Regime" in Technical Digest, Conf. on Opt. Fiber Comms., paper MF5-1, 2001

[164] A. Maruta, Y. Yamamoto, S. Okamoto, A. Suzuki, T. Morita, A. Agata and A. Hasegawa, "Effectiveness of Densely Dispersion Managed Solitons in Ultra-high Speed Transmission" Electron. Lett., Vol. 36, No. 23, pp. 1947-1949 Nov 2000

[165] L. J. Richardson, W. Forysiak and N. J. Doran, "Trans-Oceanic 160-Gb/s Single-Channel Transmission Using Short-Period Dispersion Management" IEEE Photonics Tech. Lett., Vol. 13, No. 3, pp. 209-21, Mar 2001

[166] G. P. Agrawal, "3 Group Velocity Dispersion" in Nonlinear Fiber Optics, 3rd ed. London, U.K.: Academic, 2001, pp. 63-66, 171-175.

[167] A. Sahara, H. Kubota, M. Nakazawa, "Comparison of the Dispersion Allocated WDM 910 Gbit/s x 10 channels) Optical Soliton and NRZ systems using a Q map", Opt. Comms., Vol. 160, pp. 139-145, Feb 1999

[168] C. Caspar, H. -M. Foisel, A. Gladisch, N. Hanik, F. Küppers, R. Ludwig, A. Mattheus, W. Pieper, B. Strebel, and H. G. Weber, "RZ Versus NRZ Modulation Format for Dispersion Compensated SMF-Based 10-Gb/s Transmission with more than 100-km Amplifier Spacing" IEEE Photon. Tech. Lett., Vol. 11, No. 4, pp. 481-483, Apr 1999

[169] M. I. Hayee and A. E. Willner, "NRZ Versus RZ in 10-40-Gb/s Dispersion-Managed WDM Transmission Systems" IEEE Photonics Tech. Lett., Vol. 11, No. 8, pp. 991-993, Aug 1999

[170] R. -M. Mu, T. Yu, V. S. Grigoryan and C. R. Menyuk, "Dynamics of the Chirped Return-to-Zero Modulation Format" J. Lightwave Tech. Lett., Vol. 20, No. 1, pp. 47-57, Jan 2002

[171] L. -S. Yan, Y. Xie, Q. Yu, A. E. Willner, D. Starodubov and J. Feinberg, "Performance Optimisation of Chirped Return-to-Zero Format in 10-Gb/s terrestrial Transmission Systems" Technical Digest, Conf. on Opt. Fiber Comms., paper MF1-1, 2001

[172] K. Ennser and K. Petermann, "Performance of RZ- Versus NRZ- Transmission on Standard Single-Mode Fibres" IEEE Photon. Tech. Lett., Vol. 8, No. 3, pp. 443-445, Mar 1996

[173] M. Nakazawa, H. Kubota, K. Suzuki, E. Yamada and A. Sahara, "Ultrahigh-Speed Long-Distance TDM and WDM Soliton Transmission Technologies" IEEE J. Selected Topics Quantum Electron., Vol. 6, No. 2, pp 363-396, 2000

[174] F. Forghieri, P. R. Prucnal, R. W. Tkach and A. R. Chraplyvy, "RZ Versus NRZ in Nonlinear WDM Systems" IEEE Photon. Tech. Lett., vol. 9, No. 7, pp. 1035-1037, July 1997

[175] G. P. Agrawal, Applications of Nonlinear Fiber Optics, pp. 367-438, London, U.K.: Academic, 2001, pp. 367-373.

[176] W. Forysiak, N. J. Doran, F. Knox and K. J. Blow, "Average Soliton Dynamics in Strongly Perturbed Systems" Opt. Comms., Vol, 117, pp. 65-70, May 1995

[177] T. Georges and B. Charbonnier, "Reduction of the Dispersive Wave in Periodically Amplified Links with Initially Chirped Solitons" IEEE Photon. Tech. Lett., Vol. 9, No. 1, pp. 127-129, Jan 1997

[178] Ewart Lowe, Dominique Marcenac, Tim Gilfedder, Ian Hawker "WDM and WADMs in BT's network"in Proc. Optical Add Drop Multiplexing: The First Step in Optical Networking 1998, pp 13-17, 1998